Master of Science thesis
in Climate Dynamics

The sensitivity of marine-terminating glaciers to model parameters and geometry

Nadine Steiger

University of Bergen
Faculty of Mathematics and Natural Science
Geophysical Institute

supervised by

Prof. Kerim H. Nisancioglu
Dr. Helen Johnson
MSc. Henning Åkesson

June 1, 2016

Abstract

Greenland outlet glaciers are among the largest contributors to global sea level rise. With high velocities and calving rates, they discharge large amounts of glacial ice into the ocean. During the last two decades, the mass loss of these glaciers has increased dramatically. Jakobshavn Isbræ recently experienced dramatic acceleration to peak velocities of $17\,\mathrm{km\,yr^{-1}}$; in contrast to other fast Greenland glaciers, its high velocities have persisted. Many studies have explained the observed acceleration with increased ocean water temperatures, increased surface runoff and reduced buttressing by sea ice. However, it is still not completely understood how external factors, such as changes by the atmosphere and ocean, impact marine-terminating glaciers.

Here, the impact of ice temperature, basal sliding, crevasse water depth, submarine melt rate, and buttressing by sea ice on glacier properties is studied with a numerical flowband model. A sensitivity study is conducted on an idealized marine-terminating glacier and on Jakobshavn Isbræ. Changes to the driving as well as internal parameters of the ice flow model have a great impact on the idealized glacier. Whilst a change in crevasse water depth, buttressing by sea ice, and submarine melt impact the thickness and length proportionally, basal sliding and ice rheology influence rather the shape of the glacier. The ice temperature is represented by the rate factor, a complex parameter, found to influence the glacier in opposing ways through its control on the viscosity and lateral resistance. The study of Jakobshavn Isbræ shows that stabilization at pinning points dominates the impact of parameter uncertainties. The grounding line position can therefore be stable for hundreds of years, while the thickness of the glacier continues adjusting to previous perturbations. This adjustment may eventually lead to a dramatic change of the grounding line position. It is therefore crucial for ice sheet models to involve centennial to millennial time-scales.

ACKNOWLEDGMENTS

Without my exchange semester at the University Center in Svalbard in spring 2013, I would probably still ask myself what I actually want to become when I am grown up. The magic nature of the polar regions and the beauty of ice, however, uncovered my strong wish to become a polar researcher. As a scientist, I just do not need to grow up, but can instead continue asking questions about where all this beauty comes from. During the semester at UNIS, I gained many smart and inspiring friends among which many by now have become polar scientists that share my fascination for polar regions and that I keep crossing paths with.

First of all, I very much want to thank my supervisors Kerim Nisancioglu and Helen Johnson for letting me work on a great and exciting topic with the necessary guidance and motivation during sometimes frustrating periods. I want to thank Kerim, who gave me many opportunities to attend meetings, conferences and courses, in which I not only learned a lot, but also got into contact with unbelievably friendly and competent scientists. He funded and enabled me the attendance at the Karthaus Summer School, which gave me a broad knowledge on glacier modelling, as well as the upcoming ACDC Summer School. I am also very happy that I could be part of the Ice2Ice project and that I could join the Ocean Outlook meeting at the Woods Hole Oceanographic Institution.

I am very grateful that I could be part of the best working group I could imagine, that provided me with support, advices and especially a lot of fun during the meetings. Basile de Fleurian was a great help with technical questions and as a glaciology specialist. Silje Smith-Johnson, thank you for the funny times at WHOI. A special thanks goes to (now my well-deserved third supervisor!) Henning Åkesson, who helped and supported me throughout my whole thesis. He has always been there to discuss my results and problems, supplied me with helpful MATLAB scripts, updates on the model, useful articles, and the initial input data for the model that finally enabled me to get a steady-state glacier after a long and exhausting time of searching for a stable model run. Thank you also Kerim, Helen, Henning and Basile for reviewing my thesis.

Thanks to Faezeh Nick and Andreas Vieli, who provided me with the model and who helped me out with technical problems, questions concerning the model and interpretations. I also appreciated to get started with the flowband model through the matlab version by Ellyn Enderlin. Thanks to Mahé Perrette and Johanna Beckmann for the great webglacier1d-app to extract flowline data from Greenland and also a thanks to the providers of the datasets: Jonathan Bamber, Eric Rignot, Jeremie Mouginot and

Mathieu Morlighem. Thanks to Idar Hessevik for answering all my stupid technical questions.

I also want to thank my fellow students for letting me being part of them and my friends to make the writing period more enjoyable through coffee breaks, hikes and more.

Christoffer, I am happy about sharing my big interest in nature with you!

Last but not least, I want to thank my family and my friends in Germany for always being there for me! Mama und Papa, ihr seid die Besten und ich bin unglaublich dankbar, dass ihr mich bei jedem Schritt in meinem Leben unterstützt!

Bergen, June 1, 2016

Nadine Steiger

Nadine Steiger

Contents

Abstract

Acknowledgments

1 Introduction 1
- 1.1 State of the Art 1
- 1.2 Motivation 2
- 1.3 Objectives 3
- 1.4 Outline 4

2 Theory and Background 5
- 2.1 Mass Balance 5
- 2.2 Ice Dynamics 6
  - 2.2.1 Stress and Strain 7
  - 2.2.2 Gravitational Driving Stress 7
  - 2.2.3 Basal Motion 8
  - 2.2.4 Lateral Drag 10
  - 2.2.5 Longitudinal Stress Gradient 11
  - 2.2.6 Ice Rheology 11
  - 2.2.7 Calving 12
- 2.3 Submarine Melt 13
- 2.4 Sea Ice and Ice Mélange 15
- 2.5 Jakobshavn Isbræ 15
- 2.6 Usage of a Numerical Flowband Model 16

3 Model Description 19
- 3.1 Continuity 20
- 3.2 Force Balance 20
- 3.3 Flotation Criterion 21
- 3.4 Calving Criterion 21
- 3.5 Boundary Conditions 23

4 Sensitivity of an Idealized Glacier 25
- 4.1 Description of the Initial Input and Steady-State 25
- 4.2 Perturbation Studies 28
  - 4.2.1 Basal Sliding 28
  - 4.2.2 Calving and Crevasse Water Depth 30
  - 4.2.3 Buttressing by Sea Ice and Ice Mélange 30

4.2.4 Submarine Melt Rate 32
4.2.5 Ice Temperature 34

5 Sensitivity of Jakobshavn Isbræ 37
5.1 Description of Input Data and Steady-State 37
5.2 Perturbations of Parameters 40
5.2.1 Basal Sliding 41
5.2.2 Calving and Crevasse Water Depth 41
5.2.3 Buttressing by Sea Ice and Ice Mélange 43
5.2.4 Submarine Melt Rate 45
5.2.5 Ice Temperature 46
5.3 The Relative Impact of Ice Temperatures on Viscosity and Lateral Stress 46

6 Discussion 49
6.1 Relative Importance of Parameters 49
6.2 Time Dependent Model Adjustment 53
6.3 Time Dependent Forcing 54
6.4 Stability of an Idealized Outlet Glacier versus Jakobshavn Isbræ 56

7 Conclusions and Outlook 59
7.1 Conclusions 59
7.2 Outlook 60

Notations

Appendices 65

A Different Bed Topography Data for Jakobshavn Isbræ 66

B Along-flow Stress Components 67
B.1 Idealized Glacier 67
B.2 Jakobshavn Isbræ 68

C Time Evolution for Basal Sliding 69

D Viscosity and Lateral Resistance 70

E Stabilization of Idealized Glacier 71

F Relative Importance of Parameters 72
F.1 Response after 1500 Years 72
F.2 Response of Jakobshavn Isbræ after 1500 Years 73

References 75

List of Figures 89

1

INTRODUCTION

1.1. State of the Art

One quarter of the global sea level rise during the last two decades was driven by mass loss from the Greenland ice sheet (GrIS) and the Antarctic ice sheet (AIS) (Cazenave and Llovel, 2010; Church and White, 2011). The GrIS lost three times more mass than the AIS during 2003 to 2008 ($-232\pm23\,\mathrm{Gt\,yr^{-1}}$ and $-72\pm43\,\mathrm{Gt\,yr^{-1}}$, respectively) (Shepherd et al., 2012). The GrIS contributed $7.5\pm1.8\,\mathrm{mm}$ to global sea level rise between 1992 and 2011. The most alarming fact is that the rate of ice loss from Greenland quadrupled within this period, from $-51\pm65\,\mathrm{Gt\,yr^{-1}}$ (1992 to 2000) to $-211\pm37\,\mathrm{Gt\,yr^{-1}}$ (2000 to 2011) (Shepherd et al., 2012).

Most of the GrIS is drained by marine-terminating outlet glaciers; these are characterized by fast-flowing ice, which is discharged from an ice cap or ice sheet through deep incised troughs in fjords, where the glaciers terminate with either a floating or grounded margin. The large ice fluxes, transported by outlet glaciers, are lost to the ocean by runoff, submarine melt and iceberg calving. Increased atmospheric and oceanic temperatures have caused dynamic instability of these glaciers during the last decades (e.g. Carr et al., 2013; Khan et al., 2014), such that ice discharge from the ice sheet exceeds snowfall and contributes to sea level rise. The terminus of outlet glaciers is vulnerable to regional warming on a seasonal to decadal time-scale (Joughin et al., 2004; Nick et al., 2009; Howat et al., 2010; Vieli and Nick, 2011), while the slow-moving interior of the ice sheet adjusts to perturbations on a centennial to millennial time-scale (MacGregor et al., 2016).

Despite a significant increase in mass loss of the GrIS, more than half of the ice sheet's interior has been thickening (Thomas et al., 2000; Krabill et al., 2004; Ettema et al., 2009; Schenk and Csathó, 2012) and some areas along the western margin have been decelerating (Tedstone et al., 2013). The thickening can be partly explained by higher accumulation rates (McConnell et al., 2000), but is also a slow dynamic adjustment to the last deglaciation due to a diminishing amount of soft ice (MacGregor et al., 2016).

Two processes have led to increased mass loss along the margins of the GrIS: higher surface melt rates (Van den Broeke et al., 2009; Ettema et al., 2009) and dynamic ice discharge to the ocean via marine-terminating glaciers (Thomas et al., 2003; Howat et al., 2007; Holland et al., 2008; Nick et al., 2009). The former process is driven by increased atmospheric temperatures over Greenland of about 2 °C since 1990 (Hanna et al., 2008; Box et al., 2009), causing an increase in surface melt and runoff. The latter process results from increased oceanic and atmospheric temperatures, both acting on the calving terminus of outlet glaciers and destabilizing the glaciers. Dynamic instability has initiated dramatic losses with discharge rates of tens of $\mathrm{km}^3\,\mathrm{yr}^{-1}$. Mass loss by dynamic changes dominates over mass loss by surface melt in the case of outlet glaciers, whose retreat, thinning and acceleration start at the marine terminus (Abdalati et al., 2001; Rignot and Steffen, 2008; Nick et al., 2009; Thomas et al., 2009).

Dynamic instability due to increased atmospheric and ocean temperatures is associated with different processes:

- Surface melt lubricates the ice-bedrock interface through penetration of meltwater to the bed, which may increase flow velocities (Schoof, 2010); though this effect remains debated (Tedstone et al., 2013).
- Surface meltwater enters crevasses and forces them to deepen, making the glaciers more prone to iceberg calving (Nick et al., 2009; Benn and Evans, 2010; Cook et al., 2012).
- Increased ice discharge correlates with warmer ocean water, which melts the marine terminus of outlet glaciers from below (Holland et al., 2008; Motyka et al., 2011; Straneo and Heimbach, 2013).
- Sea ice in front of marine-terminating glaciers, which binds icebergs together, is melted by warmer ocean water; as a consequence, buttressing at the front is reduced and the glaciers accelerate (Amundson et al., 2010; Cassotto et al., 2015).

The best example of an outlet glacier that has become dynamically unstable is Jakobshavn Isbræ in western Greenland. It is one of the largest outlet glaciers in Greenland and drains about 6.5% of the ice sheet (Motyka et al., 2011). In 2003, almost its whole floating tongue disintegrated, amounting to a retreat of 10 km (Vieli and Nick, 2011). As a consequence, it accelerated from $5700\,\mathrm{m\,yr^{-1}}$ in 1992 to $17\,000\,\mathrm{m\,yr^{-1}}$ in 2012 (Joughin et al., 2014) and contributed significantly to global sea level rise.

Marine-terminating glaciers experience retreat rates an order of magnitude larger than their land-terminating counterparts, due to their contact with the ocean (Carr et al., 2013). Studying outlet glaciers is therefore of high interest and their dynamics has been recognized as one of the key factors of peak loss of Arctic glacier ice (Carr et al., 2013). This thesis addresses the relative importance of the various processes outlined above for the dynamic behavior and surface elevation of an idealized as well as a realistic Greenland outlet glacier.

1.2. Motivation

Measurements and modeling of outlet glaciers have received increased attention over the last decade, thanks to the progressive awareness of the sensitivity of outlet glaciers to external forcings. Dynamic instability is a response to increased ocean and atmospheric warming (e.g. Oppenheimer, 1998; Bamber et al., 2007; Carr et al., 2013), but glacier stability is also affected by the underlying bed topography (Schoof, 2007; Jamieson et al., 2012; Enderlin et al., 2013a). The importance of external forcing and the outlet geometry is poorly understood. Measurements from the ice sheet, on the fast-flowing ice of outlet glaciers, and in the fjords could provide better knowledge but remain sparse and challenging to conduct. The key processes causing dynamic changes are therefore inadequately implemented into glacier models. A deeper understanding of these key processes is needed to improve their implementation into models and hence enable us to predict the evolution of the GrIS and its potential contribution to future sea level rise. Furthermore, many studies have focused on the recent climate change as a driver for the observed rapid retreat and acceleration of Greenland outlet glaciers (e.g. Nick et al., 2009; Straneo and Heimbach, 2013; Khan et al., 2014). However, glacier adjustment on centennial and millennial time-scales may play a larger role for the present-day observed changes than expected (MacGregor et al., 2016).

1.3. Objectives

The aim of this thesis is to understand the basic physics of marine-terminating glaciers and to correlate changes in glacier dynamics directly with the driving mechanisms. Therefore, a simple flowband model is used to conduct a parameter sensitivity study on an idealized glacier, in which five parameters are perturbed from the steady-state. With the gained insight into the sensitivity of the simple geometry to external forcing, perturbations of the same parameters are applied to the more complex geometry of Jakobshavn Isbræ to also explore the effect of topographic feature on the glacier. Instead of only focusing on the last decades, in which climate change has impacted outlet glaciers, the response of glaciers to perturbations will also be investigated on longer time-scales.

Three research questions are addressed:

1. What is the relative role of internal properties (ice temperature and basal sliding) versus the impact of terminus changes (calving, submarine melt and buttressing from sea ice) for a given, idealized geometry of a marine-terminating glacier?
2. How does the impact of changes to internal ice properties and the terminus studied in *1.* compare to the impact of fjord geometry on outlet glaciers?
3. What is the short term (decadal) versus the long term (centennial to millennial) response of the outlet glaciers?

Note, that the perturbed parameters are highly dependent on the size and geometry of the glacier. Therefore, the qualitative response of glaciers to parameter perturbations is studied rather than a quantification of realistic parameter values, or glacier length and volume changes.

1.4. Outline

Chapter 2 provides background knowledge on glacier mass balance and glacier dynamics, including the stresses that act on a glacier, as well as ice rheology, and the processes influencing the ice-ocean interface. Additionally, the advantage of using a simple model is outlined and Jakobshavn Isbræ in western Greenland is described, as it is used as a case study. Details of the numerical flowband model are given in Chapter 3, including a description of the governing equations and the calving law used. Chapter 4 presents the idealized outlet glacier model set-up and the results of the parameter sensitivity study. Moving from the idealized glacier, Chapter 5 presents a case study using the approximate geometry of Jakobshavn Isbræ. Here, the glacier set-up is described, followed by the results of a sensitivity study performed as in Chapter 4. The discussion in Chapter 6 compares the impact of the different parameters on the idealized glacier with the impact of topography on the real glacier. Moreover, the importance of different time-scales is discussed, as well as factors that cause stability of marine-terminating glaciers. Finally, Chapter 7 summarizes the study and provides an outlook with suggestions for future work.

2

THEORY AND BACKGROUND

2.1. Mass Balance

Glaciers are fed by accumulation of snowfall, snow-drift, and avalanches. In the accumulation zone, temperatures are low enough for the snow to survive several summers and to transform into ice by pressure from its own weight. Gravitational forces move the ice slowly downhill into the ablation zone, where temperatures are higher and mass loss exceeds accumulation (see Figure 2.1). The balance between accumulation of snow and ablation by surface melt is known as surface mass balance (SMB). At the equilibrium line, which is the transition between the accumulation and ablation zones, the surface mass balance is zero. Topography, local, and regional climate define the equilibrium line altitude (ELA), which rises (declines) in a warmer (colder) climate. While ablation by surface melt and consequent runoff is the main process for mass loss on land-terminating glaciers, marine-terminating glaciers, in addition, lose mass to the ocean by calving and submarine melt. A warming climate increases ablation and often also precipitation.

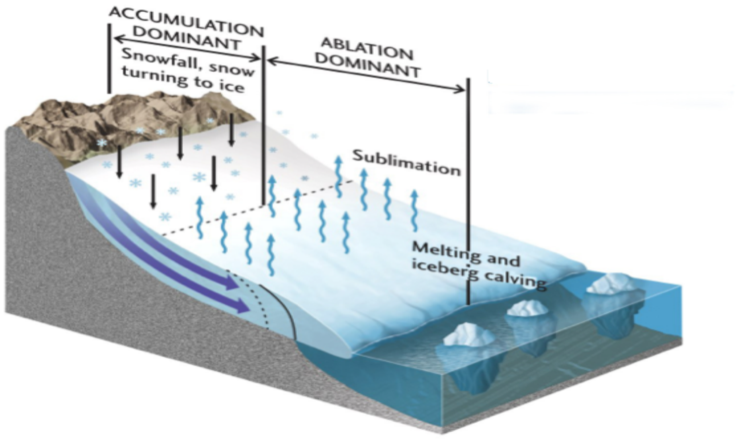

Figure 2.1.: Sketch of the glacier mass balance of a marine-terminating glacier, showing processes of accumulation and ablation; the ELA is marked as dashed line (Giffoni, 2014).

On Greenland, 90% of the ice sheet area belongs to the accumulation zone, where the SMB is positive (Ettema et al., 2009). During the last half century, precipitation in the interior of the ice sheet has increased, whereas mass loss along the coasts has increased even more as shown in Figure 2.2 (Ettema et al., 2009). Rapid mass loss first started along the southeastern coast between 2003 - 2007 but set in along the northwestern coast during the following two years (Khan et al., 2010) and has also started to increase in the northeast (Khan et al., 2014).

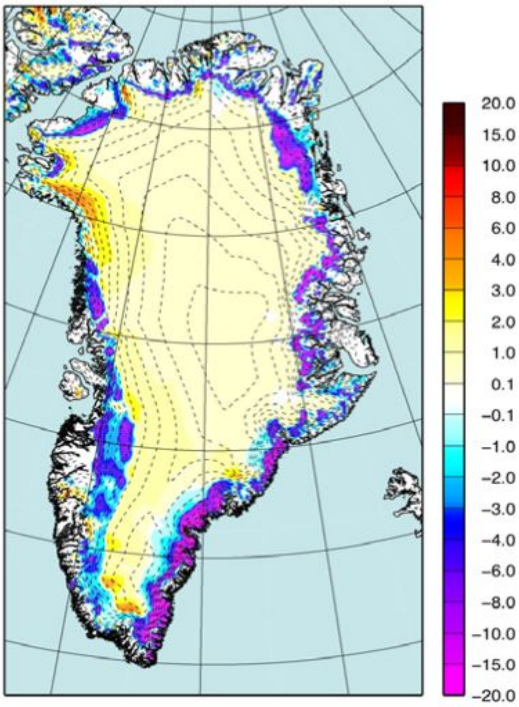

Figure 2.2.: Modeled SMB change from 1958 to 2007 in kg m^{-2} (Ettema et al., 2009). 250 m elevation contours from Bamber et al. (2001) are shown as dashed lines.

2.2. Ice Dynamics

Ablation by calving and submarine melt reaches high loss rates and influences - in addition to the glacier volume - the glacier dynamics. Dynamic mass loss is, in contrast to surface melt, more complex and difficult to calculate. It causes rapid retreat as well as thinning and acceleration through dynamic coupling (Nick et al., 2009).

This section gives an overview of the main physics that influence the dynamics of outlet glaciers. The corresponding equations, as they are used in the model, are presented in Chapter 3.

2.2.1. Stress and Strain

Motion and deformation of glacier ice are due to stresses that act on the glacier. The single components of the stress tensor are symbolized by σ_{ij}, where the index i defines the direction in which the stress is applied and j defines the direction normal to the surface. The magnitude and direction of the stresses determine how much the ice is being compressed, stretched, or sheared. Compression and stretch are caused by normal stresses that are perpendicular to a surface ($i = j$), whereas shearing is caused by shear stresses (also termed τ_{ij}, where $i \neq j$) acting parallel to a surface.

The derivation of the stress components from the hydrostatic pressure $P = \frac{1}{3}\sigma_{kk}$, where summation over repeated indices is implied, is known as deviatoric stress (σ'_{ij}) and calculated as $\sigma'_{ij} = \sigma_{ij} - \delta_{ij}P$. δ_{ij} is the Kronecker delta ($\delta_{ij} = 1$ if $i = j$, and $\delta_{ij} = 0$ if $i \neq j$). The stress components can also be divided into resistive stresses $R_{ij} = \sigma_{ij} - \delta_{ij}L$, opposing the lithostatic stress $L = \rho_i g(H - z)$, which is the weight of the ice above the level z. The shear stresses are unaffected by the hydrostatic and the lithostatic pressure (Van der Veen, 2013, pp.8-48).

Strain (ϵ_{ij}) occurs as the result of stresses and describes how a material is deformed. In glaciology strain rates are rather used - the rate at which the ice deforms - and calculated as

$$\dot{\epsilon_{ij}} = \frac{d}{dt}\epsilon_{ij} = \frac{1}{2}\left(\frac{\partial u_i}{\partial x_j} + \frac{\partial u_j}{\partial x_i}\right). \tag{2.1}$$

The form of deformation is dependent on the ice crystal structure and the viscosity (see Subsection 2.2.6). Deformation of ice happens as creep and if the applied stress exceeds a certain yield stress, it experiences failure, which becomes visible on glaciers in form of crevasses due to fracturing. Further details on stress and strain are explained by Van der Veen (2013).

2.2.2. Gravitational Driving Stress

Ice is set in motion through gravitation. Because of the slope of a glacier, the ice moves from the accumulation zone to the ablation zone. The gravitational driving stress (here simplified called τ_d, as the model only considers the x-direction) is the downslope component of the gravitational force and only determined by the steepness of the glacier surface $\frac{\partial h}{\partial x}$ and its thickness H (Benn et al., 2007a).

$$\tau_d = \rho_i g H \frac{\partial h}{\partial x} \tag{2.2}$$

where ρ_i is the ice density and g is the gravitational acceleration force.

The velocity of the flow is determined by the balance between driving stresses and resistive forces, holding the ice back. The force balance consists of the gravitational driving stress, longitudinal stress gradient, basal and lateral resistance. Figure 2.3 is a sketch of the force balance, which is described more detailed for the model in Chapter 3.

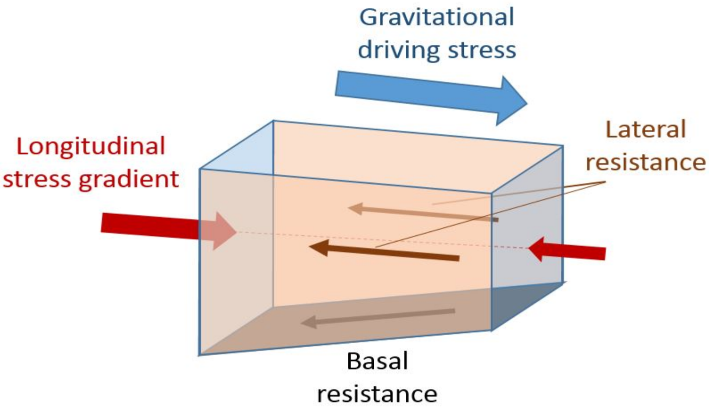
Gravitational driving stress
Longitudinal stress gradient
Lateral resistance
Basal resistance

Figure 2.3.: Sketch of the stresses acting on a glacier. Redrawn from Van der Veen (2013).

2.2.3. Basal Motion

Ice flow is - in addition to internal deformation of ice - also enabled by basal motion, which includes basal sliding and deformation of the underlying sediments. Basal motion can account for up to 90% of the surface velocities of temperate glaciers (Bamber et al., 2007). Especially ice streams experience low resistance from the bed (Shapero et al., 2016). Figure 2.4 presents vertical profiles of the flow velocity depending on the basal conditions.

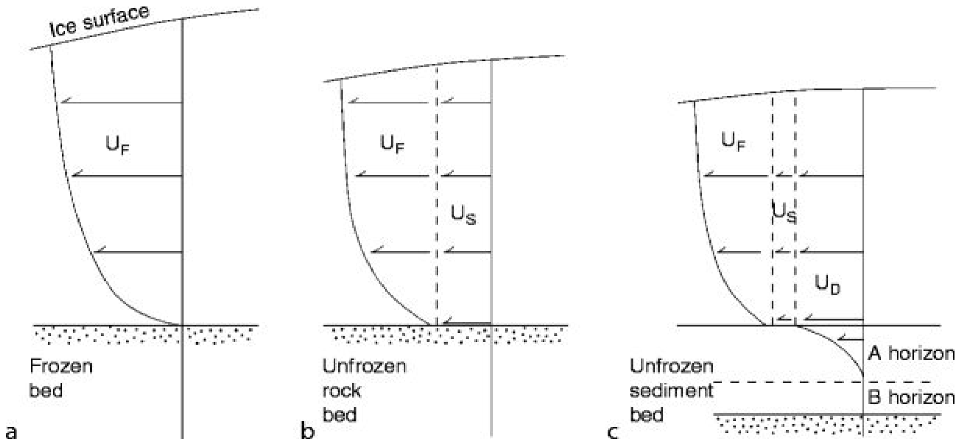
Ice surface
U_F
U_S
U_D
Frozen bed
Unfrozen rock bed
Unfrozen sediment bed
A horizon
B horizon
a
b
c

Figure 2.4.: Depth-profiles of glacier velocities for different basal conditions. (**a**) Ice flow due to creep over a frozen bed; (**b**) Velocities associated with creep and basal sliding of a warm-based glacier; (**c**) Ice flow as a combination of creep, basal sliding and deformation of subglacial sediments (Boulton, 1996).

Figure 2.4a shows the case of a cold-based glacier, whose base is frozen to the bed. Cold glaciers were originally thought to be unable to slide over their bed (Sugden and John, 1976), but later studies found basal motion even on cold glaciers (e.g. Fowler, 1986; Cuffey et al., 1999; Weber, 2000). At basal temperatures lower than −15 °C, a thin water film was found at the ice-bed interface (Cuffey et al., 1999). A subglacial water film lubricates the base and enables basal sliding, as illustrated in Figure 2.4b. Subglacial water can develop by increased pressure by the weight of the overlaying ice, which reduces the pressure-melting point and causes melting. Other processes that cause water at the ice-bed interface are geothermal heating, as it was found on Greenland by volcanic activity (Fahnestock et al., 2001), friction (Fowler, 1986), shear heating (Weber, 2000) and high saturation rates due to entrained sediments (Shreve, 1984; Cuffey et al., 1999, 2000).

Two mechanism that enable basal sliding even on the rough surface of the glacier bed and in the presence of little meltwater, are enhanced creep and regelation, first described by Weertman (1957). Enhanced creep appears due to stress concentration around an obstacle. Regelation is the process of a lowered melting temperature due to increased local pressure on the upstream side of an obstacle. This melts the ice, which flows around the obstacle and refreezes on the downsteam side, where the local pressure is low. Figure 2.5 shows schematically the process of regelation.

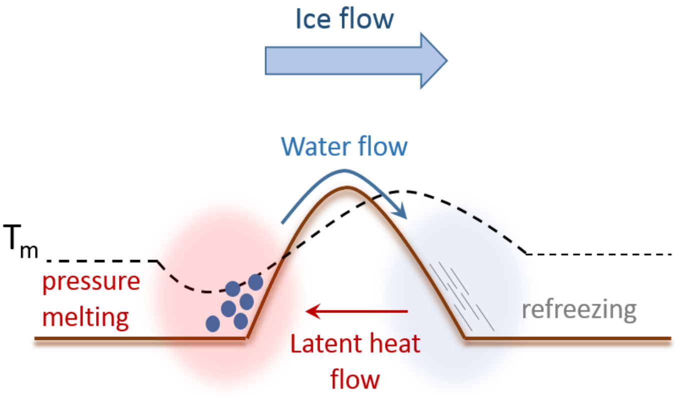

Figure 2.5.: Sliding by regelation (after Weertman, 1967). The melting temperature T_m is only illustrative.

Basal motion is, in addition, enabled by deformation of the bed (Figure 2.4 c). Especially glaciers sitting on a soft, unfrozen sediment bed experience increased sliding velocities, as wet and deformable till lubricates the base (Alley et al., 1986; Truffer et al., 2000).

In temperate glaciers, meltwater is transported through the glacier by englacial and subglacial hydrological systems. High, seasonal variations in flow velocities can be explained by a switch between an efficient and an inefficient drainage system (Sole et al., 2013; Tedstone et al., 2013, 2015), which is driven by seasonal variation in surface meltwater (Zwally et al., 2002). An efficient drainage systems transports water quickly with low pressure through well-connected channels that are either incised upward into the ice (Röthlisberger, 1972), cut down into the bedrock (Nye, 1976), or at the interface between ice and sediments (Walder and Fowler, 1994). An inefficient drainage system is spatially distributed in form of a water film (Weertman, 1972), linked cavities (Lliboutry, 1968; Walder, 1986), or groundwater flow (Shoemaker, 1986). The increase in water pressure in an inefficient system can be measured by a vertical uplift of the glacier and a springtime speed-up due to reduced basal drag (Zwally et al., 2002). The observed increase in surface melt at the coasts of Greenland (Zwally et al., 2002) was expected to increase lubrication of the bed. Joughin et al. (2008a) and Sundal et al. (2011), however, found that surface melt only influences the seasonal velocities of the ice sheet at the west coast, but it does not cause the dramatic short-term accelerations observed on several outlet glaciers. Tedstone et al. (2015) even found a decadal slow-down of glaciers after particularly high surface melting.

A formulation of a sliding law that relates basal drag to sliding velocities and effective pressure (Bindschadler, 1983; Van der Veen and Whillans, 1996; Vieli and Payne, 2005) is used in many glacier dynamics models (e.g. Pattyn, 2002).

$$U_b = k_s \tau_b^p N^{-q} \tag{2.3}$$

U_b is the basal velocity, τ_b the basal drag, k_s, p, q are constants. N is the effective pressure being the difference between ice and water pressure (p_i and p_w, respectively).

$$N = p_i - p_w. \tag{2.4}$$

2.2.4. Lateral Drag

Resistance to flow is given by drag from the lateral margins of a glacier. Resistive walls or slow-flowing ice at the margins of an ice-stream lead to variation in cross-flow resistance. Lateral stresses are more important for ice sheet stability than earlier thought. As lateral resistance increases in a narrowing ice-stream, stabilisation can even arise on a reversed bed (a bed sloping towards the interior of an ice sheet) (Jamieson et al., 2012), which was earlier thought to trigger unconditional destabilisation and rapid retreat (Weertman, 1974; Oppenheimer, 1998; Schoof, 2007; Joughin et al., 2010). High velocities of a fast-flowing ice stream cause high shear stresses along the lateral margins, which leads to softening by shear heating and mechanical fracturing (Vieli and Nick, 2011). Mechanical weakening is visible in the form of crevasses, which are typical for marine-terminating outlet glaciers. This softening causes a positive feedback between acceleration and further weakening; this plays a role in the dynamics of Antarctic ice streams (Echelmeyer et al., 1994; Vieli et al., 2007). Lateral drag, however, is important for ice streams that flow over weak beds with little resistance (Whillans and Van der Veen, 1997). The same applies to floating ice shelves, where basal drag vanishes completely and the ice is only held back by lateral resistance and along-flow stress-gradients. A mathematical expression for the lateral drag (τ_{lat}) can be derived from the lateral variation in depth-integrated resistive stresses parallel to the flow direction, $\bar{R}_{xy}$ (Van der Veen, 2013, p.54):

$$\tau_{lat} = \frac{\partial (H \bar{R}_{xy})}{\partial y} \tag{2.5}$$

2.2.5. Longitudinal Stress Gradient

Glacier ice experiences longitudinal compression or extension due to along-flow varying pushing or pulling forces. These forces are along-flow resistive stresses, whose along-flow variation cause a longitudinal stress gradient. When there is, for example, fast-ice in front of a glacier, a back-stress is acting on the glacier, which causes stronger compression downhill than further up. Where, in turn, the glacier starts floating, the along-flow compressive stresses decrease downhill and lead to extension. The longitudinal stress gradient τ_{lon} can be expressed by the along-flow variation of the depth-integrated longitudinal resistive stresses, $\bar{R}_{xx}$ (Van der Veen, 2013, p.54):

$$\tau_{lon} = \frac{\partial(H\bar{R}_{xx})}{\partial x} \tag{2.6}$$

2.2.6. Ice Rheology

Ice is a viscous material with a non-linear dependency of the effective strain rate on the effective shear. The resulting ice creep is described by *Glen's flow law* (Glen, 1954) as:

$$\dot{\epsilon_{ij}} = A\sigma_e^{n-1}\sigma'_{ij}, \tag{2.7}$$

where σ_e is the effective stress. In a simple form, where strain rates are mainly dependent on basal shear, it can be written as:

$$\dot{\epsilon} = A\tau^n \tag{2.8}$$

Measurements suggest various values for the exponent n, but $n = 3$ has primarily been chosen in numerical ice-sheet models (Cuffey and Paterson, 2010, p.57). A is the rate factor and describes the softness of the ice. It is exponentially dependent on ice temperature, but depends also on crystal fabric, impurities and water content (Cuffey and Paterson, 2010). The dependence of the rate factor on the temperature can be calculated by the Arrhenius law:

$$A = A(-10\,^{\circ}\mathrm{C}) \cdot exp\left(-\frac{Q}{R} \cdot \left(\frac{1}{T_h} - \frac{1}{T^*}\right)\right) \tag{2.9}$$

where $A(-10\,^{\circ}\mathrm{C}) = 3.5 \times 10^{-25}\,\mathrm{Pa^{-3}\,s^{-1}}$, Q is the activation energy for ice creep and R the universal gas constant. $T^* = 263 + 7 \cdot 10^{-8} \cdot P$ and $T_h = T_{ice} + 7 \cdot 10^{-8} \cdot P$, where P is the depth-averaged overburden pressure and T_{ice} is the depth- and width-averaged ice temperature. Table 2.1 lists values of A for different temperatures that were suggested by Cuffey and Paterson (2010) and which are used in this thesis. The usage of a constant rate factor may lead to large discrepancies, because strain heating within the ice and at the ice-bed interface, thermal softening of the ice by geothermal heating and impurities can change the viscosity by a factor 12 throughout the glacier (Cuffey and Paterson, 2010).

Table 2.1.: Values of the rate factor A for different ice temperatures, adapted from Cuffey and Paterson (2010).

T (°C)	A ($\mathrm{yr}^{-1}\,\mathrm{Pa}^{-3}$)
0	$7.5 \cdot 10^{-17}$
-2	$5.3 \cdot 10^{-17}$
-5	$2.9 \cdot 10^{-17}$
-10	$1.1 \cdot 10^{-17}$
-15	$6.6 \cdot 10^{-18}$
-20	$3.78 \cdot 10^{-18}$
-25	$2.15 \cdot 10^{-18}$

2.2.7. Calving

Calving is a very efficient ablation process that causes high rates of mass loss, rapid glacier retreat and thus contributes significantly to sea level rise. It occurs when fractures close to the terminus of a glacier propagate through the glacier, disintegrating ice blocks and forming icebergs. The fractures develop due to spatial velocity gradients, often caused by changes in basal sliding, such as where the glacier starts floating. The lithostatic stress from the overlain ice shuts the crevasses at a certain depth, because it increases with depth and exceeds the resistive stress (Figure 2.6). The penetration depth of surface crevasses, cd_s, equals the depth at which the resistive stress balances the lithostatic stress.

$$R_{xx}(cd_s) = \rho_i g cd_s \tag{2.10}$$

Close to the terminus, the resistive stresses can be large enough to penetrate the ice entirely. Several processes intensify the penetration of fractures and increase calving rates of marine-terminating glaciers:

- Hydrofracturing due to surface melt (Nick et al., 2013; Pollard et al., 2015). This is the effect of increased fracturing by meltwater in crevasses. The crevasse tip thereby penetrates further down, when the water pressure and the tensile stresses opening up the crevasses exceed the fracture toughness (see Figure 2.6).
- Melt-induced calving of overhanging ice at the water-line (Vieli et al., 2002; Benn et al., 2007b). Concentrated melting at the water-line due to wave erosion causes an undercut notch and leads to calving of the overhanging ice (White et al., 1980). This type of calving experiences seasonal variety due to changing water temperatures and sea ice cover.
- Reduced buttressing from sea ice (Higgins, 1991; Reeh et al., 2001; Amundson et al., 2010), which is explained in more details in Section 2.4.
- Force imbalances at the ice-ocean interface (Benn et al., 2007b)
- Torque where the ice starts floating (Benn et al., 2007b)

Especially the first three point increase significantly in a warming climate, causing higher calving rates.

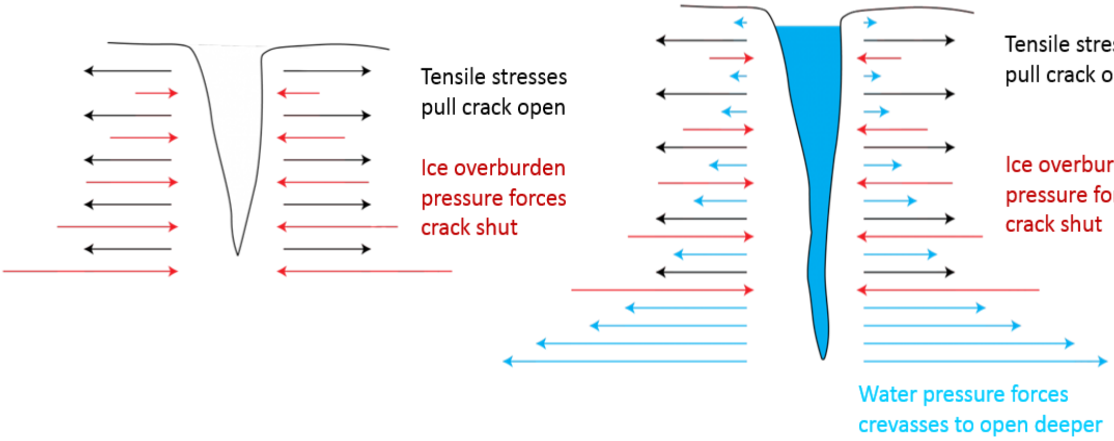
Tensile stresses pull crack open
Ice overburden pressure forces crack shut
Tensile stresses pull crack open
Ice overburden pressure forces crack shut
Water pressure forces crevasses to open deeper

Figure 2.6.: Illustration of compressive stresses in a crevasses without meltwater (left) compared to a water-filled one (right) by Benn and Evans (2010)

Calving rates show a linear relation to ocean water depth (Brown et al., 1982); therefore a retreat of the terminus into deeper waters increases the calving rates, causing a positive calving retreat feedback. Higher calving rates have recently caused increased retreat of many marine-terminating glaciers, where disintegration of floating tongues or ice shelves has caused high instability and further calving due to loss of frontal backstresses. One of the best examples is Jakobshavn Isbræ with an ice discharge that increased from $24\,\mathrm{km}^3\,\mathrm{yr}^{-1}$ in 1996 to $46\,\mathrm{km}^3\,\mathrm{yr}^{-1}$ in 2005 (Rignot and Kanagaratnam, 2006). Many calving laws have been developed and implemented into glacier models (Reeh, 1968; Iken, 1977; Vieli et al., 2001; Hughes, 2002; Nick et al., 2010), but they usually apply to a certain type of glaciers only, as calving is very dependent on parameters such as flow velocities, proglacial water body, floating or grounded terminus.

2.3. Submarine Melt

Submarine melt is an important ablation processes for tidewater glaciers. On Peterman Glacier in northern Greenland, it is more important than surface melt and calving (Rignot and Steffen, 2008). In western Greenland, subglacial melt reaches rates twice as large as surface melt but is comparable in magnitude to calving fluxes (Rignot et al., 2010). Especially on rapidly retreating Greenland outlet glaciers, high submarine melt rates up to several hundreds of meters per year have been found. Warm, saline water around Greenland originates in the North Atlantic Current. Its turning branches in the Nordic Seas are driven geostrophically along the southern coast of Greenland and northward into Baffin Bay (Straneo et al., 2013). The warm water underlies a layer of fresh, cold water coming from the Arctic through the Fram Strait. Relatively deep sills in the fjords enable an exchange between the water on the continental shelves and the fjords. Warm, subsurface Atlantic waters have therefore been found in the vicinity of the glacier fronts (Straneo et al., 2013).

An increase in ocean melt is suggested as main driver of glacier destabilization, because enhanced inflow of subtropical water into fjords correlates with increased calving rates (Holland et al., 2008; Straneo and Heimbach, 2013). On Jakobshavn Isbræ, melt rates of $228 \pm 49\,\mathrm{m\,yr^{-1}}$ were observed (Motyka et al., 2011), which is an increase by 25 % after 1997, when higher subsurface ocean temperatures from the Irminger Sea reached the west coast of Greenland (Holland et al., 2008). In Disco Bukta, off Jakobshavn Isbræ, sediment cores show a correlation between ocean temperatures and frontal position throughout the last decade (Lloyd et al., 2011).

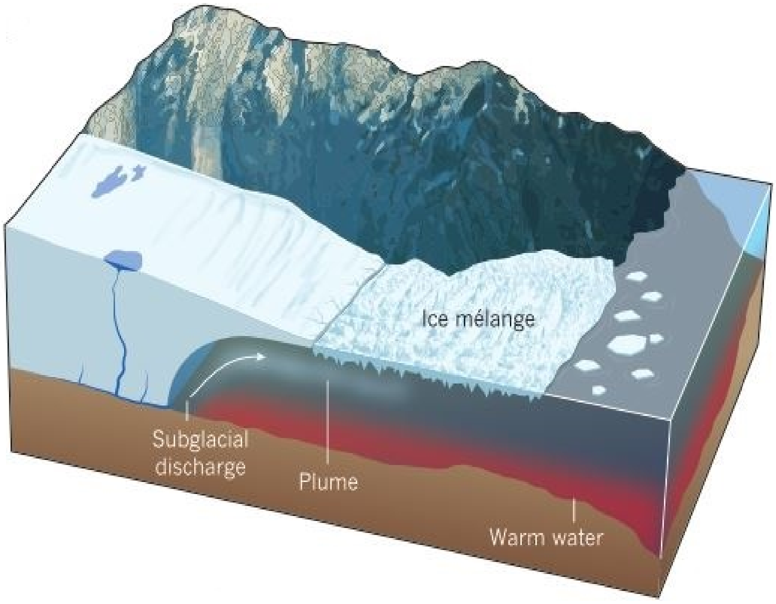

Figure 2.7.: Warm subsurface waters and plume dynamics by subglacial discharge cause submarine melting of a marine-terminating glacier. Warmer temperature cause more subglacial discharge due to increased surface melt, warmer water and reduced ice mélange. This causes higher submarine melt rates (Straneo and Heimbach, 2013).

Submarine melt is seldom a direct result of heat from the ocean. It is, instead, dependent on the turbulent heat exchange at the ice-ocean interface. Fresh, buoyant water exits from subglacial discharge at the base of the glacier and rises along the glacier front as buoyant plumes that drive convection (Jenkins, 2011). The plumes entrain the warm subsurface ocean water and enable exchange of heat between the ocean and ice (Straneo et al., 2013). The heat exchange at the interface involves complicated feedbacks, such as thermodynamics, dynamic and turbulent processes. Fresh, buoyant water originates either directly from the submarine melt at the terminus or from deep incised channels transporting subglacial meltwater into the ocean. Figure 2.7 shows a plume rising up at the front of a marine-terminating glacier, preventing the subsurface warm ocean water from melting the glacier front directly. In a warming climate, increased surface melt on glaciers rises the subglacial discharge; in addition, the overlying cold, fresh water layer in the ocean thins. Both of these effects enhance submarine melt. The rising of the subsurface ocean layer also melts the ice mélange and thereby reduces the backstress. Increased submarine melt thins the floating part of a glacier, which facilitates the penetration of crevasses through the glacier thickness, enhancing calving.

2.4. Sea Ice and Ice Mélange

Outlet glaciers terminate in fjords, where calving icebergs are bound together by sea ice during winter. The combination of icebergs and sea ice is called ice mélange and it behaves as a weak, granular ice shelf at the terminus of the glaciers (Amundson et al., 2010). Despite the low thickness of sea ice, it causes enough buttressing to prevent icebergs from calving off. On Jakobshavn Isbræ, advances of several kilometers and the formation of a floating tongue during winter have been observed as a consequence of buttressing by ice mélange (Sohn et al., 1998; Joughin et al., 2008a; Amundson et al., 2008). During summer, however, when icebergs are less bound by sea ice, calving rates increase significantly. In summer 2007, for example, calving has reached a frequency of one calving event per 75 hours on Jakobshavn Isbræ (Amundson et al., 2008). The motion of the ice mélange itself is also episodic. During winter, it is pushed downfjord by the advancing terminus and in summer it moves freely with high velocities up to $50\,\mathrm{km\,d^{-1}}$ (Amundson et al., 2010). Throughout the whole year it influences the timing of calving events.

The disintegration of several floating glacier tongues and high calving rates coincided with the melt of proglacial semi-permanent sea ice (Higgins, 1991; Copland et al., 2007; Amundson et al., 2008). Also on glaciers with fast-ice cover calving ceases; thus, when the fast-ice breaks up due to warming, large icebergs break off the glacier (Reeh et al., 2001).

2.5. Jakobshavn Isbræ

Jakobshavn Isbræ drains about 6.5 % of the GrIS (Echelmeyer et al., 1991). It has exceptional high calving rates and is therefore considered to be the most active glacier in Greenland (Legarsky and Gao, 2006). Every year it produces around $35 - 50\,\mathrm{km}^3$ of icebergs, which is more than any other Greenland outlet glacier produces (Weidick and Bennike, 2007).

The glacier attracted a lot of attention after the start of its rapid retreat in 1997. By 2003 the floating tongue was almost completely disintegrated (Vieli and Nick, 2011; Joughin et al., 2004) and ice discharge reached $50\,\mathrm{km^3\,yr^{-1}}$ - a near-doubling since 1985 (Joughin et al., 2004). During its still ongoing acceleration, ice velocities at the terminus peaked up to $17\,\mathrm{km\,yr^{-1}}$ in 2012 (Joughin et al., 2014), whereas most other destabilized glaciers decelerated again after a shorter time period (Weidick and Bennike, 2007). The consequent thinning of the frontal area happened at a rate of $> 10\,\mathrm{m\,yr^{-1}}$ (Joughin et al., 2004, 2008b; Thomas et al., 2003, 2009). The retreat history of Jakobshavn Isbræ since 1851 is shown in Figure 2.8. The retreat length during the 10 years succeeding 2001 is equal to the combined retreat over the last 100 years preceding 2001. Jakobshavn Isbræ alone contributed to the total global sea level rise by 4% in the 20th century (IPCC Working Group I, 2001).

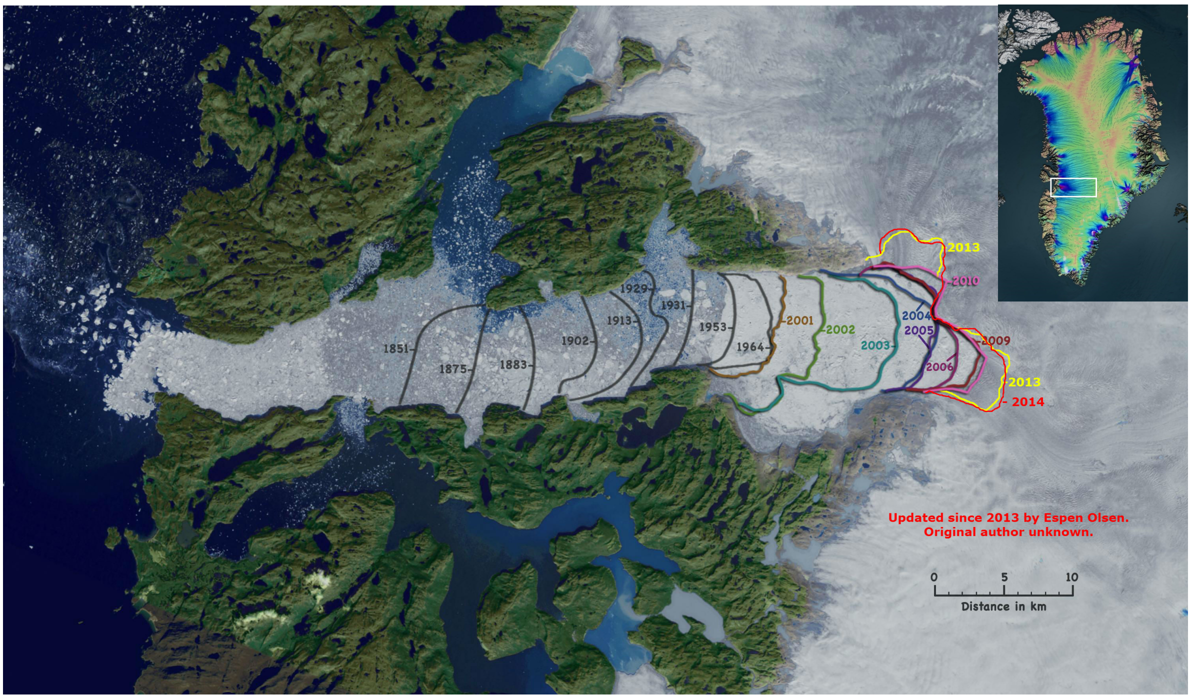

Figure 2.8.: Calving front position of Jakobshavn Isbræ from Arctic Sea Ice Blog (2015). The location of Jakobshavn Isbræ on the GrIS is marked on the inlet as a white box. NASA (2012)

2.6. Usage of a Numerical Flowband Model

Models are simplifications that help us to understand the real world. No model can represent all the details of the natural world, in part due to the lack of knowledge, but also due to the large computational effort that would be required. Numerical models help to solve more complex physical equations compared to analytical models, but they get to their computational limits, as well. It is therefore necessary to focus on smaller parts of the earth system, although it needs to be decided what to focus on and what happens at the boundaries. In glaciology, models are limited to one glacier or one ice sheet. Information about the surrounding systems is thereby needed, as glaciers are influenced by the atmosphere, ocean and geology. Large-scale ice sheet models are still unable to simulate the linkage between forcing and ice dynamics realistically (Vieli and Nick, 2011). This is due to poor understanding and the lack of observational data. Only recently developed remote sensing techniques will enable us to address some of these unknowns (e.g. Morlighem et al., 2014; Rignot et al., 2015; MacGregor et al., 2015). Their implementation into models still requires better understanding. It is therefore not always desired to include as many processes as possible but instead to focus on a better understanding of known processes in a more transparent way.

Simple models are therefore used, and they include only the basic physics and are kept computationally efficient. These models allow us to really understand how a system works. Numerical flowband models are spatially reduced to a one dimensional ice flow along the flowline of single outlet glacier basins (Nick et al., 2009, 2010). Despite their simplicity, these models have managed to agree well with observations (e.g. Nick et al., 2009; Vieli and Nick, 2011; Jamieson et al., 2012). They have been used to reconstruct the observed retreat of glaciers. A study on Hansbreen, Svalbard, by Vieli et al. (2002) linked rapid retreat during the two last decades to the bed topography and seasonal front migration to changing calving rates. Simulations of the past retreat of Marguerite Bay Ice Stream in Antarctica since the Last Glacial Maximum with a flowband model by Jamieson et al. (2012) showed that the glacier also stabilized on a reversed bed slope, due to high lateral resistance. Also future simulations were conducted with a flowband model by Nick et al. (2013), which enables an estimation of a sea-level rise contribution by four of the largest Greenland outlet glaciers.

Because of the large number of assumptions and unknowns in a flowband model, care has to be taken when interpreting and interpolating present-day model results. Sensitivity studies, as performed by Enderlin et al. (2013b), are therefore crucial for an estimation of uncertainties. The implications and issues of flowband models, when trying to understand rapid dynamic changes of marine-terminating glaciers, have been analyzed by Vieli and Nick (2011).

3

Model Description

A width-depth integrated numerical flowband model was developed by Vieli et al. (2001) and Vieli and Payne (2005) and is described in detail in Nick et al. (2009, 2010). It is a physically-based model that simulates the ice-flow and surface along the flowline of a glacier. Lateral resistance is parametrized by the horizontal shear stress integrated over the width (Van der Veen and Whillans, 1996) and the basal sliding law is of non-linear Weertman-type based on effective pressure (Fowler, 2010). The grounding line position is treated robustly and calculated with a flotation criterion. A moving spatial grid tracks the terminus position continuously so that the original grid size is stretched and squeezed with the migration of the terminus (Nick and Oerlemans, 2006). At the marine terminus, a dynamic crevasse-depth calving criterion is used (Nick et al., 2010; Benn et al., 2007b). The ice-flow dynamics is based on mass and momentum conservation, explained in the following section. The equations are solved by a Newton iteration method and computed on a staggered grid between the grid points.

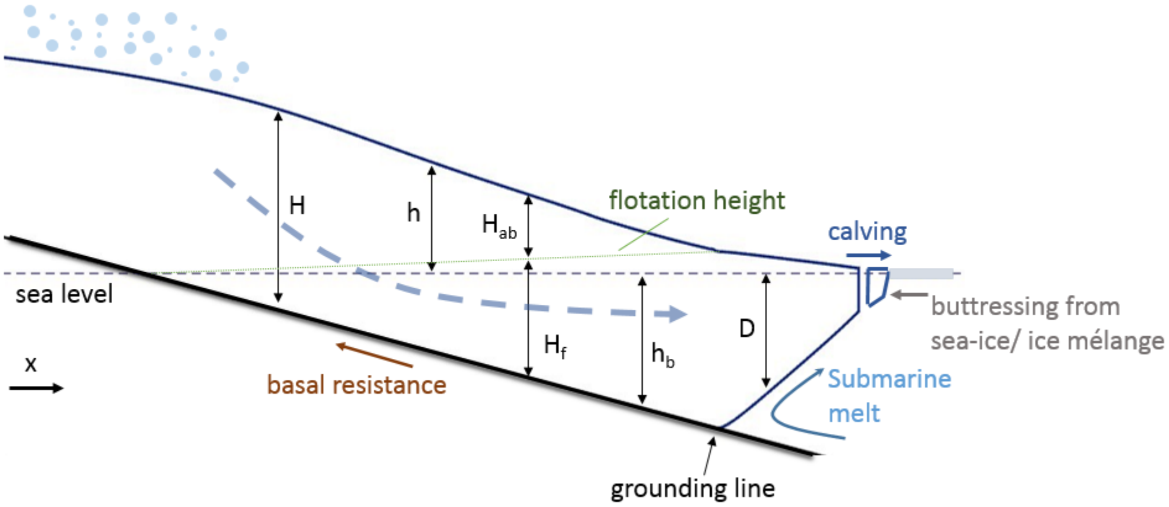

Figure 3.1.: Illustration of important factors influencing a marine-terminating glacier. The abbreviations stand for glacier thickness, H; surface elevation, h; bed elevation, h_b; ice thickness below sea level, D; height above buoyancy, H_{ab}; flotation thickness, H_f.

3.1. Continuity

As explained in Section 2.1, a glacier gains mass by accumulation of snow and loses mass by ablation. The lost mass in the ablation area is replaced by mass from the accumulation area by ice motion. If an imbalance is left, it results in a change in thickness with time. This is expressed by the depth-integrated continuity equation (here only in along-flow direction):

$$\frac{\partial H}{\partial t} = -\frac{1}{W}\frac{\partial F}{\partial x} + \dot{B} \tag{3.1}$$

H is the thickness of the glacier at the centerline, t the time, x the longitudinal coordinate and $\dot{B}$ the mass balance rate including surface mass balance and submarine melt rate. The ice flux $F = UHW$ is calculated from the vertically integrated velocity U, thickness H and width W.

3.2. Force Balance

Flow velocities along the glacier can be achieved from the force balance equation (Equation 3.2). It expresses how the gravitational driving stress is balanced by the along-flow longitudinal stress gradient, basal resistance, and lateral resistance (first, second, and third term of equation 3.2).

$$2\frac{\partial}{\partial x}\left(H\nu\frac{\partial U}{\partial x}\right) - f_s A_s\left[\left(H - \frac{\rho_w}{\rho_i}D\right)U\right]^{1/3} - \frac{2H}{W}\left(\frac{5U}{E_{lat}AW}\right)^{1/n} = \rho_i g H\frac{\partial h}{\partial x} \tag{3.2}$$

h is thereby the surface elevation, D is the depth of the glacier below sea level, ρ_i and ρ_w are the densities of the ice and ocean water, respectively.
The effective viscosity ν is non-linearly dependent on the strain rate and calculated by

$$\nu = E_\nu A^{-\frac{1}{n}}\left(\frac{\partial U}{\partial x}\right)^{\frac{1-n}{n}}. \tag{3.3}$$

A is the rate factor and $n = 3$ the exponent in Glen's flow law. I included the factor E_{lat} in Equation 3.2 and E_ν into the model to tune the size of the rate factor in the viscosity and lateral resistance terms separately, which is used later in Section 5.3.
The sliding law is adapted from Van der Veen and Whillans (1996), who used a non-linear Weertman-type sliding law (Weertman, 1957), based on a combination of regelation and creep. They included the dependency on effective basal pressure N (Equation 2.4) and set it equal to the height above buoyancy H_{ab}, following Bindschadler (1983).

$$N = H_{ab} = H - \frac{\rho_w}{\rho_i}D \tag{3.4}$$

In the balance equation, A_s and f_s are the sliding and the friction parameter, respectively, which both can be adjusted to basal water and bed roughness. The friction parameter is set equal to one where the ice is grounded and zero at the floating part. It could be used to include enhanced basal lubrication due to summer melt as it is done in Nick et al. (2013). But this is be more important on inter-annual time-scales (Howat et al., 2010), which are not resolved here.

3.3. Flotation Criterion

Marine-terminating glaciers thin towards their calving front and often reach into waters far below sea level. The density difference between ice and water causes buoyancy of the ice and detaches it from the bed, if the ratio between ice thickness and the water depth falls below the ratio of their densities. When the terminus gets afloat, it either calves off due to larger propagation of crevasses or it turns into a floating glacier tongue. The position of the transition between grounded and floating ice is called grounding line. In this model, the grounding line is located using the flotation criterion, which calculates the position at which the glacier thickness falls under the flotation thickness H_f (Van Der Veen, 1996).

$$H_f = \frac{\rho_w}{\rho_i} D \begin{cases} = H & \text{floating part} \\ < H & \text{grounded part} \end{cases} \tag{3.5}$$

The thickness everywhere at the floating tongue is equal to the flotation thickness, whereas the thickness of the grounded part exceeds the flotation thickness. When a glacier thins at the calving front, the terminus retreats until the thickness at the terminus reaches the flotation thickness again.

The floating part usually has higher velocities due to the lack of basal resistance and experiences tidal-induced vertical motion, so that grounding lines can be tracked on satellite images (Rignot et al., 2014). Tidal influence is not included in the model, as the time-scales involved are shorter than the focus of this thesis.

3.4. Calving Criterion

For the calculation of the calving front position, a crevasse-depth calving criterion has been incorporated into the model, which includes surface and basal crevasses (Nick et al., 2010). The crevasse-depth calving criterion is well suited for larger, fast-flowing outlet glaciers and is therefore chosen over a waterline-crevasse-depth criterion (Benn et al., 2007b); this only includes surface crevasses and is more appropriate for smaller and slower glaciers (Nick et al., 2010). The crevasse-depth criterion calculates a total crevasse water depth as the sum of surface crevasse depth and basal crevasse depth ($cd = cd_s + cd_b$); the calving face is then positioned, where the total crevasse water depth is equal to the glacier thickness (see Figure 3.2).

Opening of surface crevasses is caused by tensile stresses and resulting stretching, which is due to large scale gradients of surface velocities. The velocity gradients are associated with increasing velocities towards the terminus, where effective pressure diminishes as

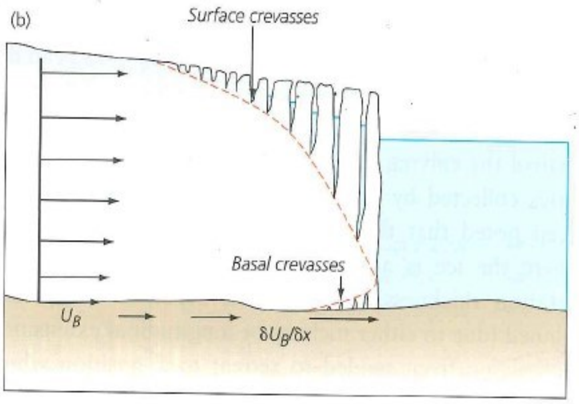

Figure 3.2.: Illustration of the crevasse-depth calving criterion (Benn and Evans, 2010).

the ice approaches flotation. The ice overburden pressure increases with depth due to the increasing weight of the ice, which shots crevasses at a certain depth. Meltwater filling up crevasses enables a further penetration down, due to the addition water pressure that acts against the fracture toughness (see Section 2.2.7 and Figure 2.6). The depth of surface crevasses can be calculated with the formulation by Nye (1957):

$$cd_s = \frac{R_{xx}}{\rho_i g} + \frac{\rho_{fw}}{\rho_i} cwd \tag{3.6}$$

where cwd is the depth of meltwater in the crevasses, ρ_{fw} the density of freshwater and R_{xx} the tensile deviatoric stress responsible for crevasse opening.

The longitudinal deviatoric stress R_{xx} is the difference between tensile stresses that pull a fraction open and the ice overburden pressure. It can be calculated from the longitudinal strain rate $\dot{\epsilon}_{xx}$ through Glen's flow law (see Chapter 2). At the same time it is balanced by the difference in hydrostatic pressure of the ice and the water at the calving front ($P_i - P_w$, see Figure 3.3).

$$R_{xx} = 2\left(\frac{\dot{\epsilon}_{xx}}{A}\right)^{1/n} = \frac{1}{2}\rho_i g\left(H - \frac{\rho_w}{\rho_i}\frac{D^2}{H}\right) \tag{3.7}$$

When rearranging Equation 3.7, the velocity at the calving front (where the spacing index $i = end$) can be calculated:

$$\dot{\epsilon_{xx}} = \left.\frac{\partial U}{\partial x}\right|_{i=end} = f_{si} A\left[\frac{\rho_i g}{4}\left(H - \frac{\rho_w}{\rho_i}\frac{D^2}{H}\right)\right]^n \tag{3.8}$$

f_{si} is thereby used to apply weakening of backstresses by sea-ice or ice mélange.

Basal crevasses are modeled for the area, where the difference between the ice thickness and the floating thickness falls below a certain threshold (here set to). The penetration depth of the basal crevasses is then depending on the tensile deviatoric stress and the height above buoyancy.

$$cd_b = \frac{\rho_i}{\rho_w - \rho_i}\left(\frac{R_{xx}}{\rho_i g} - H_{ab}\right) \tag{3.9}$$

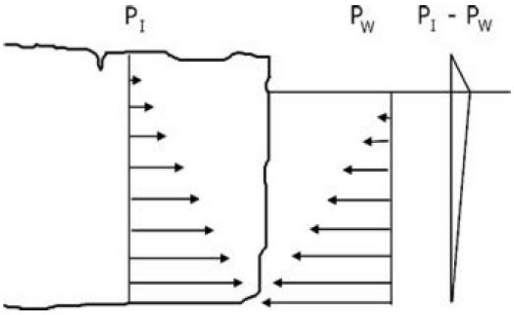

Figure 3.3.: Illustration of difference in hydrostatic pressure of ice and water at the calving front. (Benn et al., 2007b)

On grounded ice, the basal crevasse depth is smaller than on floating ice, where $H_{ab} = 0$ and the basal crevasse depth only determined by the tensile stresses.

To quantify calving, a calving rate U_c is calculated as the difference between the vertically averaged velocity at the terminus U_t and the change in length (Benn et al., 2007b).

$$U_c = U_t - \frac{\delta L}{\delta t} \tag{3.10}$$

In a steady-state, the length of the glacier is constant ($\frac{\partial L}{\partial t} = 0$) and the calving rate equals the velocity at the calving front. Together with the width and the height at the terminus, the calving flux can be calculated as

$$F_c = U_c W_t H_t. \tag{3.11}$$

The calving flux together with mass loss by surface and submarine melt balance the grounding line flux in a steady-state. The grounding line flux F_g is calculated analogously via the velocity, thickness and width at the grounding line.

$$F_g = U_g W_g H_g \tag{3.12}$$

For a glacier to be stable, the ice flux through the grounding line has to equal the cumulated surface mass balance.

3.5. Boundary Conditions

At the upper and lower boundary of the glacier the ice thickness and the depth-integrated velocity are unknown, so that two boundary conditions for each are needed. The upper boundary is at the ice divide, where the surface slope and velocity is assumed to be zero.

$$\begin{aligned} U(i = 1) &= 0 \\ H(i = 1) &= H(i = 2) \end{aligned} \tag{3.13}$$

The along-flow index i starts with 1 at the ice divide. In the model this is implemented as zero downstream mass flux at the upper boundary.
The lower boundary is at the marine-terminating calving front. The boundary conditions are solved via the calving criterion and the hydrostatic pressure between ice and water as explained in Section 3.4.

4

Sensitivity of an Idealized Glacier

Marine-terminating outlet glaciers are sensitive to increased atmospheric and oceanic temperatures, because they influence glacier dynamics through several mechanisms:

- Atmospheric warming: softening of the ice by heat diffusion into the ice; enhanced basal sliding due to surface meltwater penetrating to the base; increased calving rates by hydrofracturing
- Oceanic warming: melt of the floating tongue from below; less buttressing due to reduced sea ice

In reality, a glacier responses to a change in external forcings through more complex processes explained in Chapter 2. For example, surface meltwater may influence the whole hydrological drainage system - instead of directly enhancing basal sliding - which may cause a slow-down. However, the implementation of these mechanisms into models is challenging; their connection to atmospheric and ocean warming is therefore parameterized in the flowband model in the simplified way as listed above. Despite the simplicity and amount of approximations, flowband models have found many applications and have shown a well agreement with observations (Nick et al., 2009; Vieli and Nick, 2011; Jamieson et al., 2012), as outlined in Section 2.6. With the aid of the model, the direct impact of the above named mechanisms on marine-terminating glaciers is studied here. To isolate the response of the glacier to each parameter, an idealized glacier geometry with straight bed and walls is used. The response of a real glacier geometry (Jakobshavn Isbræ) is presented in Chapter 5 and a discussion of the relative importance of the individual factors for the glacier follows in Section 6.1.

4.1. Description of the Initial Input and Steady-State

Figure 4.1 presents the set-up of the idealized glacier. A 90 km long and 1 km thick ice block (Figure 4.1a, dark blue profile) is put on a bed, which is linearly sloping down from the ice divide to the ocean. The bed and width are kept simple in order to separate the glacier response to perturbations from its response to topographic variations. The glacier width decreases from 120 km at the ice divide to 7 km at the lower 80 km (Figure 4.1b). A glacier width changing from a wide upper area to a narrow trough is typical for Greenland outlet glaciers. The initial grid size of $\Delta x = 300\,\mathrm{m}$ is changing in time to keep the terminus at the same grid point, and the time step is $\Delta t = 0.001\,\mathrm{yr}$, which is small enough to avoid numerical instability.

For the rate factor (A), a constant value throughout the glacier is chosen, because the vertical temperature variation cannot be resolved in a depth-integrated model and a constant rate factor contributes to the simplicity of the model. It is set to a value corresponding to an ice temperature of $T = 0\,^{\circ}\mathrm{C}$ (see Table 2.1) to achieve a steady-state. This temperature may be unphysical as a depth-integrated value, but it is interesting to include warm ice. The crevasse water depth (cwd) during the spin-up is 100 m - a value similar to what was chosen by Nick et al. (2010). The surface mass balance is linearly decreasing towards the terminus and is stretched or compressed in time following the changes in glacier length. The values at the ice divide and the terminus are constant in time ($1.86\,\mathrm{m\,yr^{-1}}$ and $-4.42\,\mathrm{m\,yr^{-1}}$, respectively) and were tuned to reach a steady-state (Figure 4.1c). The submarine melt rate (smr) is set to $15\,\mathrm{m\,yr^{-1}}$ along the whole floating part (Figure 4.1c). Submarine melt is only applied vertically beneath the floating tongue of the glacier, disregarding horizontal melt at the calving front. It also follows the grounding line position spatially in time. The basal sliding parameter (A_s) is adapted from Nick et al. (2010) as $100\,\mathrm{Pa\,m^{-2/3}\,s^{-1/3}}$.

After a spin-up of 1200 years, the grounding line and terminus positions change by less than $0.1\,\mathrm{m\,yr^{-1}}$ and the volume changes by $0.003\,\mathrm{km^3\,yr^{-1}}$ (or $5.2 \times 10^{-7}\%$ of the total volume), which is close enough to a steady-state. The glacier is then 154 km long with a grounding line position at 134 km and an ice velocity at the terminus of $516\,\mathrm{m\,yr^{-1}}$. The grounding line flux in the steady-state is $3.44\,\mathrm{km^3\,yr^{-1}}$ and the calving flux is $0.84\,\mathrm{km^3\,yr^{-1}}$. The difference between grounding line and calving flux is due to mass loss by surface and submarine melt.

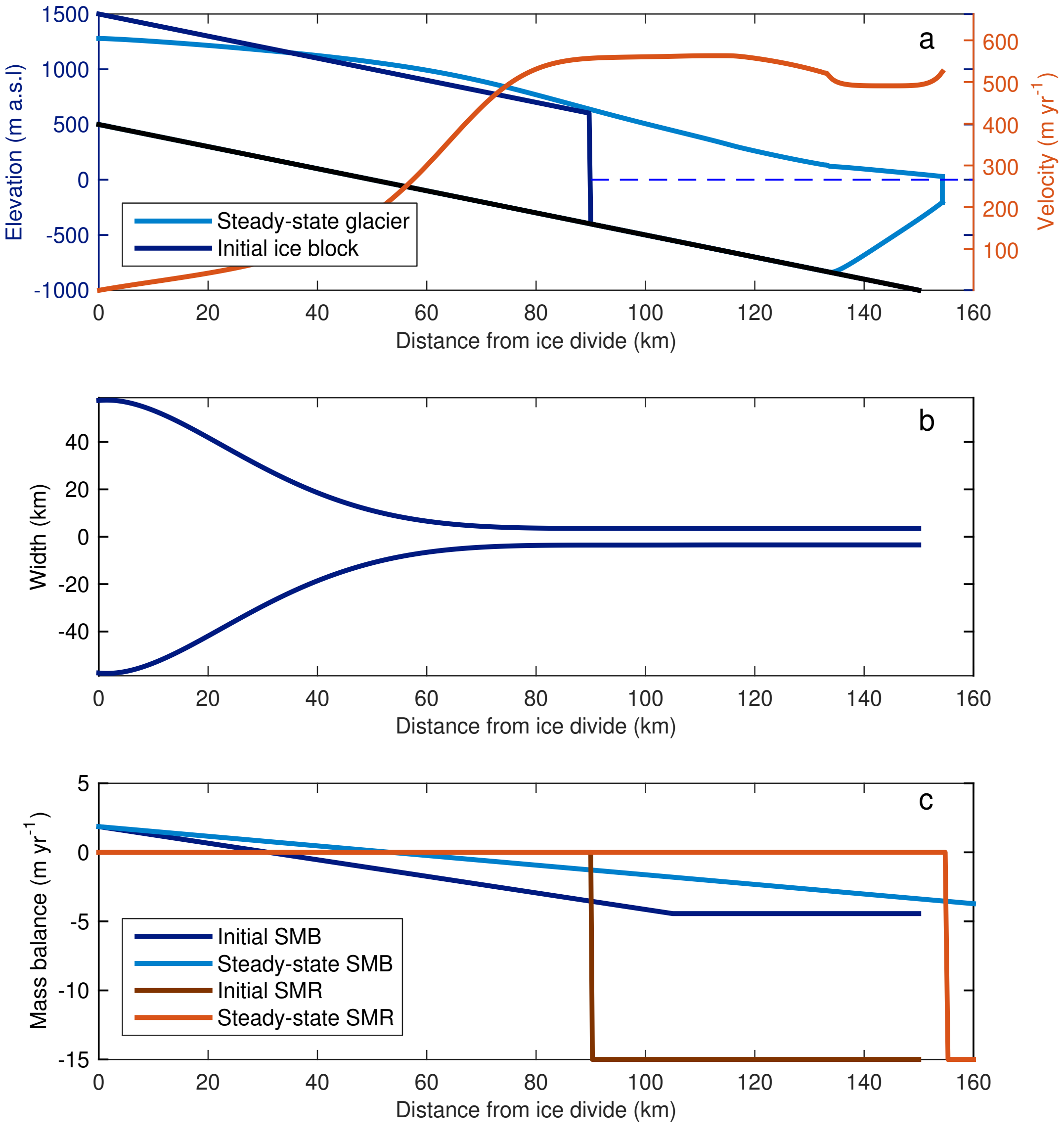

Figure 4.1.: Initial geometry and forcing of the idealized glacier configuration. (**a**) shows the initial and final steady-state glacier geometry with the along-flow velocity in the steady-state. (**b**) gives the width in planview and (**c**) shows the Surface Mass Balance (SMB) and Submarine Melt Rate (SMR) with the same y-axis, for the initial geometry and the steady-state.

4.2. Perturbation Studies

Perturbations of the sliding parameter (A_s), rate factor (A), crevasse water depth (cwd), the submarine melt rate (smr) and sea ice factor (f_{si}) are applied to the stable idealized glacier geometry presented in Section 4.1. Only one parameter is perturbed at a time to associate any response of the glacier with the respective parameter. After the perturbations, it takes the glacier several thousands of years to reach steady-state again, due to complex feedbacks within the glacier; this is discussed further in Section 6.4. In reality, a glacier is never expected to be in equilibrium, because it is always exposed to external changes. Due to the slow adjustment of the glacier and because tendencies get visible within 1500 year, only results after this time period are presented here.

Since the glacier geometry is strongly idealized and measurements or model experiments are rare, most of the parameter ranges are rather arbitrary. However, they have some physical constraints and are similar to what was used by Nick et al. (2010, 2013). The steady-state values and their ranges used for the perturbations are presented in Table 4.1. The absolute changes in glacier length, volume and ice fluxes are dependent on the range of the perturbations. Only the qualitative response of the glacier is therefore considered, instead of quantitative values after the perturbations.

Table 4.1.: Values of the initial parameters for the idealized glacier and their perturbed ranges. Corresponding values for the rate factor are found in Table 2.1.

Parameter	Symbol	Initial value	Range of perturbations	Unit
basal sliding parameter	A_s	100	40 - 160	$\mathrm{Pa\,m^{-2/3}\,s^{-1/3}}$
crevasse water depth	cwd	100	40 - 160	m
sea ice factor	f_{si}	1	1 - 2.25	
submarine melt rate	smr	15	12 - 18	$\mathrm{m\,yr^{-1}}$
rate factor	A	$A(0\,^{\circ}\mathrm{C})$	$A(0\,^{\circ}\mathrm{C})$ - $A(-20\,^{\circ}\mathrm{C})$	$\mathrm{yr^{-1}\,Pa^{-3}}$

The physical impact of the parameterized forcing on marine-terminating glaciers is explained in Chapter 2. A perturbation of the parameters in a certain direction can be linked to a warmer or colder climate. The parameter sensitivity study therefore also provides an insight into the impact of climate forcing on outlet glaciers.

4.2.1. Basal Sliding

Basal sliding is tuned in the model with the sliding parameter A_s. The smaller the sliding parameter is, the more slippery is the glacier base. The sliding parameter is $100\,\mathrm{Pa\,m^{-2/3}\,s^{-1/3}}$ in the steady-state case and perturbed in a range of $40 - 160\,\mathrm{Pa\,m^{-2/3}\,s^{-1/3}}$.

A reduction in the basal sliding parameter reduces the resistance and initially accelerates the glacier dramatically - mainly at the upstream part where the glacier bed is above sea

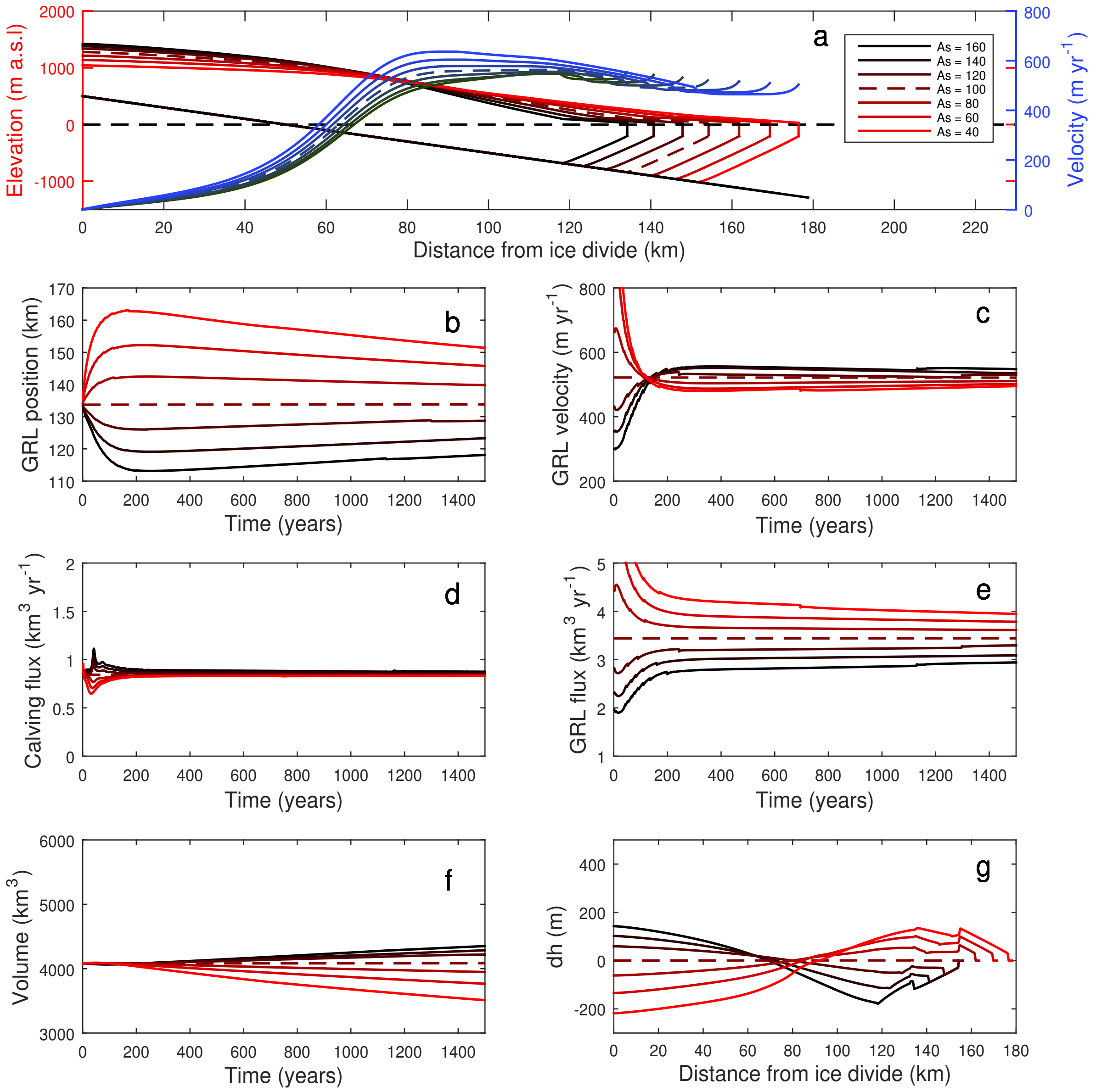

Figure 4.2.: Response to perturbations of the basal sliding parameter A_s (in $\mathrm{Pa\,m^{-2/3}\,s^{-1/3}}$) for an idealized marine-terminating glacier, from warm ice towards cold ice (red to black). Shown are the glacier shape and the corresponding velocities after 1500 years (blue to green) in (**a**), as well as the evolution of grounding line (GRL) position (**b**), grounding line velocity (**c**), calving flux (**d**), grounding line flux (**e**), volume (**f**) and difference between the surface after 1500 years and the steady-state (**g**). The steady-state is marked as dashed line.

level. At the transition where the bed reaches below sea level, the velocities are highest and reach up to three times the steady-state velocity (Appendix Figure C.1). The high velocities increase the downstream ice flux, causing an upstream thinning and a downstream thickening (Figure 4.2g). The downstream thickening provokes an advance of the grounding line position due to the floating criterion (Figure 4.2b). The thickening calving front also reduces calving fluxes (Figure 4.2d), leading to an advance of the glacier front. The upstream thinning and downstream thickening flattens the surface, which, in turn, reduces the velocity again (Figure 4.2c). After 200 years, when the velocity falls below the steady-state velocity, the grounding line retreats (Figure 4.2b). The calving flux is only marginally affected by the change in basal sliding. Note that the scales of Figures 4.6 to 4.5 is kept consistent for a better comparison. Because calving fluxes and grounding line fluxes are opposed during the first 200 years, increased basal sliding does barely affect the volume during this time period (Figure 4.2f). This means that the ice is rather redistributed by stretching of the glacier. Reduced basal sliding has a smaller impact on the changes in volume, velocity, and length than enhanced basal sliding.

4.2.2. Calving and Crevasse Water Depth

The crevasse depth criterion, used in the model, includes surface and basal crevasses (see the description of the calving criterion in Section 3.4). The surface crevasses are - in addition to stretching rates - driven by meltwater filling them up (Equation 3.6 and Figure 2.6). They are, consequently, influenced by the regional climate and the seasonal cycle via surface melt (Sohn et al., 1998; Nick et al., 2010). The crevasse water depth is parameterized as 100 m in the steady-state and perturbed within a range from 40 m to 160 m.

A larger water depth in crevasses increases calving fluxes significantly (see Figure 4.3d). An increase of the crevasse water depth by 40% rise the calving flux by 80%. The increased iceberg calving shortens the floating tongue and thickens the vertical calving front (Figure 4.3a). Because of the shortened floating tongue, upstream buttressing is reduced; thus, leading to acceleration (Figure 4.3c) and a slight increase in the grounding line flux (Figure 4.3e). The acceleration at the terminus propagates upstream, where the glacier thins (Figure 4.3g). After about 200 years, the glacier has thinned enough to reduce the grounding line flux. The grounding line flux reaches below the initial value after 1200 years (Figure 4.3e). An increase in crevasse water depth by a certain amount causes a larger migration rate than a water depth reduced by the same amount. Hence, the volume change is asymmetric (Figure 4.3f). For an increase of the crevasse water depth by 60 m, the calving rate gets so high that the glacier retreats on land after 2100 years. However, for a reduction of the crevasse water depth by 60 m, the glacier only advances 9 km within 2100 years.

4.2.3. Buttressing by Sea Ice and Ice Mélange

Ice mélange and sea ice in front of glaciers suppress calving, due to their buttressing effect. In the model, reduced buttressing is implemented as a factor that increases lateral stresses (see Equation 3.8) and opens up crevasses. The factor can only be increased from one, accounting for less buttressing. Values less than one produce no glacier respond. The effect of reduced buttressing is similar to an increase in water depth in crevasses. The calving front is destabilized, leading to a larger mass loss by calving, starting with a high, instantaneous peak flux (Figure 4.4d). The glacier,

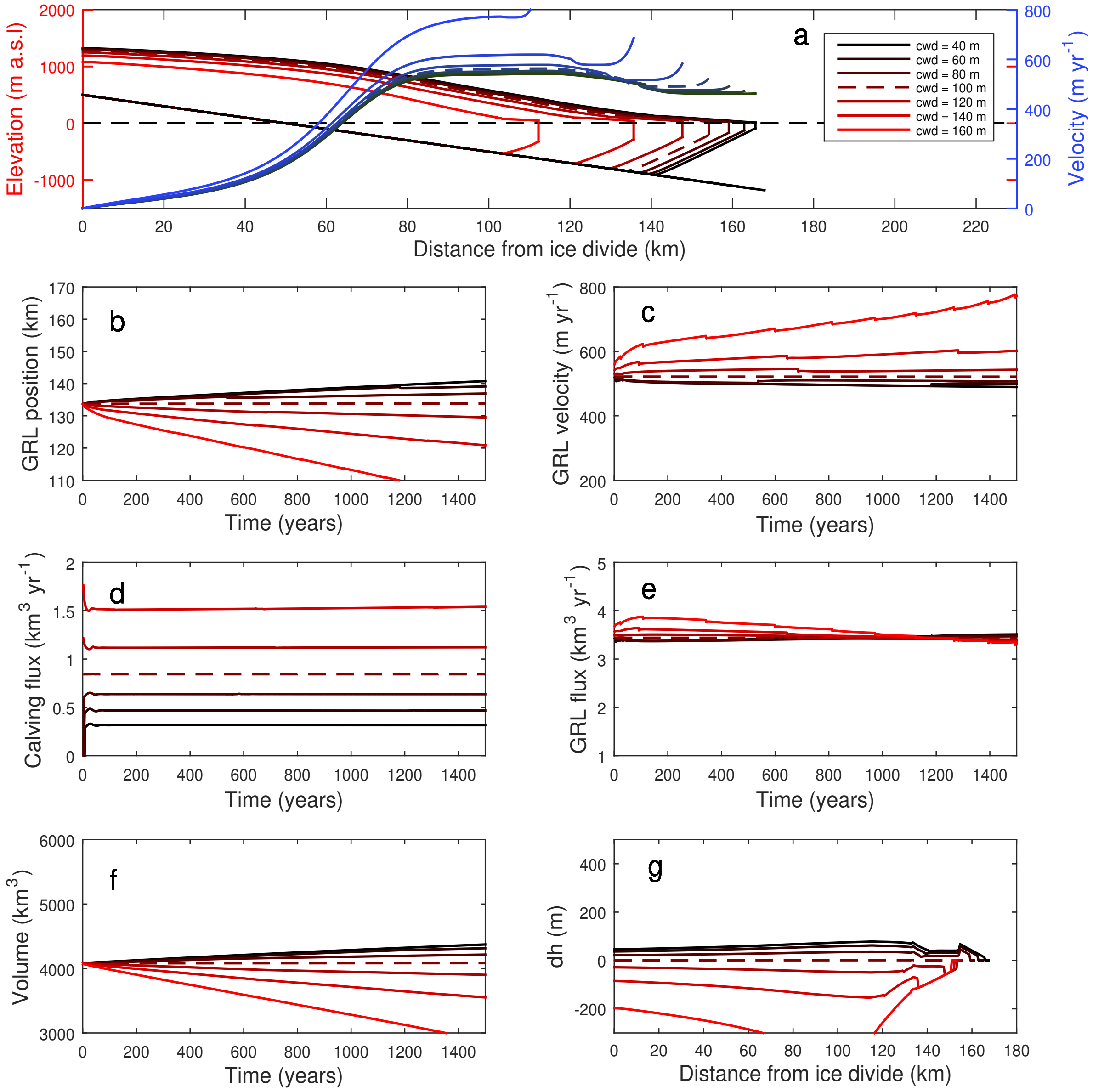

Figure 4.3.: Response to perturbations of the crevasse water depth *cwd* for an idealized marine-terminating glacier, from warm ice towards cold ice (red to black). Shown are the glacier shape and the corresponding velocities after 1500 years (blue to green) in (**a**), as well as the evolution of grounding line (GRL) position (**b**), grounding line velocity (**c**), calving flux (**d**), grounding line flux (**e**), volume (**f**) and difference between the surface after 1500 years and the steady-state (**g**). The steady-state is marked as dashed line.

therefore, retreats and accelerates (Figure 4.4c), leading to an increased grounding line flux (Figure 4.4e). The higher mass loss causes an upstream thinning (Figure 4.4g); hence, the glacier thins and retreats at the same time. For a reduction in buttressing by a factor 2.5, the glacier retreats up on land after 2500 years.

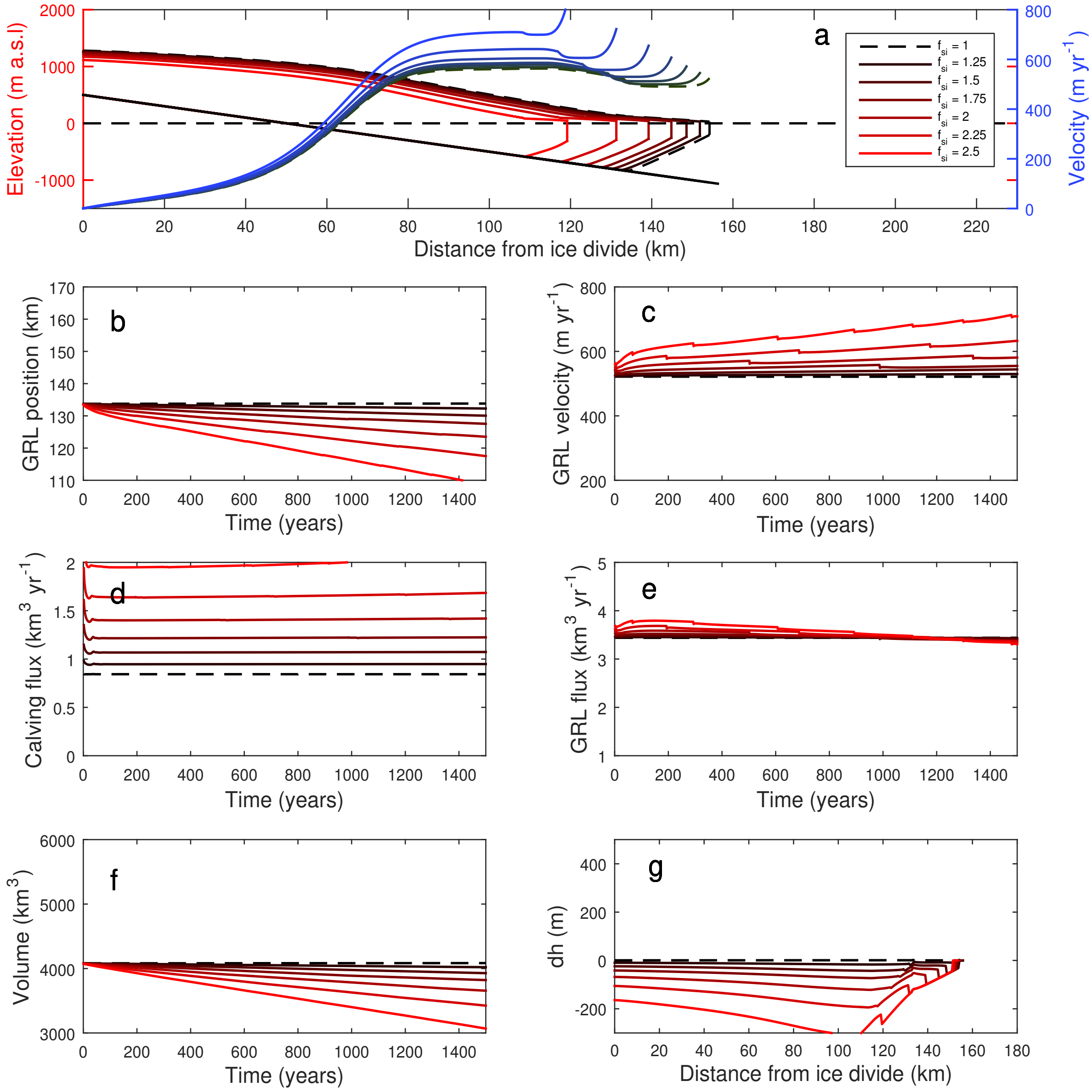

Figure 4.4.: Response to perturbations of the sea ice factor f_{si} for an idealized marine-terminating glacier, from warm ice towards cold ice (red to black). Shown are the glacier shape and the corresponding velocities after 1500 years (blue to green) in (**a**), as well as the evolution of grounding line (GRL) position (**b**), grounding line velocity (**c**), calving flux (**d**), grounding line flux (**e**), volume (**f**) and difference between the surface after 1500 years and the steady-state (**g**). The steady-state is marked as dashed line.

4.2.4. Submarine Melt Rate

Submarine melt rate (*smr*) is only applied vertically beneath the floating tongue. Melting of a floating tongue or an ice shelf from underneath causes thinning of the floating part. Consequently, calving rates increase, because the depth for crevasses to penetrate is reduced (Figure 4.5d). This causes acceleration, which then results in a larger grounding line flux. After about 1400 years, the glacier has thinned and retreated enough, such that the increased melt causes smaller grounding line fluxes (Figure 4.5e). The retreat and advance due to increased and respectively reduced submarine melt rates are symmetric, which means that it advances and retreats in the same rate for an equally large perturbation. This is in contrast to perturbations of crevasse water depth, as outlined in Section 4.2.2.

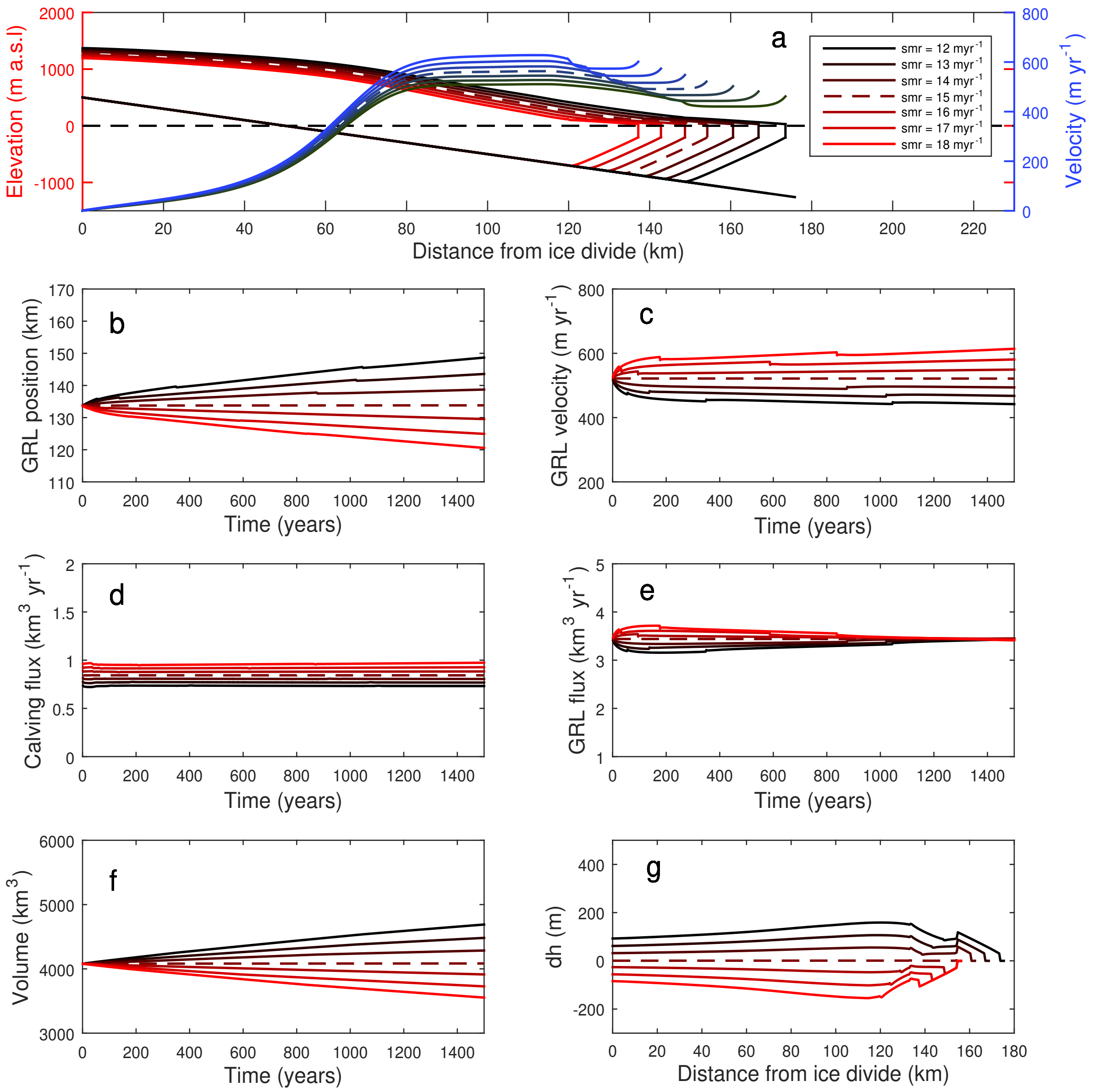

Figure 4.5.: Response to perturbations of the submarine melt rate *smr* for an idealized marine-terminating glacier, from warm ice towards cold ice (red to black). Shown are the glacier shape and the corresponding velocities after 1500 years (blue to green) in (**a**), as well as the evolution of grounding line (GRL) position (**b**), grounding line velocity (**c**), calving flux (**d**), grounding line flux (**e**), volume (**f**) and difference between the surface after 1500 years and the steady-state (**g**). The steady-state is marked as dashed line.

4.2.5. Ice Temperature

The impact of ice temperature on a glacier is governed by the rate factor (A), which defines how much the ice is deformed by an applied stress, as described by Glen's flow law (Equation 2.8). The rate factor is related to the viscosity and exponentially dependent on ice temperature. Warm ice corresponds to a large rate factor and a low viscosity (soft ice); cold ice has a small rate factor and a high viscosity (stiffer ice) (see Equation 3.3 and Table 2.1).

Because the initial temperature is $T = 0\,°\mathrm{C}$ in the steady-state, it can only be perturbed towards lower values. When glacier ice is colder, the ice deforms less readily. This results in low initial velocities (Figure 4.6c) and a small grounding line flux (Figure 4.6e). As a consequence, the glacier thickens upstream and the surface steepens. Because the calving flux first stays high (Figure 4.6d), despite a reduced grounding line flux, the floating part shortens. The surface at the lower part, which is based below sea level, is steeper for cold ice than for warm ice, which causes higher driving stresses. The velocity and the grounding line flux consequently increase and provoke a slow advance of the grounding line and the terminus. A perturbation to $-20\,°\mathrm{C}$ increases the volume by about 150% during the 1500 years (Figure 4.6f). The increase in volume is due to a thickening of the upstream part, whereas the glacier terminus retreats (Figure 4.6g).

The rate factor appears in two terms of the stress balance (Equation 3.2) and is therefore very complex. On one side, it influences the viscosity and, consequently, the longitudinal stress gradient. On the other side, it impacts the lateral resistance. These two stresses cause opposed responses of the glacier to changes in ice temperatures, which is discussed in Section 5.3.

In summary, any given type of perturbation impacts this idealized glacier, although in different ways. The initially induced response determines the glacier feedbacks which kick in to establish a new equilibrium state. The changes in grounding line or calving fluxes can thereby be of different sizes and the grounding line may move linearly or in a more complex way. The combination of changes in fluxes and length determines the final glacier shape. These aspects are discussed in detail in Chapter 6.

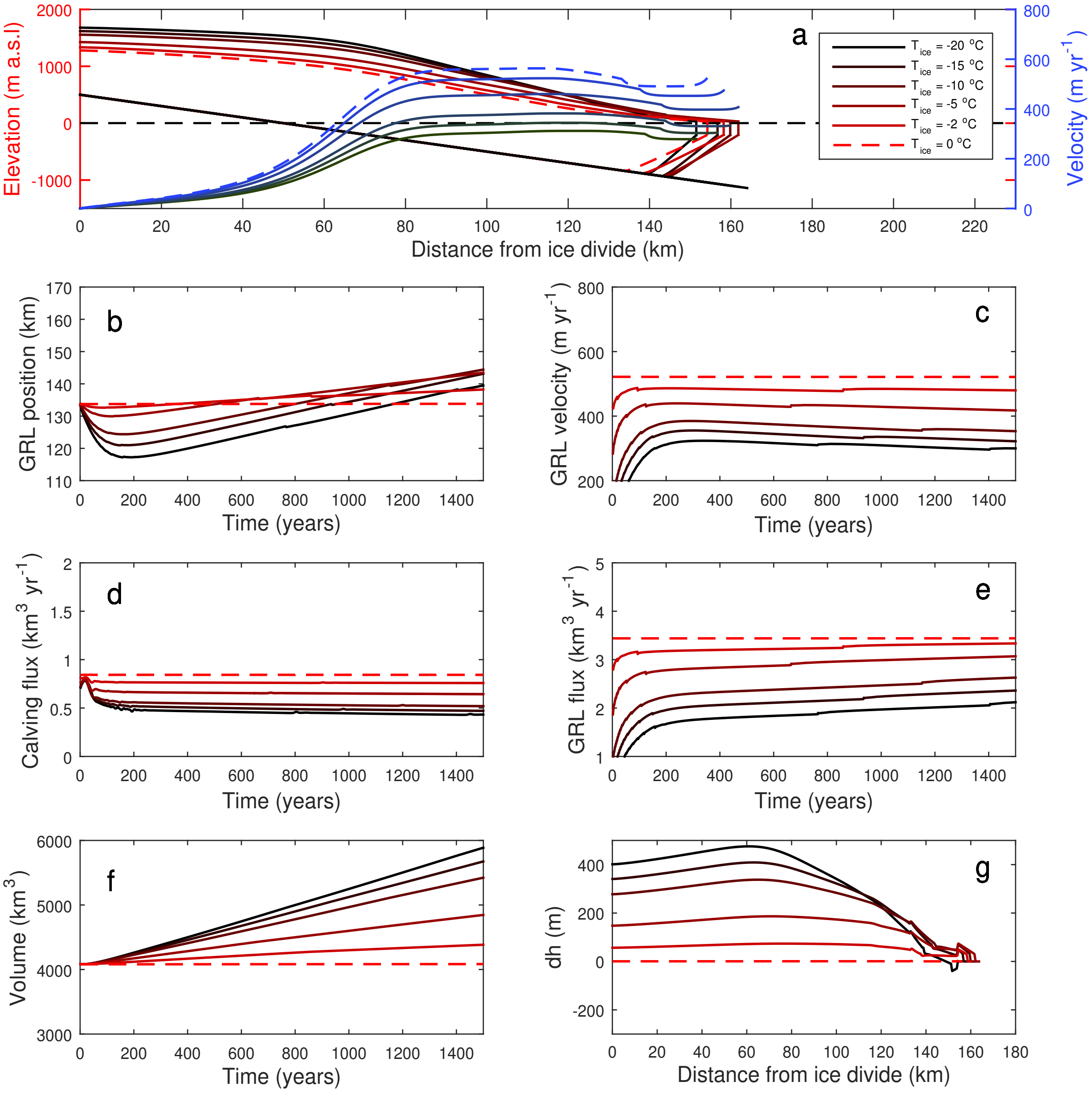

Figure 4.6.: Response to perturbations of the rate factor A for an idealized marine-terminating glacier, from warm ice towards cold ice (red to black). Shown are the glacier shape and the corresponding velocities after 1500 years (blue to green) in (**a**), as well as the evolution of grounding line (GRL) position (**b**), grounding line velocity (**c**), calving flux (**d**), grounding line flux (**e**), volume (**f**) and difference between the surface after 1500 years and the steady-state (**g**). The steady-state is marked as dashed line.

5

SENSITIVITY OF JAKOBSHAVN ISBRÆ

The model is now applied to the geometry of Jakobshavn Isbræ, western Greenland, (see Figure 2.8) to investigate the role of a realistic topography. Vieli and Nick (2011) and Nick et al. (2013) apply the flowband model to an approximate geometry of Jakobshavn Isbræ, which shows good agreement with observations from the last decade. Vieli and Nick (2011) study the impact of external forcing on the glacier and the triggered dynamical feedbacks. Ocean warming and reduced buttressing from sea ice are both able to reproduce the recent rapid changes. They also suggest a rapid adjustment to perturbations at the terminus on a short time-scale, which was also found by Nick et al. (2009) for Helheim glacier in southeast Greenland. They point out the necessity of a deeper understanding of glacier dynamics.

In this chapter, the response of Jakobshavn Isbræ to perturbations is analyzed on a decadal to millennial time-scale. First, the input geometry is described and followed by the results. Finally, the results are compare to those from the idealized glacier in Chapter 6 to evaluate the importance of the geometry.

5.1. Description of Input Data and Steady-State

Figure 5.2 shows the steady-state geometry of Jakobshavn Isbræ and the forcing. The input width is similar to the one used by Nick et al. (2013) in the area from the ice divide to 480 km downstream, where the glacier enters a deep and narrow trough. In the case of outlet glaciers which are embedded in the ice sheet, the width is difficult to define, because the glaciers are not confined by clear margins. The glacier surface calculated by the model is sensitive to the width. The width of the trouh and the depth along the flowline are picked with an interactive python-javascript webtool developed by Perrette (2015) (available on `https://github.com/perrette/webglacier1d`), which calculates width-integrated data for use with flowline models (Figure 5.1). In the tool, the centerline and two marginal lines have to be picked, from which a mesh orthogonal to the centerline at regular intervals is generated. By averaging over the cross-sections, one-dimensional data are calculated, such as topography, width, surface height, velocity, and surface mass balance. I picked the centerline following the highest surface velocities and the marginal lines in the trough following the steepest slope. The width is used for

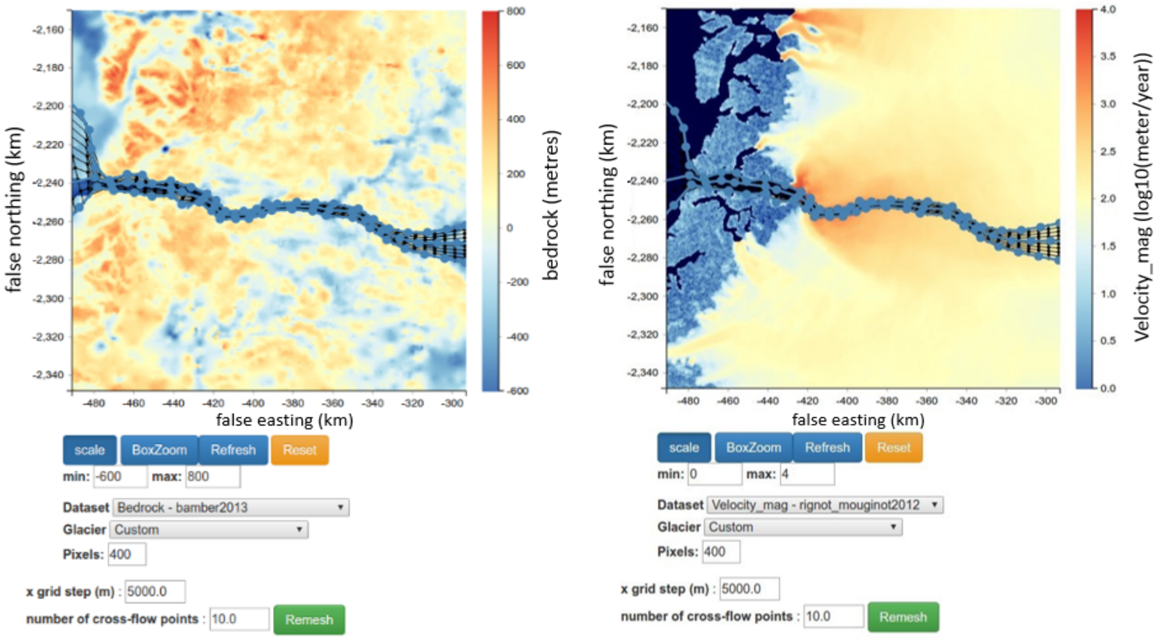

min: -600 max: 800
Dataset Bedrock - bamber2013
Glacier Custom
Pixels: 400
x grid step (m) : 5000.0
number of cross-flow points : 10.0

min: 0 max: 4
Dataset Velocity_mag - rignot_mouginot2012
Glacier Custom
Pixels: 400
x grid step (m) : 5000.0
number of cross-flow points : 10.0

(a) Bedrock

(b) Surface velocity

Figure 5.1.: Screenshot of the topography (**a**) and velocity (**b**) map of Jakobshavn Isbræ and the produced grid in the interactive webtool by Perrette (2015). The bedrock data is from Morlighem et al. (2014) and the velocity data from Rignot and Mouginot (2012). The resolution of the calculated 1D-data is 5 km.

the generation of a width-intergrated topography, and I tuned the width to achieve the observed surface in the model. Two datasets are available in the webtool by Bamber et al. (2013) and Morlighem et al. (2014). On Jakobshavn Isbræ, the two datasets differ little (see Appendix, Figure A.1); thus, I chose the data by Morlighem et al. (2014), which is more recent, is constructed using better techniques, and resolves the fast-flowing areas of the GrIS with a higher accuracy. Velocity data are from Rignot and Mouginot (2012) and surface mass balance data are from Ettema et al. (2009). Figure 5.1 shows a screenshot of the webtool with a map of the topography and velocity overlain by the mesh produced from the picked width and centerline.

The resolution of the data from the webtool is 5 km, but this was smoothed afterwards to avoid too large variations in the topography for the model. The surface mass balance is also extracted from the webtool, but lateral ice influxes at the lower 100 km have to be added to the SMB. I calculated the ice inflow from the sides via velocity, depth and width at the point of inflow. Submarine melt rates can be estimated from measurements by Motyka et al. (2011), who found melting rates of $228 \pm 49\,\mathrm{m\,yr^{-1}}$. A constant value of $250\,\mathrm{m\,yr^{-1}}$ is used here. The total mass loss by submarine melt is underestimated here, because the model applies submarine melt only vertically at the base of the floating part, which is small on Jakobshavn Isbræ. Also a seasonal cycle is disregarded, which was included by Vieli and Nick (2011) but beyond the scope of this thesis. Submarine melt rates should rather be calculated in three dimension as suggested by Fried et al. (2015), because of complex interaction of subglacial discharge and ocean waters. However, this

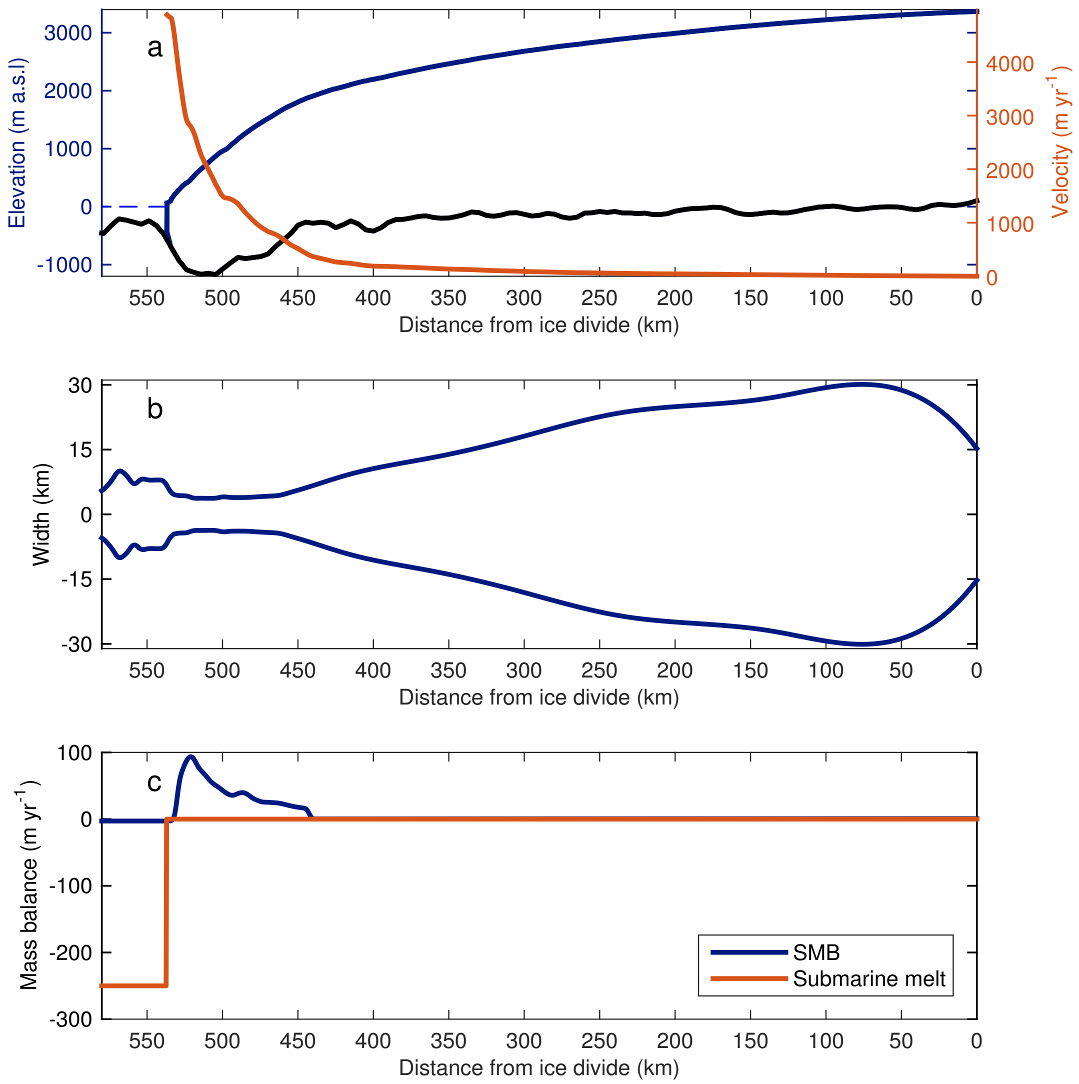

Figure 5.2.: Initial geometry and forcing of the Jakobshavn Isbræ configuration. (**a**) shows the glacier geometry with the along-flow velocity in steady-state. (**b**) gives the width in planview and (**c**) shows the surface mass balance and submarine melt rate with the same y-axis.

is not possible with this model. Figure 5.2 shows that the submarine melt rates are three times bigger than the surface ablation rates. This fits with the suggestion of Rignot et al. (2010) that submarine melt is as much larger in western Greenland than surface melt.

The ice temperature is estimated from borehole data from Iken et al. (1993) and Lüthi et al. (2002), taken at a distance of approximately 50 km from the calving front. They show ice temperatures of −5 or −10 °C at the surface, decreasing to −20 °C downward and increasing to the pressure melting point at the glacier base. A vertical integration of the observed temperatures gives a mean temperature of about −15 °C. Because ice temperature varies with elevation, I chose a linear profile along the flowline of ice temperatures reaching from −20 °C at the ice divide to −5 °C at the terminus.

Basal stress was estimated by Shapero et al. (2016) to be maximal $50 \pm 10\,\mathrm{kPa}$ at 50 km from the terminus. Van Der Veen et al. (2011) found basal stress between 50 and 350 kPa throughout the lowermost 30 km. In the steady-state a basal sliding factor of 120 is used, which corresponds to a basal stress of 120 kPa at 50 km from the terminus (see Appendix Figure B.2).

The crevasse water depth is unknown. Here, I set it to 120 m, which gives a steady-state grounding line flux of $40\,\mathrm{km}^3\,\mathrm{yr}^{-1}$. This is close to the value of $46\,\mathrm{km}^3\,\mathrm{yr}^{-1}$ found by Rignot and Kanagaratnam (2006) in 2005 and within the range of $32\,\mathrm{km}^3\,\mathrm{yr}^{-1}$ to $44\,\mathrm{km}^3\,\mathrm{yr}^{-1}$ found by Cassotto et al. (2015).

When the simulated glacier reaches an equilibrium, the grounding line stabilizes at a distance of 535 km from the ice divide on a reversed bed-slope (Figure 5.2). The stabilization at this theoretically unlikely position is discussed in Section 6.4. The velocities at the calving front reach only about $6\,\mathrm{km}\,\mathrm{yr}^{-1}$, which is much lower than the average velocity of $12\,\mathrm{km}\,\mathrm{yr}^{-1}$ found by Joughin et al. (2014). The velocity may be underestimated, because the width of the trough had to be increased, in order to reach the observed surface elevation. An alternative approach is to apply a lateral softening for ice that flows through the narrow trough, as it is done by Vieli and Nick (2011). Note also, that the calving front at steady-state is grounded, with only a small undercut. Mass loss by submarine melt is, consequently, only about $8\,\mathrm{km}^3\,\mathrm{yr}^{-1}$. The grounding line flux is therefore almost solely balanced by the calving flux. The simulated bed surface and along-flow velocities differ from the real profile of Jakobshavn Isbræ, due to the simplifications of the model and some rough parameter estimations. However, this model configuration serves as an example of how a real glacier can look like, and it is possible to make a statement on the influence of the complex geometry.

Compared to the idealized glacier, the surface of Jakobshavn Isbræ is much more rough, because bed variability is transmitted to the surface on fast-flowing glaciers (Gudmundsson, 2003). The driving stress, therefore, also shows large fluctuations along the flowline (Appendix, Figure B.2), while the driving stress is very smooth for the idealized glacier (Appendix, Figure B.1). Another difference is that the lateral stress is twice as large as the basal stress on Jakobshavn Isbræ, whereas the two stresses are equal in the idealized glacier. Shapero et al. (2016) found that basal sliding accounts for 70% of the surface velocities, which approximately fits to the result found here.

5.2. Perturbations of Parameters

This Chapter presents the results of parameter perturbations in the same way as Chapter 4 but applied on the geometry of Jakobshavn Isbræ. The x-axis in all plots in this chapter is reversed to associate the shown glacier to the east-west orientation of Jakobshavn Isbræ. A direct comparison between the two different applications is not possible, due to different dimensions of the two glaciers. The response of a glacier that is influenced by topographic features is, however, interesting in its own right. All the parameters are perturbed through large ranges, in order to get a considerable grounding line migration. The steady-state values, together with their perturbation ranges, are listed in Table 5.1.

Table 5.1.: Values of the initial parameters for the Jakobshavn Isbræ geometry and their perturbed ranges. Corresponding values for the rate factor are found in Table 2.1.

Parameter	Symbol	Initial value	Range of perturbations	Unit
basal sliding parameter	A_s	120	0 - 300	$\mathrm{Pa\,m^{-2/3}\,s^{-1/3}}$
crevasse water depth	cwd	220	60 - 380	m
sea ice factor	f_{si}	1	1 - 3.5	
submarine melt rate	smr	250	50 - 650	$\mathrm{m\,yr^{-1}}$
rate factor	A	linear	$A(0\,°\mathrm{C})$ - $A(-25\,°\mathrm{C})$	$\mathrm{yr^{-1}\,Pa^{-3}}$

5.2.1. Basal Sliding

The basal sliding parameter is perturbed in a range from $0\,\mathrm{Pa\,m^{-2/3}\,s^{-1/3}}$ (no basal resistance) to $300\,\mathrm{Pa\,m^{-2/3}\,s^{-1/3}}$. A grounding line migration is only provoked when the glacier experiences no resistance from the bed at all; it initially advances 20 km. However, the advance of the grounding line is accompanied by thinning, strong enough to move the grounding line back to its original position again (Figure 5.3b). The temporary advance is triggered by very high initial velocities after the perturbation and high grounding line fluxes (Figures 5.3c and d). Therefore, most of the mass is lost in the beginning. By the time the grounding line jumps back again (after about 1460 years), the glacier has lost about half of its mass (Figure 5.3f) and has thinned 1300 km (Figure 5.3g). In the case of removed basal resistance, the surface becomes more bumpy (Figure 5.3g). An increase in basal resistance causes a thickening of the glacier, which starts slowly and continues throughout the time period. Because the glacier is not in steady-state after 1500 years and continues thickening, it can be assumed that the grounding line may advance after some time due to the steepening of the surface slope.

5.2.2. Calving and Crevasse Water Depth

The crevasse water depth was high enough in the steady-state (220 m) to almost remove the floating tongue. A reduction in the crevasse water depth to 100 m causes a lengthening of the floating tongue by 9 km (Figure 5.4a). To also trigger a destabilization of the grounding line, the crevasse water depth has to be either reduced to 60 m or increased to 380 m, which is about half the depth of the calving front. The reduction causes an advance to the same pinning point as in the perturbation to an ice temperature of −20 °C (Figure 5.7a). The rapid advance or retreat, caused by changed crevasse water depth, occurs shortly after the perturbation. While the glacier advances, grounding line velocity and ice discharge are reduced (Figures 5.3c and e). They increase significantly, when the grounding line stabilizes. The velocity is then about 8800 m yr^{-1} and increases slowly.

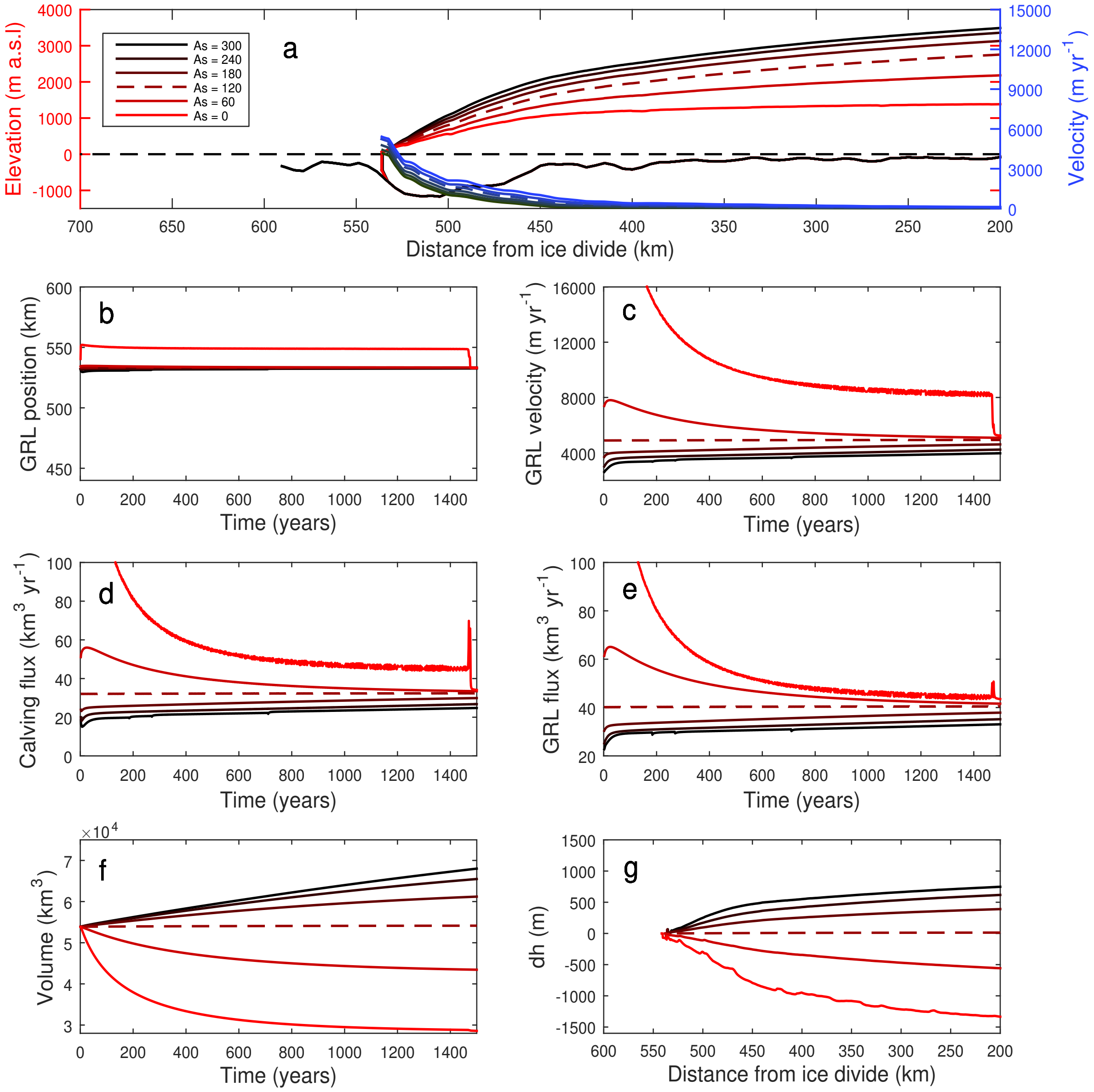

Figure 5.3.: Response to perturbations of the basal sliding A_s for the geometry of Jakobshavn Isbræ, from more to less sliding (red to black). Shown are the glacier shape and the corresponding velocities after 1500 years (blue to green) in (**a**), as well as the evolution of grounding line position (**b**), grounding line velocity (**c**), calving flux (**d**), grounding line flux (**e**), volume (**f**) and difference between the surface after 1500 years and the steady-state (**g**). The steady-state is marked as dashed line.

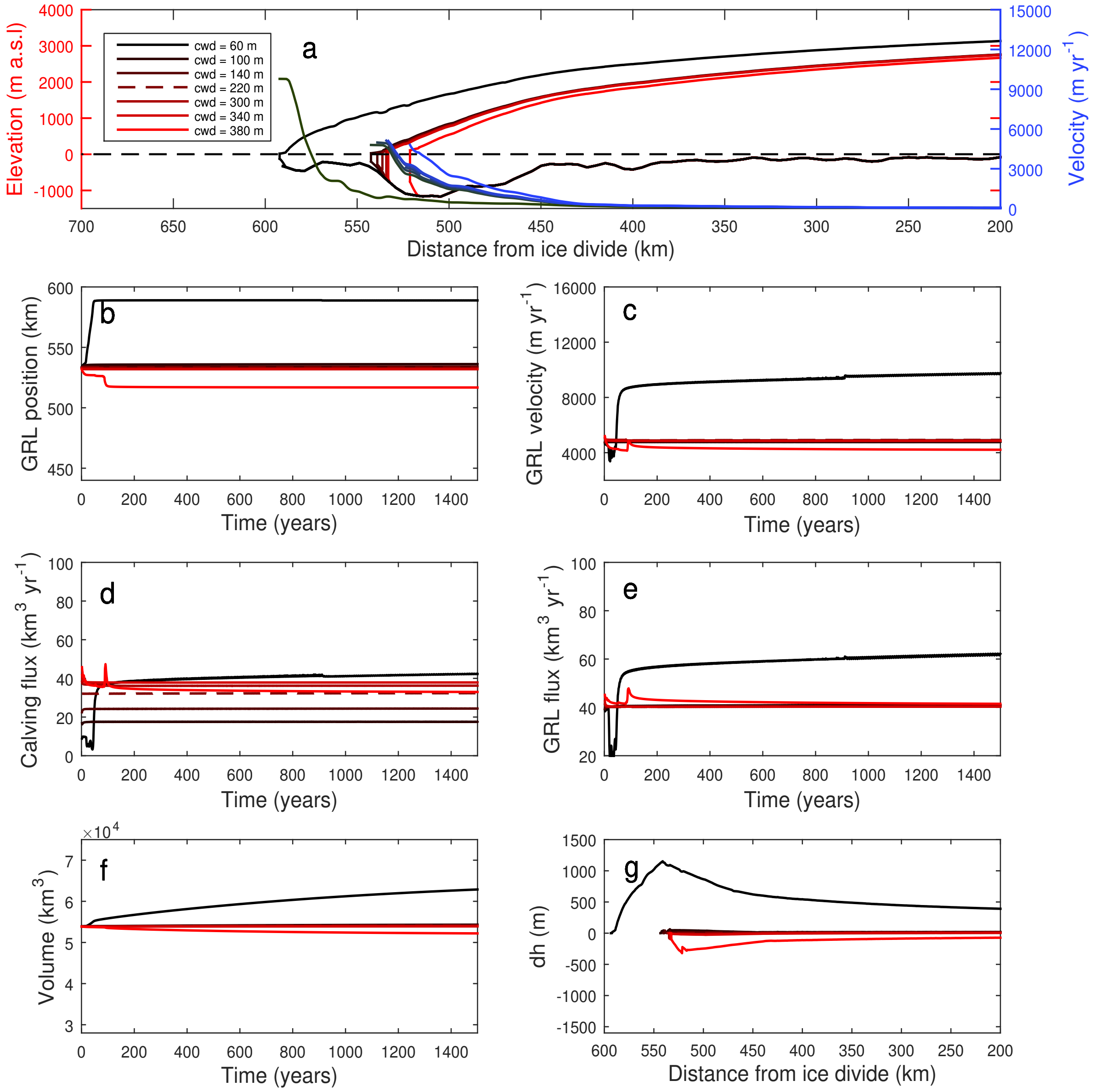

Figure 5.4.: Response to perturbations of the crevasse water depth *cwd* for the geometry of Jakobshavn Isbræ, from more to less sliding (red to black). Shown are the glacier shape and the corresponding velocities after 1500 years (blue to green) in (**a**), as well as the evolution of grounding line position (**b**), grounding line velocity (**c**), calving flux (**d**), grounding line flux (**e**), volume (**f**) and difference between the surface after 1500 years and the steady-state (**g**). The steady-state is marked as dashed line.

5.2.3. Buttressing by Sea Ice and Ice Mélange

As for the idealized glacier, the sea ice factor can only be increased, representing a reduction in buttressing. A reduction of the buttressing by a factor up to 2.5 does barely impact the glacier. The calving flux increases slightly, causing mainly a shortening of the already short floating tongue (Figure 5.5a). A sea ice factor of 3.5, however, causes a strong calving event immediately after the perturbation, causing an inland jump of about 80 km of the grounding line. A reduction of the buttressing by a factor 3 leads to the same position and thickness as a factor 3.5. Because the glacier is pushed less, the grounding line shortly stops at a position 500 km from the ice divide. Grounding line flux, velocity, and calving fluxes are significantly increased in the case of little buttressing.

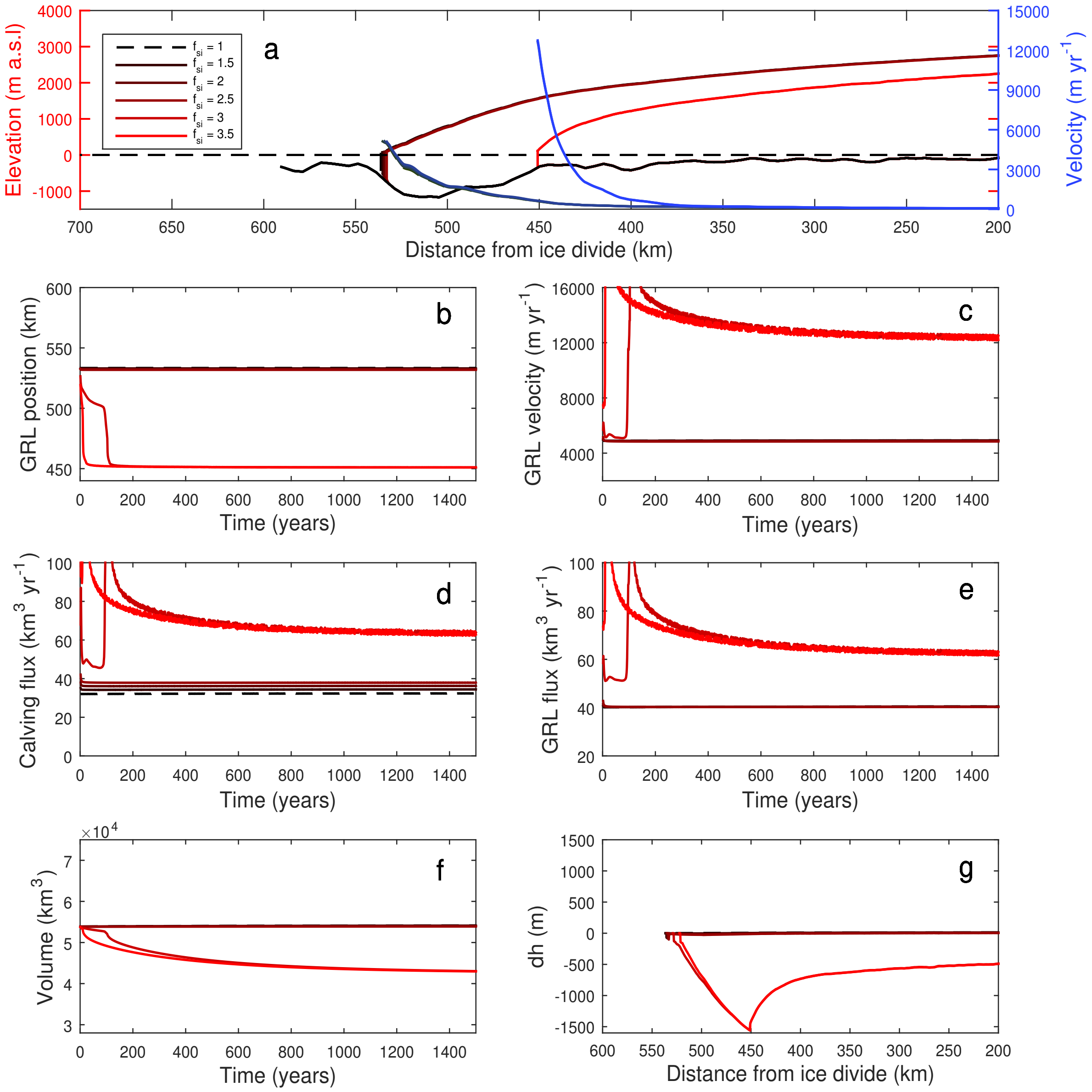

Figure 5.5.: Response to perturbations of the sea ice factor f_{si} for the geometry of Jakobshavn Isbræ, from more to less sliding (red to black). Shown are the glacier shape and the corresponding velocities after 1500 years (blue to green) in (**a**), as well as the evolution of grounding line position (**b**), grounding line velocity (**c**), calving flux (**d**), grounding line flux (**e**), volume (**f**) and difference between the surface after 1500 years and the steady-state (**g**). The steady-state is marked as dashed line.

5.2.4. Submarine Melt Rate

The submarine melt barely impacts the grounding line, because it is only applied vertically to the undercut at the terminus, which is small compared to the calving front. Within a range of 50 to 450 m yr^{-1}, it does not affect the surface of the glacier and only causes the grounding line to migrate by about 5 km. Increased melt rates thereby move the grounding line slightly upglacier and the calving flux decreases, so that a larger

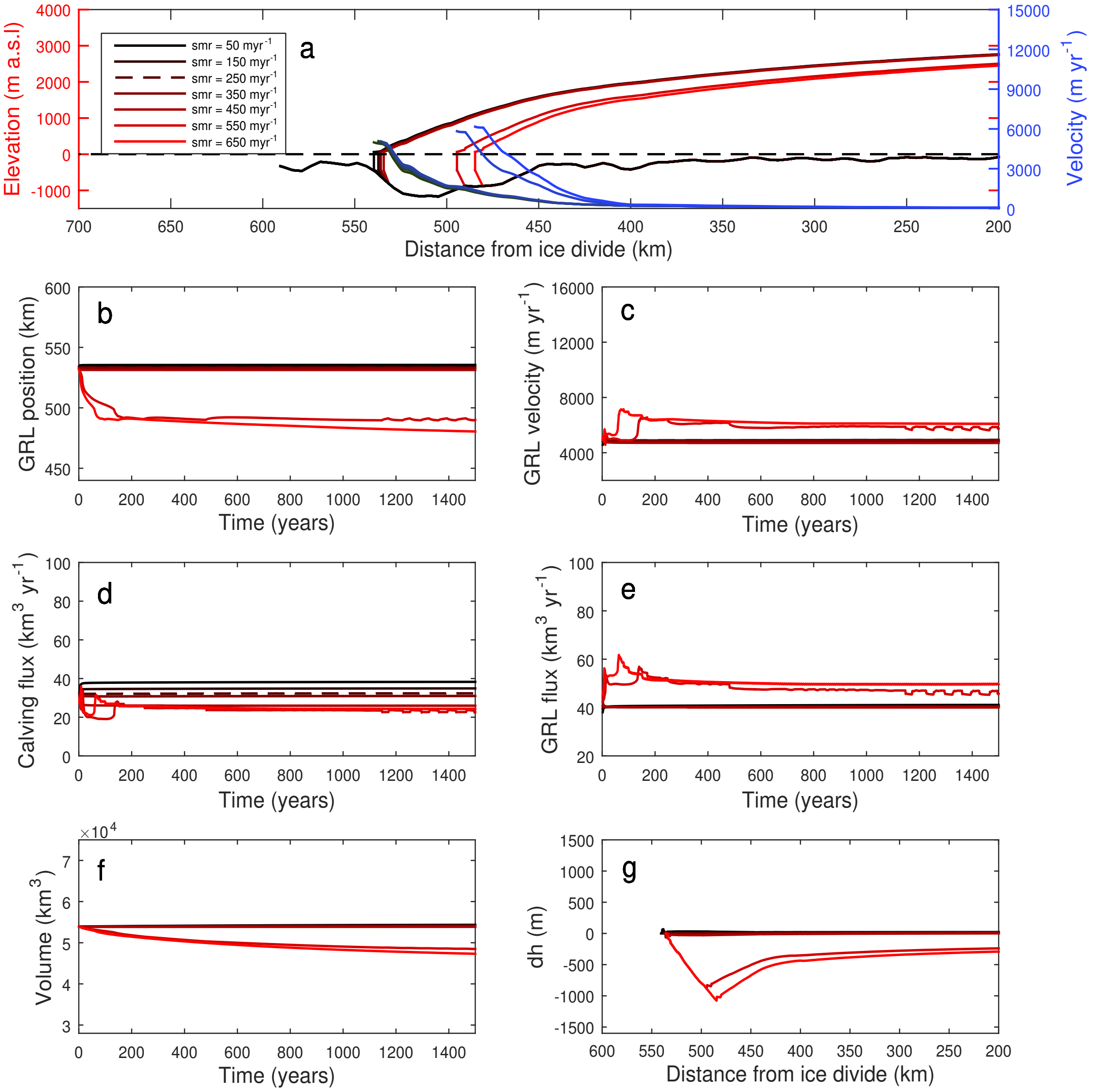

Figure 5.6.: Response to perturbations of the submarine melt rate *smr* for the geometry of Jakobshavn Isbræ, from more to less sliding (red to black). Shown are the glacier shape and the corresponding velocities after 1500 years (blue to green) in (**a**), as well as the evolution of grounding line position (**b**), grounding line velocity (**c**), calving flux (**d**), grounding line flux (**e**), volume (**f**) and difference between the surface after 1500 years and the steady-state (**g**). The steady-state is marked as dashed line.

floating part appears. A dramatic change in grounding line position is only achieved when the submarine melt rate increases to 550 m yr^{-1} (or 550 m yr^{-1}). It retreats then to 480 km (490 km, respectively) from the ice divide after 1400 years and continues slowly to retreat.

5.2.5. Ice Temperature

The rate factor in the steady-state is a linear function of the distance from the ice divide with values corresponding to ice temperatures of −20 °C to −5 °C. For the perturbations, instead of using a linear function, constant values throughout the glacier are used as in Chapter 4. The steady-state surface (Figure 5.7a, dashed line) is similar to a constant rate factor corresponding to −5 °C, which shows that the ice flow is mostly influenced by the ice temperature at its narrow trough. The grounding line does not move significantly as long as the temperature is between −2 °C and −15 °C (Figure 5.7b). The velocity, however, is influenced by the change in ice temperature, causing an increased grounding line flux for warmer ice and reduced ice discharge for colder ice. When the ice is perturbed to very cold temperatures, the surface steepens significantly, and the grounding line destabilizes after 150 years. It then advances 52 km within 51 years, causing a doubling in velocity (Figure 5.7c) and a strong increase in grounding line fluxes (Figure 5.7e). During the rapid advance, the velocity and the ice discharge are reduced but increase a lot when it stabilizes at the new position.

To summarize, Jakobshavn Isbræ has to be pushed hardly to destabilize its grounding line. Perturbations in basal sliding and rate factor cause a strong change in thickness, although the grounding line stays at the same position. When a destabilization of the grounding line is triggered, it moves rapidly to another point of stabilization.

5.3. The Relative Impact of Ice Temperatures on Viscosity and Lateral Stress

Englacial ice temperatures are poorly known. They can only be measured in-situ with thermistors lowered into the ice through boreholes. On Jakobshavn Isbræ, boreholes were drilled at around 50 km from the terminus (Iken et al., 1993; Lüthi et al., 2002, therein Figure 7). All profiles show ice temperatures of −5 °C at the surface, decreasing downward to −23 °C in the interior, and increasing again to the pressure melting point at the base of the glacier. This change in temperature with depth cannot be resolved in the depth-integrated model used here, which requires a depth-averaged temperature. Because air temperatures - and therefore also ice temperatures - decrease with elevation, a linear function for the along-flow temperature can be used, and a constant value throughout the glacier provides simplicity.

Figure 5.7a shows that a glacier with decreasing ice temperature from −20 °C at the ice divide to −5 °C at the glacier front, behaves very similar to a glacier with a constant ice temperature of −5 °C. This means that the flow of outlet glaciers depends mostly on the temperature in the narrow trough at the proximity of the terminus rather than

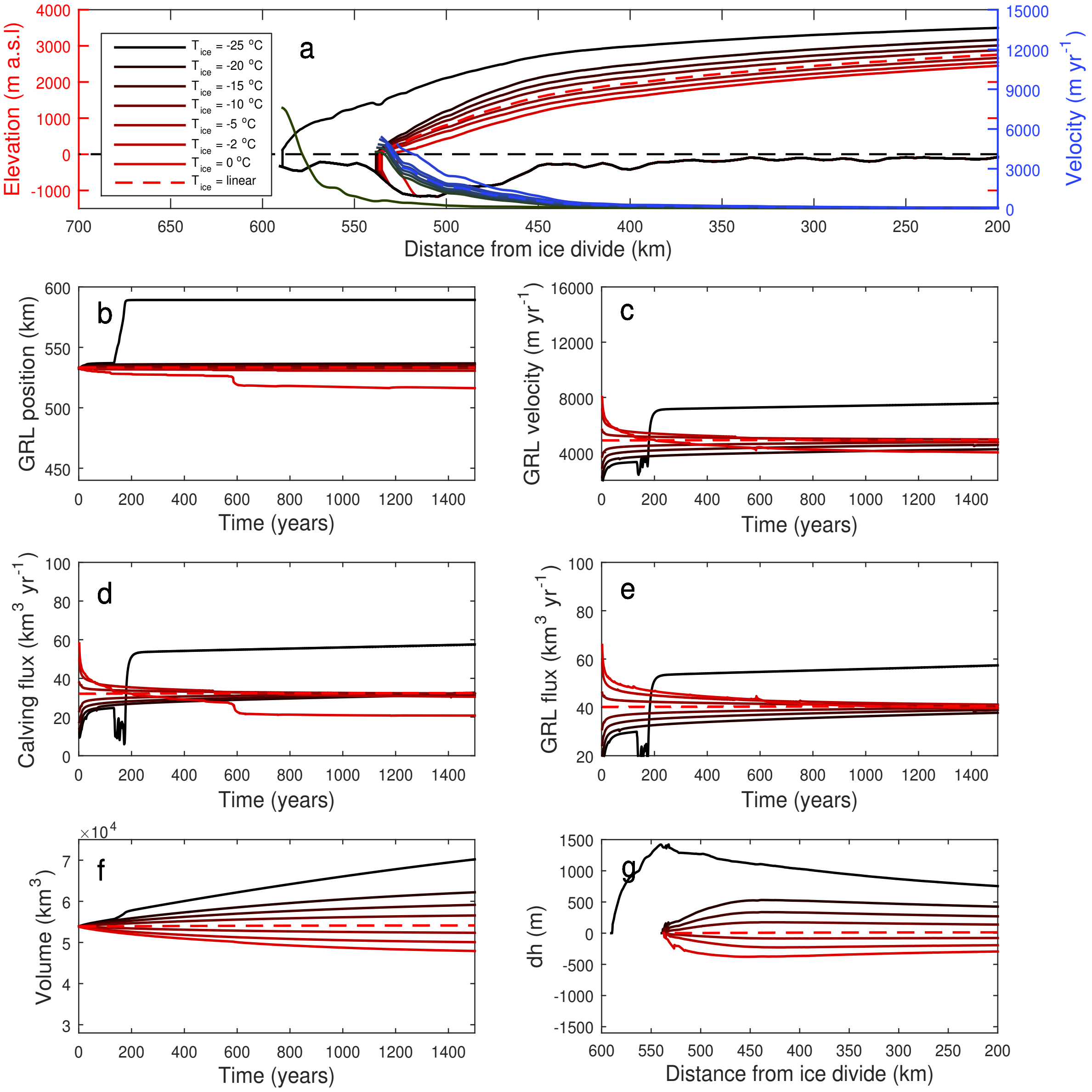

Figure 5.7.: Response to perturbations of the rate factor A for the geometry of Jakobshavn Isbræ, from more to less sliding (red to black). Shown are the glacier shape and the corresponding velocities after 1500 years (blue to green) in (**a**), as well as the evolution of grounding line position (**b**), grounding line velocity (**c**), calving flux (**d**), grounding line flux (**e**), volume (**f**) and difference between the surface after 1500 years and the steady-state (**g**). The steady-state is marked as dashed line.

on upstream temperatures. The reason is that margins influence ice velocities mostly in narrow areas, but their resistance is dependent on the ice temperature.

In the model, the ice temperature is only an indirect input via the rate factor, which it influences exponentially. The rate factor appears in three different terms in the model: the viscosity (Equation 3.3), the lateral resistance (Equation 3.2) and the strain rate (Equation 3.8). The strain rate, however, is again divided by A for the calculation of the resistive stress R_{xx} (Equation 3.7), so that it cancels out. The effect of a changed viscosity compared to the lateral resistance is still interesting.

To reveal the contribution of both these terms, I implemented a factor in front of each of the rate factors (E_ν and E_{lat} in Equation 3.2), which can be tuned independently. Since the steady-state run uses the highest rate factor of A($T_{ice} = 0\,°C$), I reduced the factors for viscosity and lateral resistance stepwise by factors that correspond to the reduction in the rate factor values in Table 2.1 (0.5, 0.25, 0.125, 0.0625, 0.031). The response of the idealized glacier to the individually changed viscosity and lateral resistance is shown in Figures 5.8b and c, compared to the total effect of both in a. The time evolution during the first 200 years for a reduction by a factor 0.031 (corresponding to an ice temperature of −20 °C) is shown.

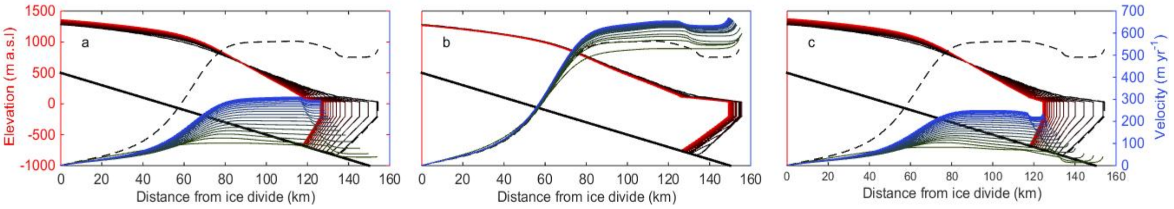

Figure 5.8.: Time evolution of the glacier for the first 200 years after a perturbation in the rate factor (**a**), viscosity (**b**), and lateral resistance (**c**), with values corresponding to to −20 °C. Time steps are 10 years from black (green) to red (blue). The steady-state glacier and velocity are plotted in black with a dashed line.

A increase in viscosity to a value corresponding to −20 °C makes the ice stiffer. In the part of the glacier with a bed below sea level, the velocity decreases slightly as a consequence of the less readily deformed ice (Figure 5.8b). Hence, the surface steepens slightly and the grounding line retreats. Because the floating tongue thins, the calving flux increases, reducing back-stresses. Thus, the velocities increase again. Overall, the stiffer ice leads to a volume loss and grounding line retreat. This is more pronounced after a longer time period of 3000 years (see Appendix Figure D.1).

An increase in lateral resistance to a value corresponding to −20 °C reduces the flow velocity initially to below 100 m yr^{-1} (Figures 5.8c). The grounding line flux decreases, the glacier consequently thickens and the front retreats. Although the velocity increases slowly due to the steepening surface slope, the velocities - and also the grounding line flux - still stay small. The resulting increase in volume opposes the impact of increased viscosity. Figure D.1 in the Appendix confirms the opposed glacier response in thickness, length, grounding line and calving fluxes.

To conclude, the impact on glacier dynamics due to lowered ice temperature is a combination of mass loss caused by higher viscosities and mass gain due to increased lateral stresses. The lateral resistance is found to be the dominant process, leading to a thickening of the surface in the upper area and a shortening of the lower part, as well as a slow-down of the whole glacier. Enderlin et al. (2013b) also investigate the glacial response to softening of the ice and and get an acceleration for warmer ice, which is in agreement with my results.

6

Discussion

The individual impact of perturbations of different forcings on the idealized geometry and Jakobshavn Isbræ were described in Chapters 4 and 5. Here, I summarize the impact of the various parameters on the glaciers. Here, I summarize the results and compare the relative impact of the various parameters on the glaciers. This is followed by a discussion of the time-scales of the response, as well as the time-scales of the applied external forcings. Subsequently, stabilization of the idealized glacier is compared to Jakobshavn Isbræ.

6.1. Relative Importance of Parameters

The impact of all parameters studied in Chapter 4 and 5 on glacier properties, such as volume, length, and fluxes is presented in Figure 6.1. The results after 200 years are shown, because the transient response during the first 200 years determines to a large degree the successive adjustment of the glacier. The difference between this first period to the following time period is discussed in Section 6.2.

All parameters that were perturbed in the sensitivity study are connected to temperature: Basal sliding is enhanced when more surface meltwater penetrates down to the glacier bed (if the hydrological drainage system is disregarded, which makes the feedback more complicated). Crevasses open deeper if there is more meltwater filling them or less buttressing by sea ice at the terminus. Higher submarine melt rates are linked to increased ocean temperatures. The internal temperature of the ice increases when warmer air diffuses into the ice.

Figure 6.1a shows that the glacier volume decreases in the case of increasing temperatures for all parameters, except for basal sliding, which keeps the volume almost unaffected. Note also that only submarine melt changes the volume linearly (see also Figure 4.5f). This is because the parameter is perturbed in equal steps and submarine melt influences the volume linearly in the model, as it directly removes mass. The impact of crevasse water depth and buttressing by sea ice are reduced towards lower temperatures (smaller water depth and larger buttressing), giving smaller changes in ice volume; this means that in these two cases the glacier stabilizes faster when growing than when shrinking. Changes in basal sliding have little effect on the volume during the transient phase. After a longer time period, however, it causes a significant change in volume (see Appendix Figure F.1).

The impact on glacier length is shown in Figure 6.1b. It is divergent for the different parameters: Crevasse water depth, buttressing by sea ice and submarine melt all act on the floating part of a glacier. They cause a retreat of the terminus and the grounding line with higher temperatures. In contrast, the rate factor and basal sliding parameter act on the grounded part of the glacier and cause an advance for perturbations towards higher temperatures. Note however, that in these cases were the glacier front advances, the volume still decreases.

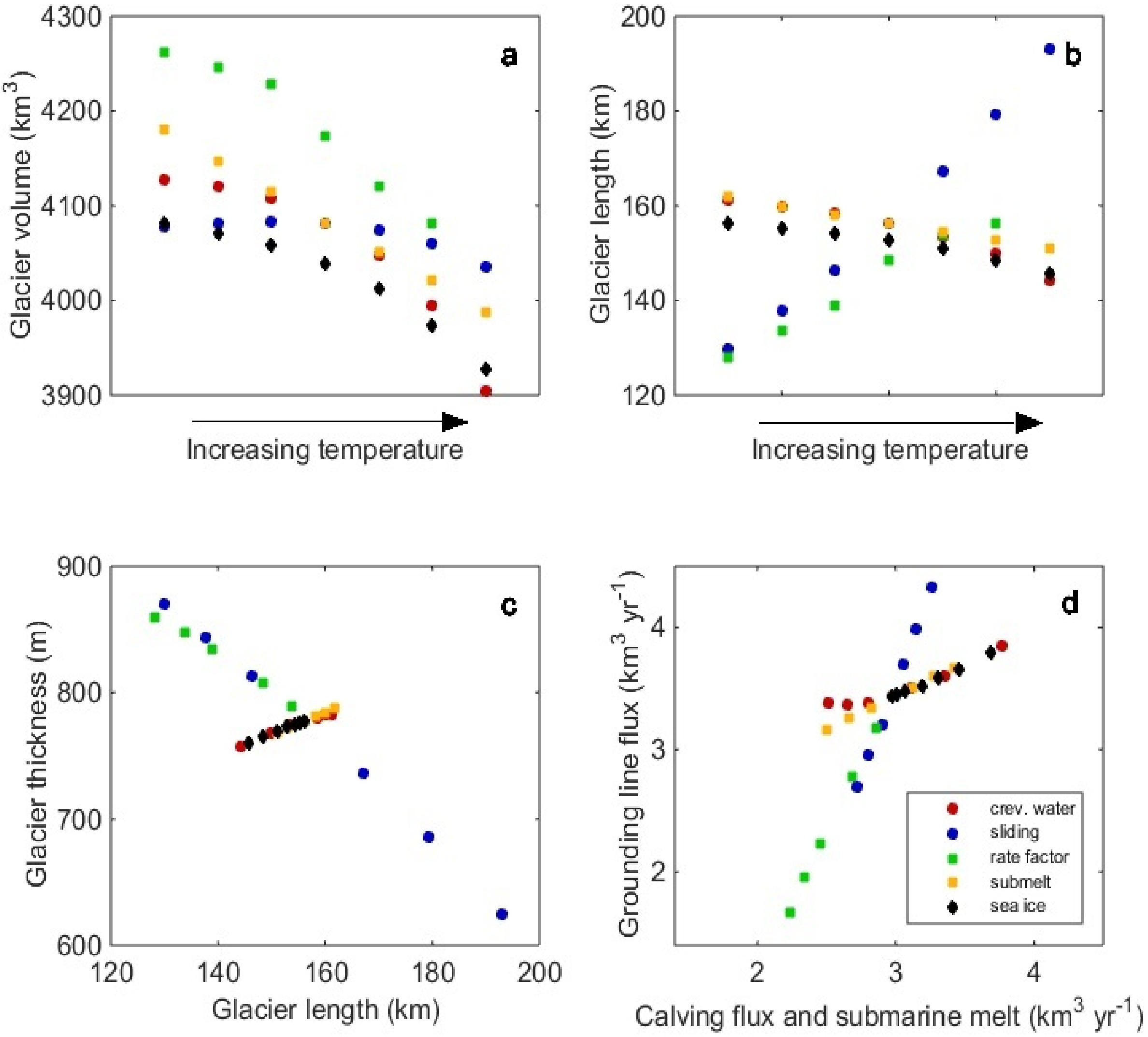

Figure 6.1.: Combined presentation of property changes for the perturbed parameters after 200 model years: crevasse water depth (*cwd*, red), sliding factor (A_s, blue), rate factor (A, green), submarine melt rate (*smr*, orange) and sea ice factor (f_{si}, black). (**a**) and (**b**) show change in glacier volume and temperature in case of changed parameters towards higher temperatures, where the temperatures are only to be taken relatively. (**c**) presents the change in thickness at the ice divide versus length and (**d**) shows the change in calving and submarine melt flux versus grounding line flux.

Figure 6.1c shows the correlations between length and thickness. For changes in crevasse water depth, sea ice factor, and submarine melt, length and thickness correlate positively. These parameters cause thinning and retreat of the glacier for warmer temperatures and therefore tend to keep the surface slope constant. For changes in rate factor and basal sliding, however, length and thickness correlate negatively. These parameters cause thinning and advance of the glacier for warmer temperatures. Thus, they flatten the surface and reduce the driving stress. The change in the surface slope results in a reversal of the grounding line movement with time (Figures 4.6b and 4.2b).

On longer time-scales, the impact of the rate factor on glacier length is more complex and non-linear (see Appendix Figure F.1). For a smaller rate factor, a warming causes lengthening and thinning, whereas for a larger rate factor, a warming causes shortening and thinning. For Jakobshavn Isbræ, the parameters can also be grouped by their relative impact on glacier length and volume, although the impact is less pronounced (Appendix Figure F.2c). A free movement of the grounding line is impeded here by stabilizing pinning points, so that the parameters rather influence the glacier volume than the glacier length. The effect of pinning points on glacier stability is further explained in Section 6.4.

In a steady-state, the grounding line flux is roughly balanced by the sum of submarine melt flux and calving flux. An offset of $0.4\,\mathrm{km}^3\,\mathrm{yr}^{-1}$ arises due to ablation by surface melt, which is small compared to the other fluxes. In Figure 6.1d, the steady-state values are, where the dots cross. Perturbations to the rate factor and basal sliding change the grounding line flux more than the calving and submarine melt fluxes. This results in an enlargement of the floating part, when the glacier thins upstream; and a reduction in the floating part, when the glacier thickens upstream.

Perturbations in the crevasse water depth, buttressing by sea ice, and submarine melt, however, change the calving and submarine melt flux more than the grounding line flux. This results in a larger loss of floating ice compared to the grounded ice; or a larger gain of floating ice compared to the grounded ice. While the crevasse water depth and buttressing by sea ice change the volume mainly by calving (i.e. shortening), ocean melt is implemented in the model to only remove ice from the bottom of the floating tongue (i.e. thinning). The resulting changes, however, are similar for crevasse water depth, sea ice buttressing and submarine melt, because a thinning of the floating tongue also initiates calving.

Based on the findings in this thesis, Figure 6.2 provides a conceptual model summarizing the studied idealized glacier responses to a shift in external forcing towards a colder (left panel) or warmer (right panel) climate. The parameters can be divided into two categories: those that act on the grounded ice (rate factor and basal sliding) and those that affect the floating tongue (crevasse water depth, sea ice buttressing and submarine melt). The impact of crevasse water depth, sea ice buttressing and submarine melt is qualitatively similar, because they all lead to mass loss at the front, acceleration and thinning due to dynamic coupling given warmer temperatures. Basal sliding and viscosity, however, change the glacier shape, leading to inversely proportional transient responses in length and thickness.

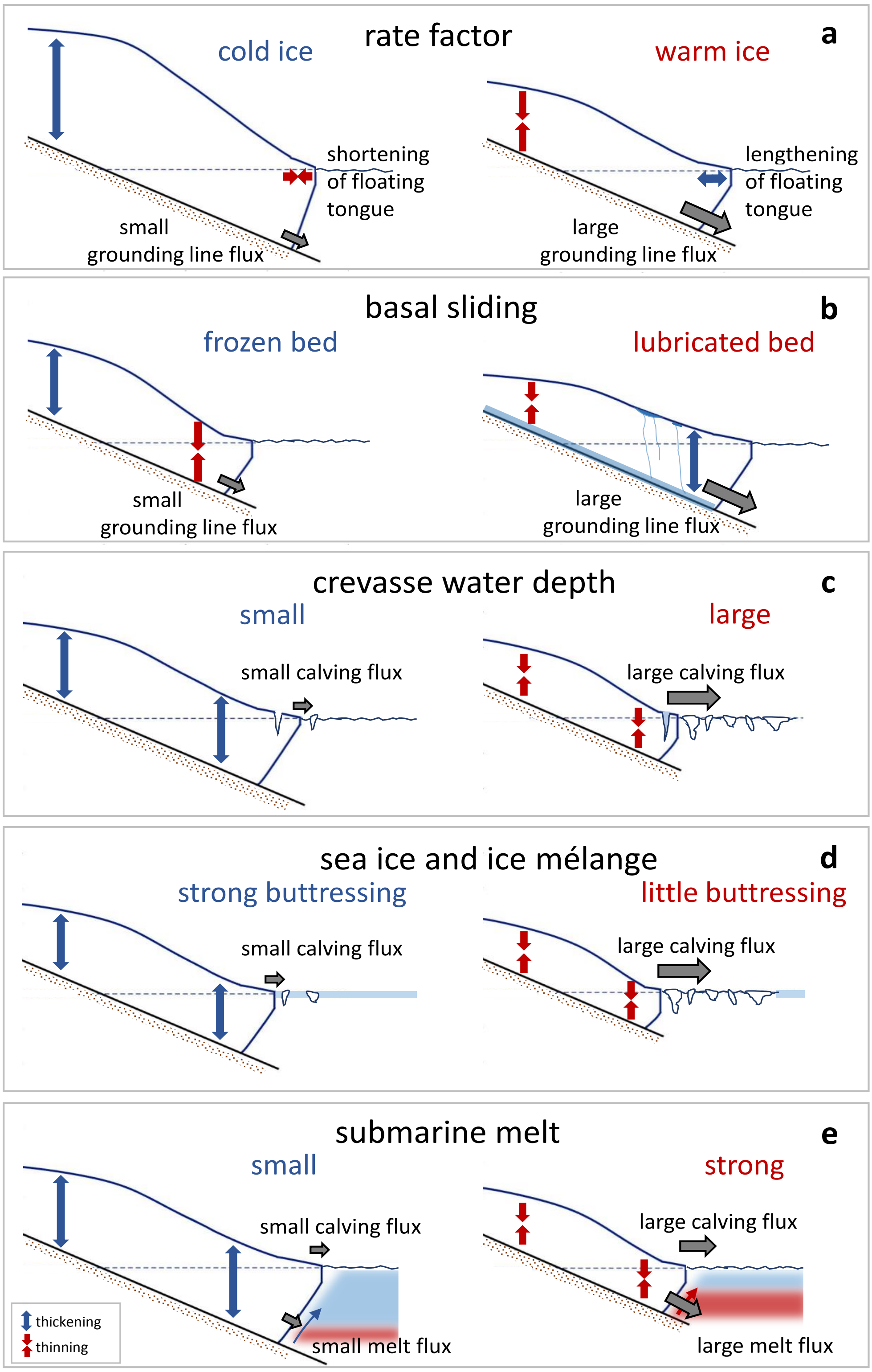
rate factor
a
cold ice
warm ice
shortening of floating tongue
lengthening of floating tongue
small grounding line flux
large grounding line flux
basal sliding
b
frozen bed
lubricated bed
small grounding line flux
large grounding line flux
crevasse water depth
c
small
large
small calving flux
large calving flux
sea ice and ice mélange
d
strong buttressing
little buttressing
small calving flux
large calving flux
submarine melt
e
small
strong
small calving flux
large calving flux
small melt flux
large melt flux
thickening
thinning

Figure 6.2.: Sketch of the impacts of the five parameter perturbations on a marine-terminating glacier. The panels show the impact of the rate factor (**a**), basal sliding (**b**), crevasses water depth (**c**), buttressing by sea ice (**d**), and submarine melt rate (**e**).

In reality, a changing climate initiates several processes synchronously, leading to more complex glacier responses. As long as perturbations are concentrated at the terminus (changes in submarine melt, buttressing and calving), their combined effect would enhance each other, as these parameters cause similar changes to a glacier. If submarine melt and calving by reduced buttressing increase due to a warming ocean, they cause an enhanced retreat and thinning of a glacier. If, in addition, a glacier gets more lubricated due to for example more meltwater finding its way to the bed, advance and retreat counteract each other. Also an adjustment of the ice temperature to warming - combined with warmer ocean - may cancel out the retreat due to increased calving and submarine melt by the advance due to softer ice. Simultaneous perturbations were not performed for this thesis and the predominant glacier response may depend on the magnitude of each perturbation. However, when studying changes on glaciers, it has to be considered that competing processes are involved.

6.2. Time Dependent Model Adjustment

The perturbations presented in Chapter 4 were applied as step-changes to the model parameters. Throughout the subsequent response to these perturbations, the parameters were kept constant. The response of the glacier to perturbations depends highly on the time-scale of interest. To begin with, the glacier reacts instantaneously to the perturbations; this changes the glacier properties significantly for a period of approximately 200 years. After these 200 years, the glacier adjusts slowly to the change in glacier properties and finally reaches a new steady-state.

Initial Response The initial responses to perturbations during the first 200 years were presented in Section 6.1. The division into two groups is the consequence of different instantaneous reactions to the perturbations. The step-perturbations in basal sliding and rate factor cause a large instantaneous change in grounding line velocity and flux (Figures 4.2 and 4.6, c and d), whereupon changes in grounding line position and volume follow. The perturbations in crevasse water depth, buttressing by sea ice and submarine melt rate, however, cause a large instantaneous change in calving fluxes (Figures 4.3d, 4.4d and 4.5d) and submarine melt fluxes (not shown), which initiate the changed grounding line, velocity and volume. These instantaneous changes are large in comparison to the subsequent longterm response and determine the glacier shape.

Longterm Response The subsequent longterm response leads in all cases to a retreat of the grounding line in a warming scenario (see Figures 4.2 to 4.6). Despite the unequal instantaneous responses to the different perturbations, higher temperatures leaded in all cases to thinning and mass loss. The grounding line flux therefore always decreases, when the initial period of 200 years is over. For the parameters acting on the floating part, the grounding line flux decreases due to a decrease in the cross-section, whereas for basal sliding and rate factor the grounding line decreases due to decreasing velocities. On millennial time-scales, lower temperatures cause a growth of the glacier and the initial response appears insignificant (see Appendix Figure E.1 as an example). However, real glaciers are perturbed on smaller time-scales, so that the glacier continuously adjusts to new changes and the initial response gains importance.

6.3. Time Dependent Forcing

In reality, step-perturbations are unlikely and glaciers are exposed to changes in external forcings on various time-scales. Here, potential time-scales involved for each perturbation that a marine-terminating glacier is exposed to are linked to the sensitivity study conducted in this thesis.

Basal Sliding The impact of increased surface melting on the Greenland ice sheet in a warming climate has been highly debated. Studies suggested that increased surface melt may increase flow velocities due to lubrication of the bed (Zwally et al., 2002). But later studies found that surface melt is insignificant to mean flow velocities (Tedstone et al., 2013; Sole et al., 2013), or could even cause a slow-down on decadal time-scales (Tedstone et al., 2015). On seasonal time-scales, however, surface meltwater causes variations in flow speeds due to a switch in the hydrological system as explained in Section 2.2.3. In the model used here, only basal sliding by a lubricated bed is taken into account, with no implied switch in the hydrological system. This corresponds to lubrication of the bed due to geothermal heating or pressure melting, rather than surface melt. However, a system with low effective pressure develops on a seasonal time-scale and the induced rapid speed-up may - on a seasonal time-scale - cause a flattening of the surface and an upstream thinning, as it was shown in Section 4.2.1.

Sea ice and Ice Mélange Ice mélange impacts Greenland glaciers on a seasonal time-scale (Cassotto et al., 2015; Amundson et al., 2010). It influences the timing of calving events through the shift between strong buttressing during winter, when icebergs are bounded together by sea ice, and weak buttressing, when the sea ice breaks up. Jakobshavn Isbræ, for example, advances several kilometers during winter, when sea ice stiffens the ice mélange (Amundson et al., 2010). Glaciers that terminate in fjords with permanent fast-ice are buttressed all year round. Break-up of this fast-ice has been found to influence the terminus stability on a time-scale of several decades, enabling a complete disintegration of the floating tongue. (Reeh et al., 2001) suggest that the absence of the 60 km long floating tongue of Nioghalvfjerdfjorden glacier in northeast Greenland during 7.7 and 4.5 ka B.P. correlated with the breakup of fast sea ice. As the model with the set-up used here disregards seasonal variations in the buttressing by sea ice or ice mélange, the step-perturbation in buttressing corresponds to such a breakup of fast-ice. This initiates a retreat, acceleration and thinning (Figure 4.4), until the grounding line reaches a stabilizing point or external forcing opposes the retreat. The Northeast Greenland Ice Stream calved heavily and retreated in correlation with reduced sea ice concentrations and caused the retreat into deeper waters, causing further instability.

Meltwater in Crevasses Meltwater fills crevasses on a seasonal cycle, following surface melt (Weertman, 1973; Sohn et al., 1998; Nick et al., 2010), and thus causes interannual terminus migration. Higher melt rates during summer deepen the crevasses by hydrofracturing and cause more calving. The seasonal variability is transfered by non-linear processes to the long-term dynamics of marine-terminating glaciers that are close to flotation (Amundson et al., 2010; Cassotto et al., 2015). The seasonal cycle of surface melt is neglected in the model, but local warming has increased the annual surface melt at the Greenlandic margins (Ettema et al., 2009). The step-increase in crevasse water depth applied in the model would therefore represent increased annual surface melt. Once increased calving rates theoretically initiate a continuous ice loss (Figure 4.3f) until the calving front is grounded on a sill, where calving rates decrease again.

Submarine Melt Increased ocean temperatures correlate with glacier retreat and acceleration over several years on many Greenland outlet glaciers (Moon and Joughin, 2008) (see Section 2.3). Motyka et al. (2011) suggested an increase in submarine melt rates by 25% after 1997 due to a warming ocean in the vicinity of Jakobshavn Isbræ. An increase of submarine melt by 25% applied to the idealized glacier caused a volume reduction of $0.5\,\mathrm{km}^3\,\mathrm{yr}^{-1}$ or a retreat rate of $60\,\mathrm{m}\,\mathrm{yr}^{-1}$ during the first 20 years. Compared to Jakobshavn Isbræ this is little, but the idealized glacier is much smaller and the steady-state submarine melt rate is only $15\,\mathrm{m}\,\mathrm{yr}^{-1}$ compared to $228\,\mathrm{m}\,\mathrm{yr}^{-1}$ on Jakobshavn Isbræ. An increase in the submarine melt rate by 25% in the modeled Jakobshavn Isbræ has little effect. This is due to the lack of submarine melt at the vertical calving front and the small size of the undercut, exposed to submarine melt.

Ice Temperatures Seroussi et al. (2013) suggested that the thermal regime of the Greenland ice sheet is in steady-state on a century-scale projection. The variation in ice rigidity is less than 5%, which impacts the basal motion and the evolution of the ice sheet negligibly, compared to external forcing by the ocean and atmosphere. On long time-scales, however, glacier ice integrates the history of past surface temperature variations over thousands of years. Through the shape of temperature profiles of boreholes, the past climate can be inferred. Changes in air temperatures have to span long time-scales to be significant in the depth-profiles in the ice. As an example, the layer of ice from the Little Ice Age (LIA) (from 1550 to 1850 AD) only shows a negative deviation in ice temperature of 0.1 °C; this was found from borehole profiles on two different locations from GRIP and Dye 3 by Dahl-Jensen et al. (1998). But signals of the Last Glacial Maximum (LGM) (25 ka B.P.), which was about 23 °C colder, are stored in the ice as a reduction in temperatures by 5 °C. During the last part of the Holocene (last 9 ka) and continuing up until today the interior of the GrIS has been thickening and decelerating, which can only partly be explained by higher Holocene accumulation rates. In addition, the deceleration is due to a dynamic response to the last deglaciation (MacGregor et al., 2016). Although the ice was colder during the LGM, it was softer than during the Holocene, due to a large amount of impurities. Thus, during the Holocene the soft ice has been continuously replaced by stiff ice and the thickening results from an overall stiffening of the ice sheet. Consequently, ice viscosity depends to a high degree on the amount of impurities.

Although temperature may not be the main driver, ice viscosity is of high interest when studying long-term variations of the GrIS. Because the response time of the interior of an ice sheet is up to several thousands of years (Appendix Figure E.1), a response of the glacier to historical changes in ice rheology should be taken into account when studying glacier dynamics. The results in Sections 4.2.5 and 5.2.5 also showed that a shift in the rate factor (which could be caused by several factors, including changes in impurities) does make a difference for the glacier. If the perturbation is large enough or is combined with other perturbations, a destabilization can be triggered after a long time period (Figure 5.7).

In summary, the different time-scales of glacier responses have to be considered when studying dynamic changes. Ice sheet models should therefore include the glacial history in order to study the present-day responses to climatic events. Even slow adjustments that are still ongoing from climatic changes many thousands years ago, may cause sudden changes such as a destabilization of the grounding line. Although studies suggest that glaciers were in steady-state before they rapidly retreated during the last two decades, these observations were mostly based on measuring changes in the grounding line position. As found in this study, even given a stable grounding line, a glacier can still be undergoing slow adjustments in thickness.

6.4. Stability of an Idealized Outlet Glacier versus Jakobshavn Isbræ

Outlet glaciers and ice-streams have been found to become unstable on a reversed sloping bed (Weertman, 1974; Thomas, 1979; Schoof, 2007). Once a retreat of such a glacier is triggered, the glacier is grounded in deeper waters. Ice discharge at the grounding line increases with increasing ice thickness (Schoof, 2007). If the grounding line moves into deeper waters, the ratio between total ice thickness at the grounding line and ice thickness below sea level decreases, and the front approaches flotation. This results in higher calving fluxes and cavity melting. As a consequence, further acceleration and retreat is initiated. This positive feedback provokes a continuous retreat of the glacier until the bed slope reverses again.

In the model run with the geometry of Jakobshavn Isbræ, I found that the grounding line in the steady-state is situated on a reversed-bed (i.e. deepening inland) (Figure 5.2a), which, theoretically, is an unlikely position for stabilization. This shows that fast-flowing ice can actually be stable on a reversed bed, if the channel is narrowing and enables stabilization by increased lateral resistance, as was also shown by Jamieson et al. (2012); Enderlin et al. (2013a); Gudmundsson et al. (2012). Figure 6.3d (dashed line) shows that the grounding line is located at the transition between the narrow trough and a wider section. The grounding line can barely advance, because the widening of the margins reduces lateral resistance, which accelerates the glacier and leads to high calving fluxes due to high strain rates. A retreat is also difficult, due to the high lateral resistance.

When applying perturbations to the external forcing, as conducted in Chapter 5 the grounding line is trapped at its steady-state position until it is pushed hard enough to eventually destabilize. Once moved from its stable position, rapid advance or retreat is initiated until the grounding line stabilizes at another pinning point. This new pinning point might be 80 km away, as in the case of a large reduction in the buttressing by sea ice (see Figures 6.3d). Such a dramatic acceleration of the grounding line after its destabilization was also found by Vieli and Nick (2011) for Jakobshavn Isbræ. Studies with a flowband model in Marguerite Bay, Antarctica, by Jamieson et al. (2014) revealed that the unrealistically large magnitude of perturbations needed to initiate retreat is reduced, when several processes are perturbed simultaneously. Also in this thesis, several parameters could have be perturbed synchronously to achieve more realistic results. If perturbing crevasse water depth together with submarine melt and buttressing, each perturbation could be much smaller to reach destabilization, as the three forcings impact a glacier similarly. However, simultaneous perturbations together with basal sliding or rate factor may keep the grounding line stable for a longer time, as advance and retreat would act against each other.

The idealized glaciers in Chapter 4 has no pinning points in the bed or the width. The bed is sloping down towards the ocean and is expected to stabilize after it has been perturbed. This takes long time, because the loss in buttressing is transfered upstream by complex feedbacks, such as longitudinal stresses within the glacier, and surface adjustment. The response time is defined as the time it takes for the glacier to reach a steady-state after an instantaneous perturbation and depends on the glacier thickness, the rate of mass turnover and the ablation rate (Jóhannesson et al., 1989; Bamber et al., 2007). It is, in addition, inversely proportional to the flow velocity (Nye, 1960) and varies therefore within the ice sheet. The fast-flowing areas close to the terminus adjust to changes within several years to decades, whereas slow flowing inland ice may take several millennia to adapt to changes.

On inland Antarctica, the response time is estimated to be 10,000 years or more, while Greenland adjusts within a few thousand years (Bamber et al., 2007). For the idealized glacier used in this thesis, the response time is about 15,000 model years, depending on the strength of the perturbation. Appendix Figure E.1 shows the change in time of the glacier shape, velocity, length, volume and fluxes following a perturbation to an ice temperature of $-5\,^{\circ}\mathrm{C}$ until the glacier stabilized. Although it may look like the glacier will never find a steady-state within the 1500 years presented in Figure 4.6, it just takes a long time, because the glacier is long, has a large drainage area, and has relatively low flow speeds. It also takes more time due to the lack of a pinning point. Eventually, a steady-state is reached when the ice flux at the grounding line equals the balance flux, which is the net mass balance cumulated over the area above the grounding line.

In reality, a surface elevation feedback should be included in the surface mass balance. In the model presented here, the surface mass balance is only stretched or compressed due to a change in glacier length, but it is not adjusted to a change in surface elevation. When a glacier thins, lowering of the surface causes more ablation, which lowers the surface even more. When, in turn, a glacier thickens in the accumulation area, its surface reaches colder air, which causes less ablation and - to be precise - also less accumulation due to the dryer air.

Chapter 5 showed that the response of a real glacier to perturbations is less smooth than an idealized glacier (see also Figure 6.3). It is also shown that the upstream area of the glacier may respond to perturbations even while the grounding line stays constant. Appendix Figure F.2b shows that the glacier length is barely responding to changing temperatures, except for large jumps to a new pinning point when the glacier is pushed very hard. The volume, however, leads to the same conclusion as Figure 6.1, that increasing temperatures reduce the volume for all parameter perturbations.

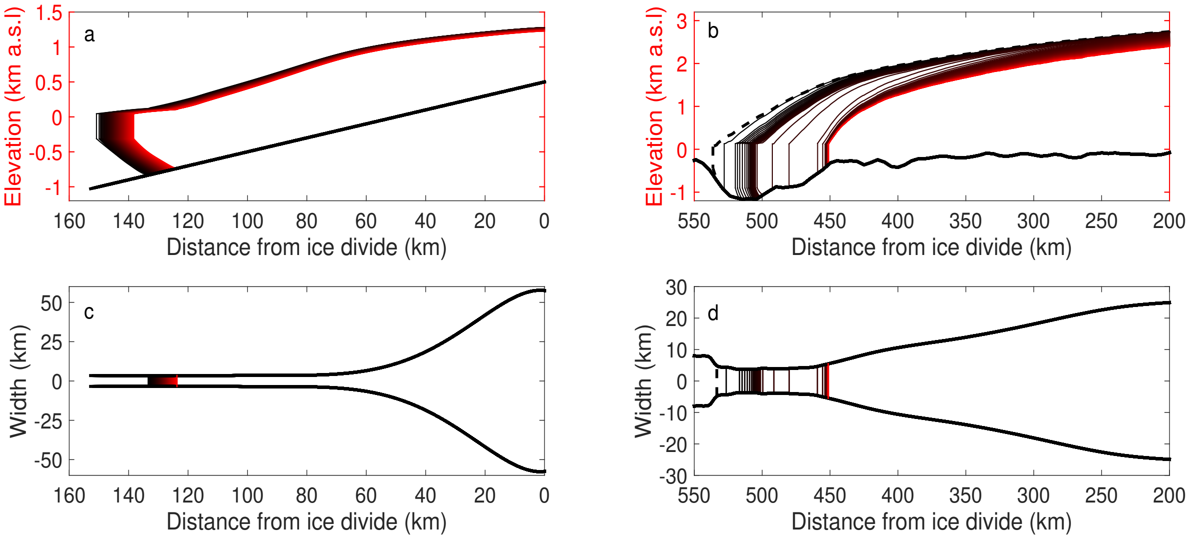

Figure 6.3.: Time evolution of the idealized glacier and Jakobshavn Isbræ for the first 500 years after a reduction in buttressing by sea ice by a factor 3.5. Shown are the evolution of the glacier shape and velocity (**a** and **b**) and the change in length on a planview (**c** and **d**). The time step is 5 years from black to red. The steady-state is illustrated with a dashed line.

To summarize, two significant differences between the idealized glacier and Jakobshavn Isbræ are as follows:

1. Stabilization of the idealized glacier is given by the sea level through flotation. On a real glacier, positions for grounding line stabilization are predefined by pinning points in the bed topography or the width.
2. The idealized glacier is sensitive to small perturbations, while the real glacier requires strong perturbations in order to trigger a change in grounding line position.

7

CONCLUSIONS AND OUTLOOK

7.1. Conclusions

The impact of ice temperature, basal sliding, water in crevasses, buttressing by sea ice, and submarine melt on marine-terminating glaciers was analyzed in this thesis. An idealized glacier with a simplified geometry was compared with a more complex geometry, resembling Jakobshavn Isbræ in western Greenland. The used numerical flowband model is physically-based, but uses many parameterizations. An investigation of the isolated impact of the individual parameters on the glaciers and the effect of topography brought the following main findings:

1. An idealized glacier, which has a flat bed and straight walls, is sensitive to perturbations with a strong initial transient response, that determines the glacier shape and the successive processes. The following adjustment is a slow process due to dynamic feedbacks and induces a new steady-state after more than thousand years.
2. The perturbed parameters can be divided into two categories, each of which leads to different initial glacier responses:
    a) Changes in processes that act only on the terminus of the modeled marine-terminating glacier initiate a proportional response in thickness and length. A warming climate causes a synchronous thinning and retreat.
    b) Changes in processes that act on the grounded part of the ice sheet affect its thickness and length anti-correlated, and thus provoke a change in the surface slope. A warming climate initially causes a thinning and lengthening.
3. The rate factor is a complex parameter, because it influences two stresses in opposed ways on the here used glacier.
    a) Longitudinal stress gradient: The rate factor influences the viscosity and therefore the along-flow stress gradient. Colder ice is stiffer, leading to a retreat of the grounding line, steepening of the surface slope and consequently increasing the ice discharge. The volume of the glacier decreases.
    b) Lateral resistance: Colder ice increases the lateral resistance, leading to decreased velocities in the narrow channel, decreased grounding line flux, and an upstream

thickening of the glacier. The volume of the glacier increases. The softening or stiffening of the lateral margins is of larger importance for the glacier than a change in viscosity.

4. On the real glacier, stabilization is faster to reach due to pinning points on the bed and the margins. Therefore, perturbations have to be strong to destabilize the grounding line. But once destabilized, the grounding line jumps rapidly to the next stable point, which may be tens of kilometers away. A combination of several perturbations, that lead to the same glacier response, may cause a faster destabilization and a weaker, more realistic jump to the next pinning point.

The implications of the findings are that the grounding line stabilization is less influenced by parameters uncertainty, as long as there are topographic features. A glacier, whose grounding line is located on a pinning point, however, may appear to be in steady-state, while it is still adjusting the surface in the upstream slow-moving area. This mass loss may - after several hundreds or thousands of years - finally destabilize the grounding line.

7.2. Outlook

During the evolution on this thesis, some questions were answered but even more arose. This section provides an overview of ideas and suggestions for future research with the flowband model and Jakobshavn Isbræ.

Idealized Glacier similar to Jakobshavn Isbræ

For a better comparison of the parameter impacts on Jakobshavn Isbræ with their impact on an idealized glacier geometry, the latter one should have similar dimensions and shape as the real geometry. The same ranges of parameters could then be used, allowing a more quantitative comparison. Because the real geometry is grounded at the terminus and far from flotation, the idealized glacier should have a grounded calving front, as well.

Parameterization of Submarine Melt Rate at the Vertical Calving Front

Processes at the ice-ocean interface are implemented in the model in a highly simplified way. An idea is to include a plume-model such as developed by Jenkins (2011) to get a more realistic representation of submarine melt. On Jakobshavn Isbræ and several other Greenlandic outlet glaciers, submarine melt is an important ablation process, but on grounded calving fronts, the model highly underestimates submarine melt. The included plume-model should therefore also be able to apply submarine melt at the vertical calving front.

Reconstruction of the Retreat of Jakobshavn Isbræ through the Fjord

Even though the model is a simple model and constructed to better understand the main processes influencing marine-terminating glaciers, it can, nevertheless, be used to model real glaciers. Nick et al. (2013) modeled the prospective evolution of Jakobshavn Isbræ until 2200, using possible future warming scenarios. It would be interesting to also simulate the history of Jakobshavn Isbræ since the Little Ice Age. The best approach would be to start from the known present-day geometry and let it grow to a dated grounding line position. A reasonable time period is the LIA in ca. 1850, since which the retreat history, including halt positions, is well known (Weidick and Bennike, 2007, and Figure 2.8). Lateral moraines are found along the fjord and give information on the thickness during the LIA (see Figure 7.1). In addition, the ice between the LIA position and today is unaffected by marginal influxes, which is a good condition for the flowband model.

As a further exercise, the retreat through the whole fjord from Ilulissat, where Disko Bugt begins can be simulated. Outside Ilulissat, the Marrait and Tasiussaq moraine systems were found and dated to 9500 B.P. and 8000 B.P., respectively (see Figure 7.1 and Weidick and Bennike, 2007). This, however, is more difficult, because the width is not confined to the steep fjord walls any more and ice fluxes from the sides are unknown.

After the growth of Jakobshavn Isbræ to either the LIA position or to Ilulissat, the forcing should be reversed to trigger a glacier retreat again. To simulate the advance, accumulation has to increase, submarine melt rate and calving rates decrease. The reversal of the forcing may reveal whether retreat and advance are symmetric and if the glacier stabilizes at the same points.

The retreat and advance simulations could, in addition, include two variations to discover whether the width or the bed topography determine the pinning points, at which the glacier stabilizes during its retreat. One model run may therefore include a linear width through the whole fjord and another run might contain a flat bed topography.

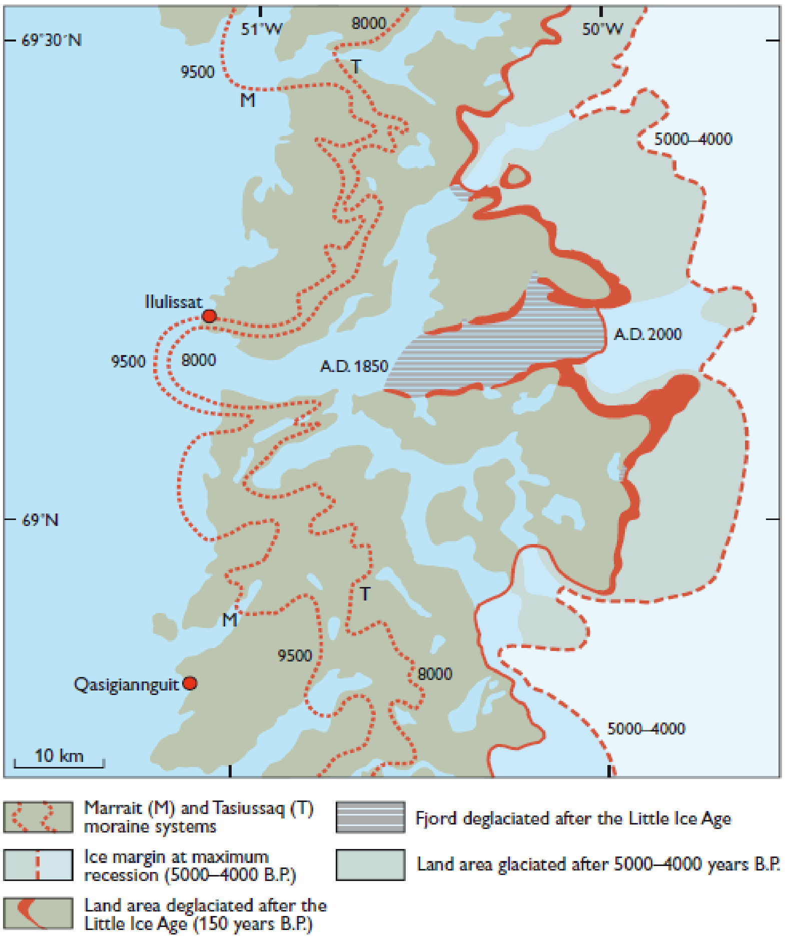
69°30'N
51°W
8000
50°W
9500
T
M
5000–4000
Ilulissat
A.D. 2000
9500
8000
A.D. 1850
69°N
T
M
9500
8000
Qasigiannguit
5000–4000
10 km
Marrait (M) and Tasiussaq (T) moraine systems
Ice margin at maximum recession (5000–4000 B.P.)
Land area deglaciated after the Little Ice Age (150 years B.P.)
Fjord deglaciated after the Little Ice Age
Land area glaciated after 5000–4000 years B.P.

Figure 7.1.: Reconstructions of the ice margins of Jakobshavn Isbæ and the Greenland Ice Sheet back to 9500 B.P (Weidick and Bennike, 2007).

Notations

GrIS	Greenland Ice Sheet
AIS	Antarctic Ice Sheet
SMB	Surface mass balance
B	Mass balance
ELA	Equilibrium Line Altitude
LIA	Little Ice Age
LGM	Last Glacial Maximum
x, y, z	longitudinal, lateral and vertical coordinates
σ	stress
τ	shear stress
σ'	deviatoric stress
ϵ	strain
$\dot{\epsilon_{xx}}$	strain rate
ρ_i	density of ice
ρ_w	density of sea water
ρ_{fw}	density of fresh water
g	gravitational acceleration
H	thickness
α	bed slope
T	temperature
U	velocity in flow direction
U_c	calving rate
U_t	velocity at terminus
N	effective pressure
A	rate factor
n	exponent in Glen's flow law
Q	activation energy for ice creep
R	universal gas constant
p_i	ice pressure
p_w	water pressure
t	time
W	width
L	length from ice divide to terminus
F	flux

F_c	calving flux
F_g	grounding line flux
ν	effective viscosity
f_s	friction parameter
A_s	sliding parameter
D	depth of the ice below sea level
h	surface elevation
H_f	flotation height
H_{ab}	height above flotation
h_b	bed elevation
cd	crevasse-depth
R_{xx}	longitudinal resistive stress
cwd	water depth in the crevasses
smr	submarine melt rate
f_{si}	sea ice factor

Appendices

A

DIFFERENT BED TOPOGRAPHY DATA FOR JAKOBSHAVN ISBRÆ

In the webtool by Perrette (2015), the bed topography along the flowline can be calculated from either the dataset by Morlighem et al. (2014) or Bamber et al. (2013). Figure A.1 shows both bed topographies.

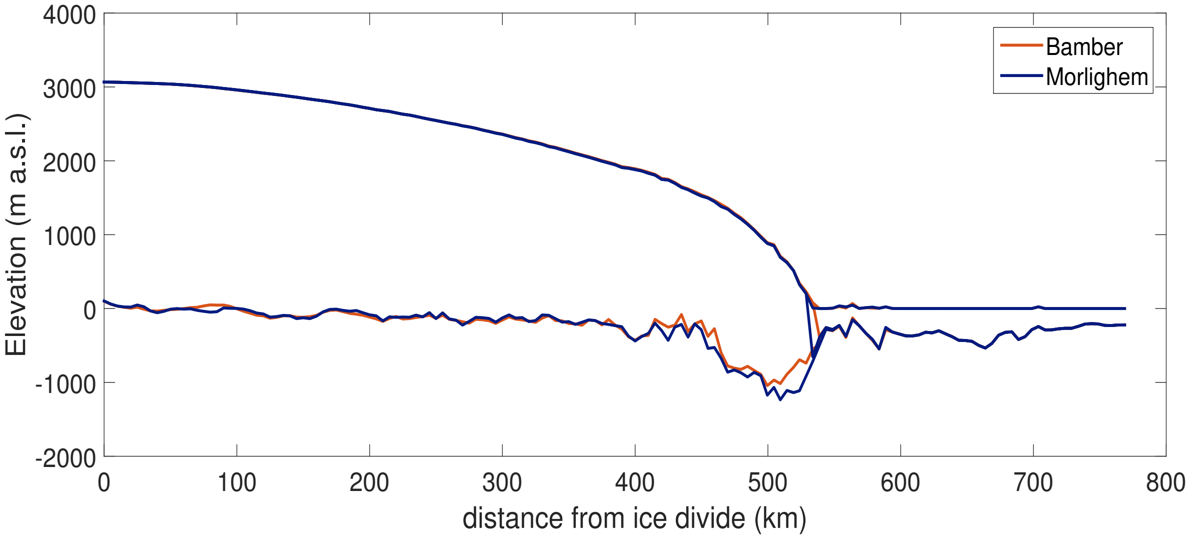

Figure A.1.: Comparison of the unsmoothened bed topography data by Bamber et al. (2013) and Morlighem et al. (2014) along the flowline of Jakobshavn Isbæ, calculated by cross-sections with the interactive webtool by Perrette (2015)

.

B

ALONG-FLOW STRESS COMPONENTS

The model calculates the four stress components acting on a glacier to calculated the flow velocity. They are presented separately in Figure B.1 for the idealized glacier and in Figure B.2 for Jakobshavn Isbræ.

B.1. Idealized Glacier

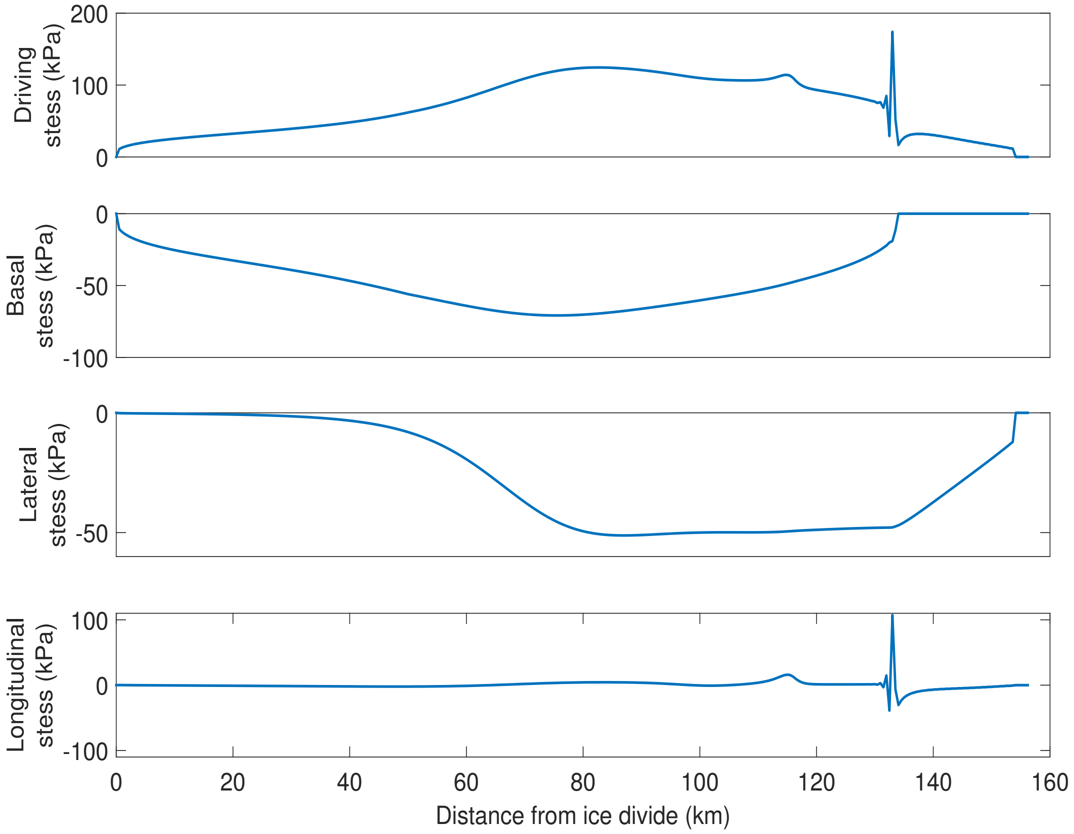

Figure B.1.: The four stress components along the flowline of the idealized glacier for the steady-state solution.

.

B.2. Jakobshavn Isbræ

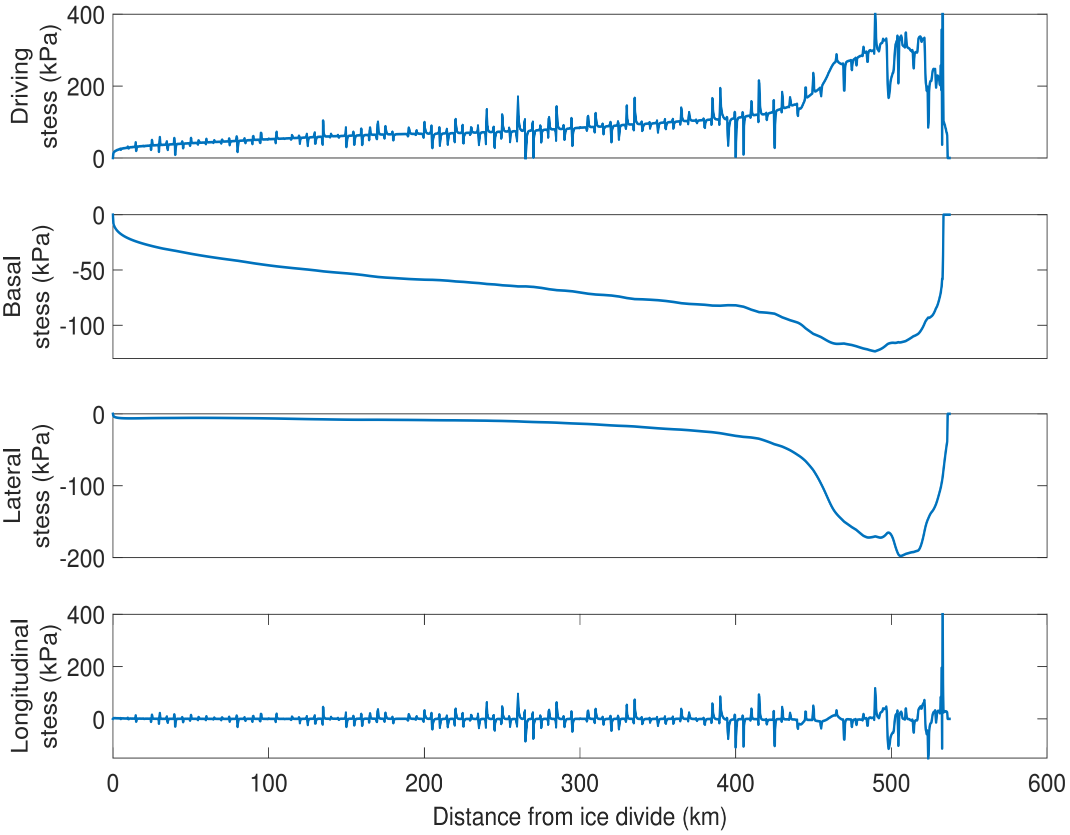

Figure B.2.: The four stress components along the flowline of Jakobshavn Isbræ for the steady-state solution.

.

C

TIME EVOLUTION FOR BASAL SLIDING

To better explain the chain of processes initiated by a perturbation in basal sliding, the time evolution of the along-flow surface and velocity is presented here.

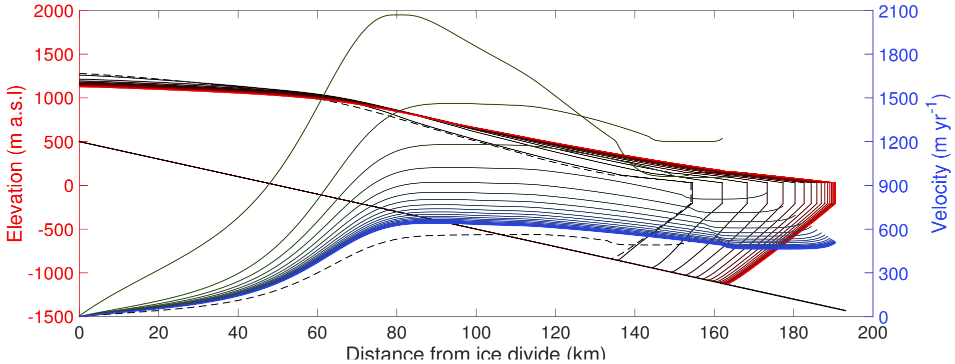

Figure C.1.: Time evolution during the first 200 years of the surface and velocity after a perturbation to increased basal sliding ($A_s = 40\,\mathrm{Pa\,m^{-2/3}\,s^{-1/3}}$). The time step is 10 years from black to red (green to blue). The steady-state profile is drawn as dashed line.

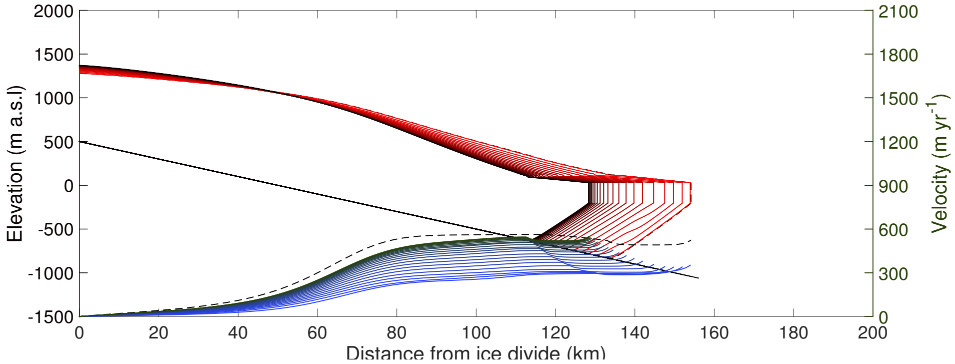

Figure C.2.: Time evolution during the first 200 years of the surface and velocity after a perturbation to reduced basal sliding ($A_s = 160\,\mathrm{Pa\,m^{-2/3}\,s^{-1/3}}$). The time step is 10 years from red to black (blue to green). The steady-state profile is drawn as dashed line.

D

VISCOSITY AND LATERAL RESISTANCE

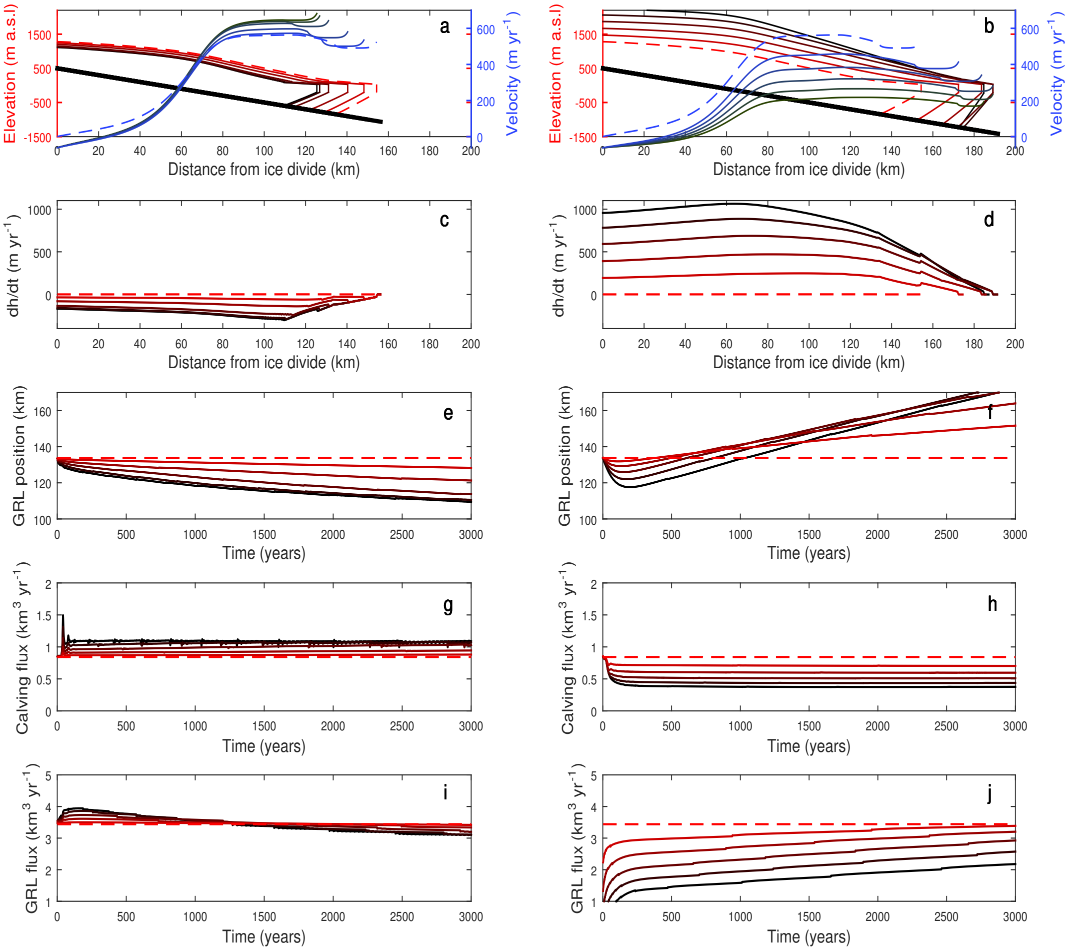

Figure D.1.: Glacier response during the first 3000 years to parameter perturbations in viscosity (left column) and lateral resistance (right column) towards values representative for ice temperatures of 0 °C (red) to −20 °C (black). Showing the surface elevation and velocity (**a** and **b**), the change in the surface elevation between first year and last year (**c** and **d**), evolution of grounding line position with time (**e** and **f**), the calving flux (**g** and **h**) and grounding line flux (**i** and **j**).

E

Stabilization of Idealized Glacier

In Chapter 4, only the first 1500 years after the perturbation were shown, in which the glacier did not reach steady-state again. More time is needed until the glacier adjusts to the perturbations. Figure E.1 shows results of the perturbations of the ice temperature to $-5\,^{\circ}\mathrm{C}$ as an example for the glacier changes until stabilization. After the 20,000 years, the grounding line only changes $0.05\,\mathrm{m\,yr^{-1}}$.

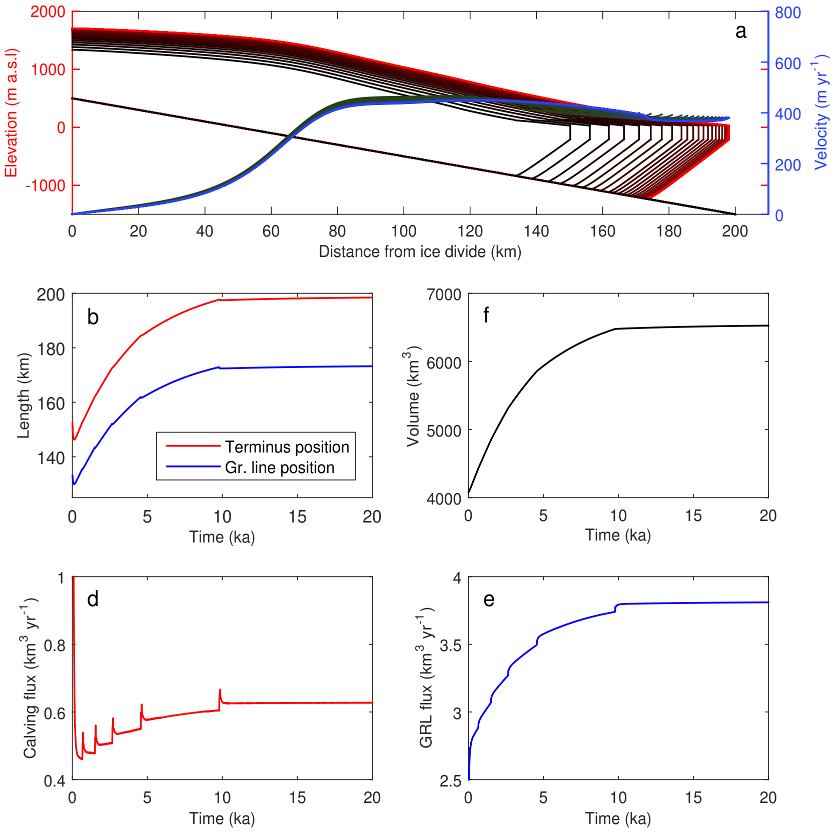

Figure E.1.: Model run of the perturbation to a rate factor corresponding to $-5\,^{\circ}\mathrm{C}$ for 20,000 years, showing stabilization. Shown are the glacier shape and the corresponding velocities in time steps of 500 years (black to red and green to blue, respectively) in (**a**), as well as the evolution of grounding line position (**b**), volume (**c**), calving flux (**d**) and grounding line flux (**e**).

F

Relative Importance of Parameters

F.1. Response after 1500 Years

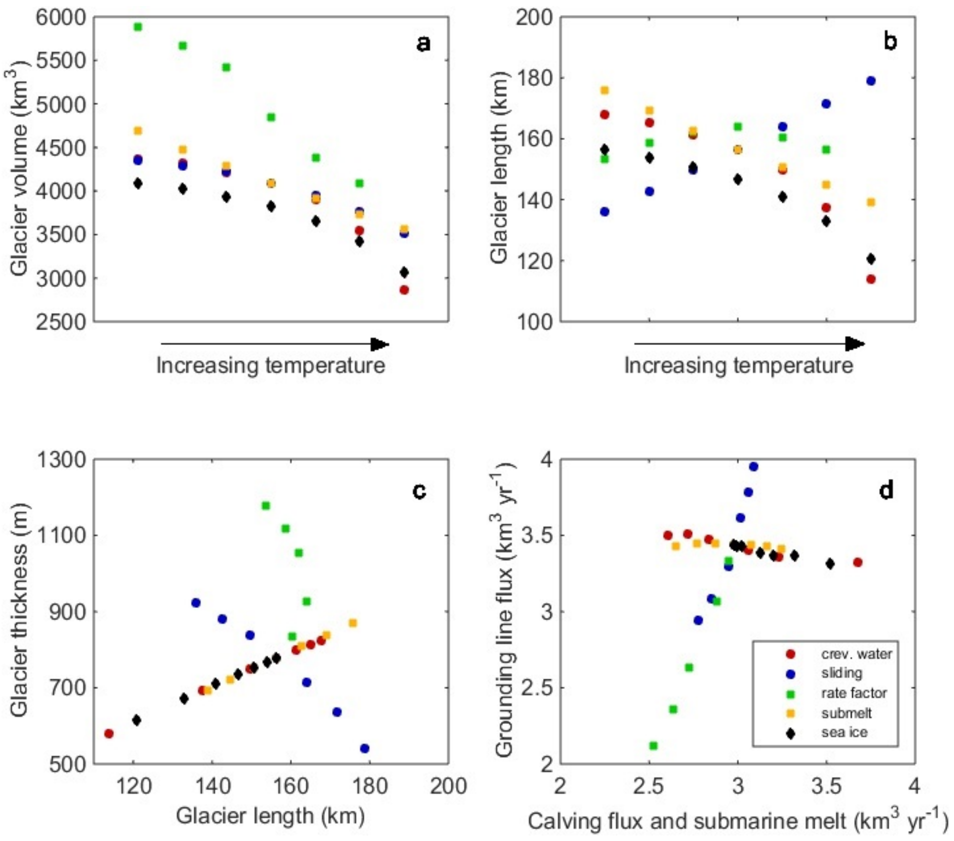

Figure F.1.: Combined presentation of property changes for the perturbed parameters after 1500 model years: crevasse water depth (cwd, red), sliding factor (A_s, blue), rate factor (A, green), submarine melt rate (smr, orange) and sea ice factor (f_{si}, black). (**a**) and (**b**) show change in glacier volume and temperature in case of changed parameters towards higher temperatures, where the temperatures are only to be taken relatively. (**c**) presents the change in thickness at the ice divide versus length and (**d**) shows the change in calving and submarine melt flux versus grounding line flux.

F.2. Response of Jakobshavn Isbræ after 1500 Years

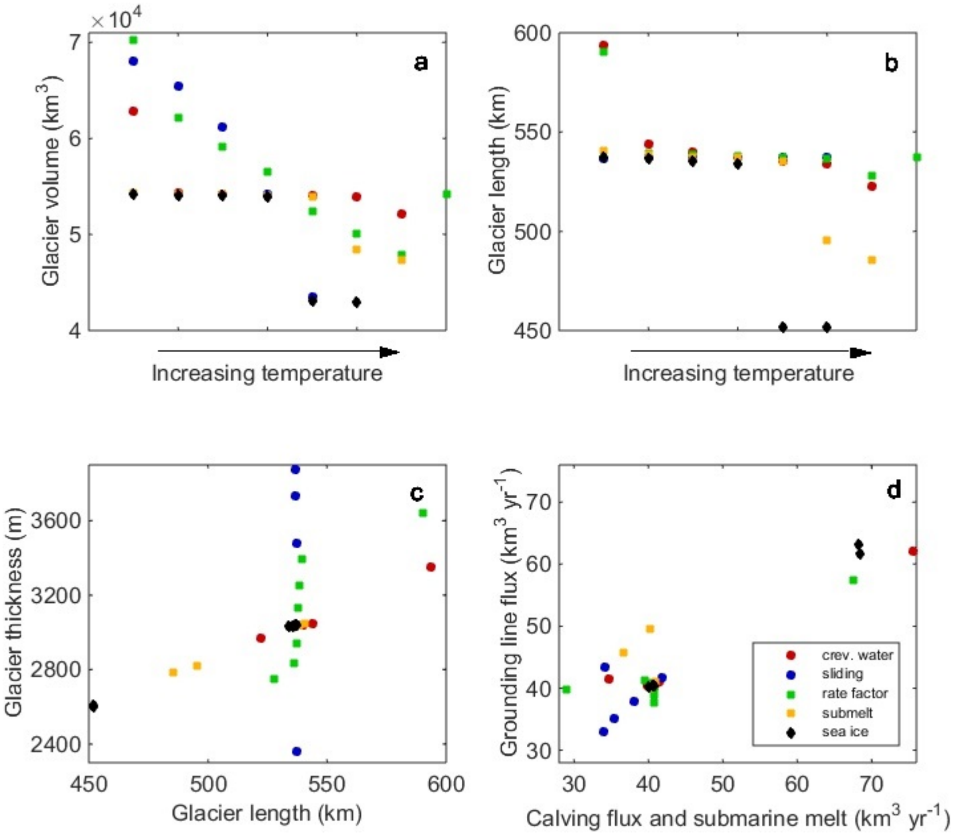

Figure F.2.: Combined presentation of property changes for the perturbed parameters of the approximate geometry of Jakobshavn Isbræ after 1500 model years: crevasse water depth (cwd, red), sliding factor (A_s, blue), rate factor (A, green), submarine melt rate (smr, orange) and sea ice factor (f_{si}, black). (**a**) and (**b**) show change in glacier volume and temperature in case of changed parameters towards higher temperatures, where the temperatures are only to be taken relatively. (**c**) presents the change in thickness at the ice divide versus length and (**d**) shows the change in calving and submarine melt flux versus grounding line flux.

REFERENCES

Abdalati, W., Krabill, W., Frederick, E., Manizade, S., Martin, C., Sonntag, J., Swift, R., Thomas, R., Wright, W., and Yungel, J. (2001). Outlet glacier and margin elevation changes: Near-coastal thinning of the Greenland ice sheet. *Journal of Geophysical Research*, 106(D24):33,729 – 33,741.

Alley, R. B., Blankenship, D. D., Bentley, C. R., and Rooney, S. T. (1986). Deformation of till beneath ice stream B, West Antarctica. *Nature*, 322(6074):57–59.

Amundson, J. M., Fahnestock, M., Truffer, M., Brown, J., Lüthi, M. P., and Motyka, R. J. (2010). Ice mélange dynamics and implications for terminus stability, Jakobshavn Isbræ, Greenland. *Journal of Geophysical Research: Earth Surface*, 115(1):1–12.

Amundson, J. M., Truffer, M., Lüthi, M. P., Fahnestock, M., West, M., and Motyka, R. J. (2008). Glacier, fjord, and seismic response to recent large calving events, Jakobshavn Isbræ, Greenland. *Geophysical Research Letters*, 35(22):2–6.

Arctic Sea Ice Blog (2015). http://neven1.typepad.com/blog/2015/08/jakobshavn-record-retreat.html, Accessed: 2016-05-30.

Bamber, J. L., Alley, R. B., and Joughin, I. (2007). Rapid response of modern day ice sheets to external forcing. *Earth and Planetary Science Letters*, 257(1-2):1–13.

Bamber, J. L., Griggs, J. A., Hurkmans, R. T. W. L., Dowdeswell, J. A., Gogineni, S. P., Howat, I., Mouginot, J., Paden, J., Palmer, S., Rignot, E., and Steinhage, D. (2013). A new bed elevation dataset for Greenland. *Cryosphere*, 7(2):499–510.

Bamber, J. L., Layberry, R. L., and Gogineni, S. P. (2001). A new ice thickness and bed data set for the Greenland ice sheet: 1. Measurement, data reduction, and errors.

Benn, D. I. and Evans, D. J. A. (2010). *Glaciers and glaciation.* Hodder Education, London, 2nd edition.

Benn, D. I., Hulton, N. R. J., and Mottram, R. H. (2007a). 'Calving laws', 'sliding laws' and the stability of tidewater glaciers. *Annals of Glaciology*, 46(1):123–130.

Benn, D. I., Warren, C. R., and Mottram, R. H. (2007b). Calving processes and the dynamics of calving glaciers. *Earth-Science Reviews*, 82(3-4):143–179.

Bindschadler, R. (1983). The importance of pressurized subglacial water in separation and sliding at the glacier bed. *Journal of Glaciology*, 29(101):3–19.

Boulton, G. S. (1996). Theory of glacial erosion, transport and deposition as a consequence of subglacial sediment deformation. *Journal of Glaciology*, 42(140):43–62.

Box, J. E., Yang, L., Bromwich, D. H., and Bai, L.-S. (2009). Greenland Ice Sheet Surface Air Temperature Variability: 1840–2007. *Journal of Climate*, 22(14):4029–4049.

Brown, C. S., Meier, M. F., and Post, A. (1982). Calving Speed of Alaska Tidewater Glaciers, with Application to Columbia Glacier. *U.S. Geological Survey Professional Paper*, pages 1258–C.

Carr, J. R., Stokes, C. R., and Vieli, A. (2013). Recent progress in understanding marine-terminating Arctic outlet glacier response to climatic and oceanic forcing: Twenty years of rapid change. *Progress in Physical Geography*, 37:436–467.

Cassotto, R., Fahnestock, M., Amundson, J. M., Truffer, M., and Joughin, I. (2015). Seasonal and interannual variations in ice melange and its impact on terminus stability, Jakobshavn Isbræ, Greenland. *Journal of Glaciology*, 61(225):76–88.

Cazenave, A. and Llovel, W. (2010). Contemporary Sea Level Rise. *Annual Review of Marine Science*, 2:145–173.

Church, J. A. and White, N. J. (2011). Sea-Level Rise from the Late 19th to the Early 21st Century. *Surveys in Geophysics*, 32(4-5):585–602.

Cook, S., Zwinger, T., Rutt, I. C., O'Neel, S., and Murray, T. (2012). Testing the effect of water in crevasses on a physically based calving model. *Annals of Glaciology*, 53(60):90–96.

Copland, L., Mueller, D. R., and Weir, L. (2007). Rapid loss of the Ayles Ice Shelf, Ellesmere Island, Canada. *Geophysical Research Letters*, 34(21):1–6.

Cuffey, K., Conway, H., and Hallet, B. (1999). Interfacial water in polar glaciers and glacier sliding at -17 C. *Geophysical Research*, 26(6):751–754.

Cuffey, K. and Paterson, W. (2010). *The Physics of Glaciers*. Butterworth-Heinemann/Elsevier, Burlington, MA, fourth edition.

Cuffey, K. M., Conway, H., Gades, A. M., Hallet, B., Lorrain, R., Severinghaus, J. P., Steig, E. J., Vaughn, B., and White, J. W. C. (2000). Entrainment at cold glacier beds. *Geology*, 28(4):351–354.

Dahl-Jensen, D., Mosegaard, K., Gundestrup, N., Clow, G. D., Johnsen, S. J., Hansen, A. W., and Balling, N. (1998). Past Temperatures Directly from the Greenland Ice Sheet. *Science*, 282(5387):268–271.

Echelmeyer, K., Clarke, T. S., and Harrison, W. D. (1991). Surficial glaciology of Jakobshavn Isbrae, West Greenland: Part I. Surface Morphology. *Journal of Glaciology*, 37(127):368–382.

Echelmeyer, K. A., Harrison, W. D., Larsen, C., and Mitchell, J. E. (1994). The role of the margins in the dynamics of an active ice stream. *Journal of Glaciology*, 40(136):527–538.

Enderlin, E. M., Howat, I. M., and Vieli, A. (2013a). High sensitivity of tidewater outlet glacier dynamics to shape. *Cryosphere*, 7:1007–1015.

Enderlin, E. M., Howat, I. M., and Vieli, A. (2013b). The sensitivity of flowline models of tidewater glaciers to parameter uncertainty. *Cryosphere*, 7(5):1579–1590.

Ettema, J., Van Den Broeke, M. R., Van Meijgaard, E., Van De Berg, W. J., Bamber, J. L., Box, J. E., and Bales, R. C. (2009). Higher surface mass balance of the Greenland ice sheet revealed by high-resolution climate modeling. *Geophysical Research Letters*, 36(12):4–8.

Fahnestock, M., Abdalati, W., Joughin, I., Brozena, J., and Gogineni, P. (2001). High Geothermal Heat Flow, Basal Melt, and the Origin of Rapid Ice Flow in Central Greenland. *Science*, 294:2338–2342.

Fowler, A. (1986). Sub-temperate basal sliding. *Journal of Glaciology*, 32(110):3–5.

Fowler, A. C. (2010). Weertman, Lliboutry and the development of sliding theory. *Journal of Glaciology*, 56(200):965–972.

Fried, M. J., Catania, G. A., Bartholomaus, T. C., Duncan, D., Davis, M., Stearns, L. A., Nash, J., Shroyer, E., and Sutherland, D. (2015). Distributed subglacial discharge drives significant submarine melt at a Greenland tidewater glacier.

Giffoni, A. (2014). The physics of glaciers. `http://ffden-2.phys.uaf.edu/webproj/212_spring_2014/Alison_Giffoni/alison_giffoni/Slide2.html`, Accessed: 2016-05-30.

Glen, J. W. (1954). The creep of polycrystalline ice. *Proceedings of the Royal Society Series A*, 228(1175):519–38.

Gudmundsson, G. H. (2003). Transmission of basal variability to a glacier surface. *Journal of Geophysical Research*, 108(May):1–19.

Gudmundsson, G. H., Krug, J., Durand, G., Favier, L., and Gagliardini, O. (2012). The stability of grounding lines on retrograde slopes. *Cryosphere*, 6(6):1497–1505.

Hanna, E., Huybrechts, P., Steffen, K., Cappelen, J., Huff, R., Shuman, C., Irvine-Fynn, T., Wise, S., and Griffiths, M. (2008). Increased runoff from melt from the Greenland Ice Sheet: A response to global warming. *Journal of Climate*, 21(2):331–341.

Higgins, A. K. (1991). North Greenland Glacier Velocities and Calf Ice Production. *Polarforschung*, 60(1):1–23.

Holland, D. M., Thomas, R. H., de Young, B., Ribergaard, M. H., and Lyberth, B. (2008). Acceleration of Jakobshavn Isbræ triggered by warm subsurface ocean waters. *Nature Geoscience*, 1(10):659–664.

Howat, I. M., Box, J. E., Ahn, Y., Herrington, A., and McFadden, E. M. (2010). Seasonal variability in the dynamics of marine-terminating outlet glaciers in Greenland. *Journal of Glaciology*, 56:601–613.

Howat, I. M., Joughin, I., and Scambos, T. a. (2007). Rapid changes in ice discharge from Greenland outlet glaciers. *Science*, 315(March):1559–1561.

Hughes, T. (2002). Calving bays. *Quaternary Science Reviews*, 21(1-3):267–282.

Iken, A. (1977). Movement of a large ice mass before breaking off. *Journal of Glaciology*, 19(8):595–604.

Iken, A., Echelmeyer, K., Harrison, W., and M., F. (1993). Mechanisms of fast flow in Jakobshavns Isbræ, West Greenland: Part I. Measurements of temperature and water level in deep boreholes. *Journal of Glaciology*, 39(131):15–25.

IPCC Working Group I (2001). *Climate Change 2001: The Scientific Basis.* Cambridge Univ. Press, Cambridge.

Jamieson, S. S., Vieli, A., Livingstone, S. J., Ó Cofaigh, C., Stokes, C., Hillenbrand, C.-D., and Dowdeswell, J. a. (2012). Ice-stream stability on a reverse bed slope. *Nature Geoscience*, 5:799–802.

Jamieson, S. S. R., Vieli, A., Cofaigh, C. Ó., Stokes, C. R., Livingstone, S. J., and Hillenbrand, C. D. (2014). Understanding controls on rapid ice-stream retreat during the last deglaciation of Marguerite Bay, Antarctica, using a numerical model. *Journal of Geophysical Research: Earth Surface*, 119(2):247–263.

Jenkins, A. (2011). Convection-driven melting near the grounding lines of ice shelves and tidewater glaciers. *Journal of Physical Oceanography*, 41(12):2279–2294.

Jóhannesson, T., Raymond, C. F., and Waddington, E. D. (1989). *A Simple Method for Determining the Response Time of Glaciers*, volume 6, chapter A Simple M, pages 343–352. Springer Netherlands, Dordrecht.

Joughin, I., Abdalati, W., and Fahnestock, M. (2004). Large fluctuations in speed on Greenland's Jakobshavn Isbræ glacier. *Nature*, 432(7017):608–610.

Joughin, I., Das, S. B., King, M. A., Smith, B. E., Howat, I. M., and Moon, T. (2008a). Seasonal speedup along the western flank of the Greenland Ice Sheet. *Science*, 320:781–3.

Joughin, I., Howat, I. M., Fahnestock, M., Smith, B., Krabill, W., Alley, R. B., Stern, H., and Truffer, M. (2008b). Continued evolution of Jakobshavn Isbrae following its rapid speedup. *Journal of Geophysical Research*, 113(F4):F04006.

Joughin, I., Smith, B. E., Howat, I. M., Scambos, T., and Moon, T. (2010). Greenland flow variability from ice-sheet-wide velocity mapping. *Journal of Glaciology*, 56(197):415–430.

Joughin, I., Smith, B. E., Shean, D. E., and Floricioiu, D. (2014). Brief Communication: Further summer speedup of Jakobshavn Isbræ. *Cryosphere*, 8(1):209–214.

Khan, S. a., Kjaer, K. H., Bevis, M., Bamber, J. L., Wahr, J., Kjeldsen, K. K., Bjork,

A. a., Korsgaard, N. J., Stearns, L. a., van den Broeke, M. R., Liu, L., Larsen, N. K., and Muresan, I. S. (2014). Sustained mass loss of the northeast Greenland ice sheet triggered by regional warming. *Nature Climate Change*, 4:292–299.

Khan, S. A., Wahr, J., Bevis, M., Velicogna, I., and Kendrick, E. (2010). Spread of ice mass loss into northwest Greenland observed by GRACE and GPS. *Geophysical Research Letters*, 37:1–5.

Krabill, W., Hanna, E., Huybrechts, P., Abdalati, W., Cappelen, J., Csatho, B., Frederick, E., Manizade, S., Martin, C., Sonntag, J., Swift, R., Thomas, R., and Yungel, J. (2004). Greenland Ice Sheet: Increased coastal thinning. *Geophysical Research Letters*, 31(24):1–4.

Legarsky, J. J. and Gao, X. (2006). Internal layer tracing and age-depth relationship from the ice divide toward Jakobshavn, Greenland. *IEEE Geoscience and Remote Sensing Letters*, 3(4):471–475.

Lliboutry, L. (1968). General theory of subglacial cavitation and sliding of temperate glaciers. *Journal of Glaciology*, 7:21–58.

Lloyd, J., Moros, M., Perner, K., Telford, R. J., Kuijpers, A., Jansen, E., and McCarthy, D. (2011). A 100 yr record of ocean temperature control on the stability of Jakobshavn Isbrae, West Greenland. *Geology*, 39(9):867–870.

Lüthi, M., Funk, M., Iken, A., Gogineni, S., and Truffer, M. (2002). Mechanisms of fast flow in Jakobshavn Isbrae, West Greenland: Part III. Measurements of ice deformation, temperature and cross-borehole conductivityin boreholes to the bedrock. *Journal of Glaciology*, 48(162):369–385.

MacGregor, J. A., Colgan, W. T., Fahnestock, M. A., Morlighem, M., Catania, G. A., Paden, J. D., and Gogineni, S. P. (2016). Holocene deceleration of the Greenland Ice Sheet. *Science*, 351(6273):590–593.

MacGregor, J. A., Fahnestock, M. A., Catania, G. A., Paden, J. D., Gogineni, S. P., Young, S. K., Rybarski, S. C., Mabrey, A. N., Wagman, B. M., and Morlighem, M. (2015). Radiostratigraphy and age sturcture of the Greenland Ice Sheet. *Journal of Geophysical Research: Earth Surface*, 120:212–241.

McConnell, J., Arthern, R., Mosley-Thompson, E., Davis, C., Bales, R., Thomas, R., Burkhart, J., and Kyne, J. (2000). Changes in Greenland ice sheet elevation attributed primarily to snow accumulation variability. *Nature*, 406(6798):877–9.

Moon, T. and Joughin, I. (2008). Changes in ice front position on Greenland's outlet glaciers from 1992 to 2007. *Journal of Geophysical Research: Earth Surface*, 113(2):1–10.

Morlighem, M., Rignot, E., Mouginot, J., Seroussi, H., and Larour, E. (2014). Deeply incised submarine glacial valleys beneath the Greenland ice sheet. *Nature Geoscience*, 7:18–22.

Motyka, R. J., Truffer, M., Fahnestock, M., Mortensen, J., Rysgaard, S., and Howat,

I. (2011). Submarine melting of the 1985 Jakobshavn Isbrae floating tongue and the triggering of the current retreat. *Journal of Geophysical Research: Earth Surface*, 116(F1):1–17.

NASA (2012). NASA/Goddard Space Flight Center Scientific Visualization Studio. http://svs.gsfc.nasa.gov/3962, Accessed: 2016-05-30.

Nick, F. M. and Oerlemans, J. (2006). Dynamics of tydewater glaciers: comparison of three models. *J. Glaciol.*, 52(177):183–190.

Nick, F. M., Van Der Veen, C. J., Vieli, A., and Benn, D. I. (2010). A physically based calving model applied to marine outlet glaciers and implications for the glacier dynamics. *Journal of Glaciology*, 56(199):781–794.

Nick, F. M., Vieli, A., Andersen, M. L., Joughin, I., Payne, A., Edwards, T. L., Pattyn, F., and van de Wal, R. S. W. (2013). Future sea-level rise from Greenland's main outlet glaciers in a warming climate. *Nature*, 497(7448):235–8.

Nick, F. M., Vieli, A., Howat, I. M., and Joughin, I. (2009). Large-scale changes in Greenland outlet glacier dynamics triggered at the terminus. *Nature Geoscience*, 2(2):110–114.

Nye, J. (1957). The distribution of stress and velocity in glaciers and ice-sheets. *Proceedings of the Royal Society of London. Series A, Mathematical and Physical Sciences*, 239(1216):123–133.

Nye, J. F. (1960). The Response of Glaciers and Ice-Sheets to Seasonal and Climatic Changes. *Proceedings of the Royal Society of London A: Mathematical, Physical and Engineering Sciences*, 256(1287):559–584.

Nye, J. F. (1976). Water flow in glaciers: Jøkulhlaups, tunnels and veins. *Journal of Glaciology*, 17:1881–207.

Oppenheimer, M. (1998). Global warming and the stability of the West Antarctic Ice Sheet. *Nature*, 393(6683):325–332.

Pattyn, F. (2002). Transient glacier response with a higher-order numerical ice-flow model. *Journal of Glaciology*, 48(162):467–476.

Perrette, M. (2015). Community interactive webtool to explore Greenland datasets. https://github.com/perrette/webglacier1d, accessed: 2015-09-28.

Pollard, D., Deconto, R. M., and Alley, R. B. (2015). Potential Antarctic Ice Sheet retreat driven by hydrofracturing and ice cliff failure. *Earth and Planetary Science Letters*, 412:112–121.

Reeh, N. (1968). On the calving of ice from floating glaciers. *Journal of Glaciology*, 7(50):215–232.

Reeh, N., Thomsen, H. H., Higgins, A. K., and Weidick, A. (2001). Sea ice and the stability of north and northeast Greenland floating glaciers. *Annals of Glaciology*, 33(1):474–480.

Rignot, E., Fenty, I., Xu, Y., Cai, C., and Kemp, C. (2015). Undercutting of marine-terminating glaciers in West Greenland. *Geophysical Research Letters*, 42:5909–5917.

Rignot, E. and Kanagaratnam, P. (2006). Changes in the Velocity Structure of the Greenland Ice Sheet. *Science*, 311:986–990.

Rignot, E., Koppes, M., and Velicogna, I. (2010). Rapid submarine melting of the calving faces of West Greenland glaciers. *Nature Geoscience*, 3(3):187–191.

Rignot, E. and Mouginot, J. (2012). Ice flow in Greenland for the International Polar Year 2008-2009. *Geophysical Research Letters*, 39(11):1–7.

Rignot, E., Mouginot, J., Morlighem, M., Seroussi, H., and Scheuchl, B. (2014). Widespread, rapid grounding line retreat of Pine Island, Thwaites, Smith, and Kohler glaciers, West Antarctica, from 1992 to 2011. *Geophysical Research Letters*, 41(10):3502–3509.

Rignot, E. and Steffen, K. (2008). Channelized bottom melting and stability of floating ice shelves. *Geophysical Research Letters*, 35(2):L02503.

Röthlisberger, H. (1972). Water Pressure in Subglacial Channels. *Journal of Glaciology*, 2(62):177–203.

Schenk, T. and Csathó, B. (2012). A new methodology for detecting ice sheet surface elevation changes from laser altimetry data. *IEEE Transactions on Geoscience and Remote Sensing*, 50(9):3302–3316.

Schoof, C. (2007). Ice sheet grounding line dynamics: Steady states, stability, and hysteresis. *Journal of Geophysical Research: Earth Surface*, 112(3):1–19.

Schoof, C. (2010). Ice-sheet acceleration driven by melt supply variability. *Nature*, 468(7325):803–806.

Seroussi, H., Morlighem, M., Rignot, E., Khazendar, A., Larour, E., and Mouginot, J. (2013). Dependence of century-scale projections of the Greenland ice sheet on its thermal regime. *Journal of Glaciology*, 59(218):1024–1034.

Shapero, D. R., Joughin, I. R., Poinar, K., Morlighem, M., and Gillet-Chaulet, F. (2016). Basal resistance for three of the largest Greenland outlet glaciers. *Journal of Geophysical Research: Earth Surface*, 121:168–180.

Shepherd, A., Ivins, E. R., A, G., Barletta, V. R., Bentley, M. J., Bettadpur, S., Briggs, K. H., Bromwich, D. H., Forsberg, R., Galin, N., Horwath, M., Jacobs, S., Joughin, I., King, M. A., Lenaerts, J. T. M., Li, J., Ligtenberg, S. R. M., Luckman, A., Luthcke, S. B., McMillan, M., Meister, R., Milne, G., Mouginot, J., Muir, A., Nicolas, J. P., Paden, J., Payne, A. J., Pritchard, H., Rignot, E., Rott, H., Sørensen, L. S., Scambos, T. A., Scheuchl, B., Schrama, E. J. O., Smith, B., Sundal, A. V., van Angelen, J. H., van de Berg, W. J., van den Broeke, M. R., Vaughan, D. G., Velicogna, I., Wahr, J., Whitehouse, P. L., Wingham, D. J., Yi, D., Young, D., and Zwally, H. J. (2012). A Reconciled Estimate of Ice-Sheet Mass Balance. *Science*, 338:1183–1189.

Shoemaker, E. M. (1986). Subglacial hydrology for an ice sheet resting on a deformable aquifer. *Journal of glaciology*, 32(110):20–30.

Shreve, R. L. (1984). Glacier sliding at subfreezing temperatures. *Journal of Glaciology*, 30(106):341–347.

Sohn, H., Jezek, K. C., and van der Veen, C. J. (1998). Jakobshavn Glacier, west Greenland: 30 years of spaceborne observations. *Geophysical Research Letters*, 25(14):2699–2702.

Sole, A., Nienow, P., Bartholomew, I., Mair, D., Cowton, T., Tedstone, A., and King, M. A. (2013). Winter motion mediates dynamic response of the Greenland Ice Sheet to warmer summers. *Geophysical Research Letters*, 40(15):3940–3944.

Straneo, F. and Heimbach, P. (2013). North Atlantic warming and the retreat of Greenland's outlet glaciers. *Nature*, 504:36–43.

Straneo, F., Heimbach, P., Sergienko, O., Hamilton, G., Catania, G., Griffies, S., Hallberg, R., Jenkins, A., Joughin, I., Motyka, R., Pfeffer, W. T., Price, S. F., Rignot, E., Scambos, T., Truffer, M., and Vieli, A. (2013). Challenges to understanding the dynamic response of Greenland's marine terminating glaciers to oc eanic and atmospheric forcing. *Bulletin of the American Meteorological Society*, 94:1131–1144.

Sugden, D. and John, B. (1976). *Glaciers and Landscape: A Geomorphological Approach*. Arnold Education, London.

Sundal, A. V., Shepherd, A., Nienow, P., Hanna, E., Palmer, S., and Huybrechts, P. (2011). Melt-induced speed-up of Greenland ice sheet offset by efficient subglacial drainage. *Nature*, 469(7331):521–524.

Tedstone, A. J., Nienow, P. W., Gourmelen, N., Dehecq, A., Goldberg, D., and Hanna, E. (2015). Decadal slowdown of a land-terminating sector of the Greenland Ice Sheet despite warming. *Nature*, 526(7575):692–695.

Tedstone, A. J., Nienow, P. W., Sole, A. J., Mair, D. W. F., Cowton, T. R., Bartholomew, I. D., and King, M. a. (2013). Greenland ice sheet motion insensitive to exceptional meltwater forcing. *Proceedings of the National Academy of Sciences of the United States of America*, 110(49):19719–24.

Thomas, R., Akins, T., Csatho, B., Fahnestock, M., Gogineni, P., Kim, C., and Sonntag, J. (2000). Mass Balance of the Greenland Ice Sheet at High Elevations. *Science*, 289:426–428.

Thomas, R., Frederick, E., Krabill, W., Manizade, S., and Martin, C. (2009). Recent changes on Greenland outlet glaciers. *Journal of Glaciology*, 55(189):147–162.

Thomas, R. H. (1979). The Dynamics of Marine Ice Sheets. *Journal of Glaciology*, 24(90):167 – 177.

Thomas, R. H., Abdalati, W., Frederick, E., Krabill, W. B., Manizade, S., and Steffen, K. (2003). Investigation of surface melting and dynamic thinning on Jakobshavn Isbræ, Greenland. *Journal of Glaciology*, 49:231–239.

Truffer, M., Harrison, W. D., and Echelmeyer, K. A. (2000). Glacier motion dominated by processes deep in underlying till. *Journal of Glaciology*, 46(153):213–221.

Van den Broeke, M., Bamber, J. L., Ettema, J., Rignot, E. J., Schrama, E., Van de Berg, W., Van Meijgaard, E., Velicogna, I., and Wouters, B. (2009). Partitioning Recent Greenland Mass Loss. *Science*, 326(5955):984–986.

Van Der Veen, C. J. (1996). Tidewater calving. *Journal of Glaciology*, 42(141):375–385.

Van der Veen, C. J. (2013). *Fundamentals of Glacier Dynamics*. CRC Press, 2nd edition.

Van Der Veen, C. J., Plummer, J. C., and Stearns, L. a. (2011). Controls on the recent speed-up of Jakobshavn Isbræ, West Greenland. *Journal of Glaciology*, 57(204):770–782.

Van der Veen, C. J. and Whillans, I. M. (1996). Model experiments on the evolution and stability of ice streams. *Annals of Glaciology*, 23:129–137.

Vieli, A., Funk, M., and Blatter, H. (2001). Flow dynamics of tidewaterg laciers: A numerical modelling approach. *Journal of Glaciology*, 47:595–606.

Vieli, A., Jania, J., and Kolondra, L. (2002). The retreat of a tidewater glacier: Observations and model calculations on Hansbreen, Spitsbergen. *Journal of Glaciology*, 48(163):592–600.

Vieli, A. and Nick, F. M. (2011). Understanding and Modelling Rapid Dynamic Changes of Tidewater Outlet Glaciers: Issues and Implications. *Surveys in Geophysics*, 32(4-5):437–458.

Vieli, A. and Payne, A. J. (2005). Assessing the ability of numerical ice sheet models to simulate grounding line migration. *Journal of Geophysical Research: Earth Surface*, 110(F1):1–18.

Vieli, A., Payne, A. J., Shepherd, A., and Du, Z. (2007). Causes of pre-collapse changes of the Larsen B ice shelf: Numerical modelling and assimilation of satellite observations. *Earth and Planetary Science Letters*, 259(3-4):297–306.

Walder, J. and Fowler, A. (1994). Channelized subglacial drainage over a deformable bed. *Journal of Glaciology*, 40(134):3–15.

Walder, J. S. (1986). Hydraulics of subglacial cavities. *Journal of Glaciology*, 32(112):439–445.

Weber, J. E. (2000). Non-temperate glacier flow over wavy sloping ground. *Journal of Glaciology*, 46(154):453–458.

Weertman, J. (1957). On the sliding of glaciers. *Journal of Glaciology*, 3:33–38.

Weertman, J. (1967). Sliding of nontemperate glaciers. *Journal of Geophysical Research*, 72(2):521–523.

Weertman, J. (1972). General Theory of Water Flow at the Base of a Glacier or Ice Sheet. *Reviews of Geophysics and Space Physics*, 10(1):287–333.

Weertman, J. (1973). Creep of ice. *Physics and Chemistry of Ice*, pages 320–337.

Weertman, J. (1974). Stability of the junction of an ice sheet and an ice shelf. *Journal of Glaciology*, 13(67):3–11.

Weidick, A. and Bennike, O. (2007). Quaternary glaciation history and glaciology of Jakobshavn Isbrae and the Disko Bugt region, West Greenland: a review. *Geological Survey of Denmark and Greenland Bulletin*, (14):78.

Whillans, I. M. and Van der Veen, C. J. (1997). The role of lateral drag in the dynamics of Ice Stream B, Antarctica. *Journal of Glaciology*, 43(144):231–237.

White, F. M., Spaulding, M. L., and Gominho, L. (1980). Theoretical estimates of the various mechanisms involved in iceberg deterioration in the open ocean environment. *U.S. Coast Guard Report*, CG-D-62-80:136.

Zwally, H., Abdalati, W., Herring, T., Larson, K., Saba, J., and Steffen, K. (2002). Surface Melt-Induced Acceleration of Greenland Ice-Sheet Flow. *Science*, 297:218–222.

List of Figures

2.1 Sketch of the glacier mass balance of a marine-terminating glacier, showing processes of accumulation and ablation; the ELA is marked as dashed line (Giffoni, 2014). 5

2.2 Modeled SMB change from 1958 to 2007 in kg m^{-2} (Ettema et al., 2009). 250 m elevation contours from Bamber et al. (2001) are shown as dashed lines. 6

2.3 Sketch of the stresses acting on a glacier. Redrawn from Van der Veen (2013). 8

2.4 Depth-profiles of glacier velocities for different basal conditions. (**a**) Ice flow due to creep over a frozen bed; (**b**) Velocities associated with creep and basal sliding of a warm-based glacier; (**c**) Ice flow as a combination of creep, basal sliding and deformation of subglacial sediments (Boulton, 1996). 8

2.5 Sliding by regelation (after Weertman, 1967). The melting temperature T_m is only illustrative. 9

2.6 Illustration of compressive stresses in a crevasses without meltwater (left) compared to a water-filled one (right) by Benn and Evans (2010) 13

2.7 Warm subsurface waters and plume dynamics by subglacial discharge cause submarine melting of a marine-terminating glacier. Warmer temperature cause more subglacial discharge due to increased surface melt, warmer water and reduced ice mélange. This causes higher submarine melt rates (Straneo and Heimbach, 2013). 14

2.8 Calving front position of Jakobshavn Isbræ from Arctic Sea Ice Blog (2015). The location of Jakobshavn Isbræ on the GrIS is marked on the inlet as a white box. NASA (2012) 16

3.1 Illustration of important factors influencing a marine-terminating glacier. The abbreviations stand for glacier thickness, H; surface elevation, h; bed elevation, h_b; ice thickness below sea level, D; height above buoyancy, H_{ab}; flotation thickness, H_f. 19

3.2 Illustration of the crevasse-depth calving criterion (Benn and Evans, 2010). 22

3.3 Illustration of difference in hydrostatic pressure of ice and water at the calving front. (Benn et al., 2007b) 23

4.1 Initial geometry and forcing of the idealized glacier configuration. (**a**) shows the initial and final steady-state glacier geometry with the along-flow velocity in the steady-state. (**b**) gives the width in planview and (**c**) shows the Surface Mass Balance (SMB) and Submarine Melt Rate (SMR) with the same y-axis, for the initial geometry and the steady-state. 27

4.2 Response to perturbations of the basal sliding parameter A_s (in $\mathrm{Pa\,m^{-2/3}\,s^{-1/3}}$) for an idealized marine-terminating glacier, from warm ice towards cold ice (red to black). Shown are the glacier shape and the corresponding velocities after 1500 years (blue to green) in (**a**), as well as the evolution of grounding line (GRL) position (**b**), grounding line velocity (**c**), calving flux (**d**), grounding line flux (**e**), volume (**f**) and difference between the surface after 1500 years and the steady-state (**g**). The steady-state is marked as dashed line. 29

4.3 Response to perturbations of the crevasse water depth *cwd* for an idealized marine-terminating glacier, from warm ice towards cold ice (red to black). Shown are the glacier shape and the corresponding velocities after 1500 years (blue to green) in (**a**), as well as the evolution of grounding line (GRL) position (**b**), grounding line velocity (**c**), calving flux (**d**), grounding line flux (**e**), volume (**f**) and difference between the surface after 1500 years and the steady-state (**g**). The steady-state is marked as dashed line. 31

4.4 Response to perturbations of the sea ice factor f_{si} for an idealized marine-terminating glacier, from warm ice towards cold ice (red to black). Shown are the glacier shape and the corresponding velocities after 1500 years (blue to green) in (**a**), as well as the evolution of grounding line (GRL) position (**b**), grounding line velocity (**c**), calving flux (**d**), grounding line flux (**e**), volume (**f**) and difference between the surface after 1500 years and the steady-state (**g**). The steady-state is marked as dashed line. . . . 32

4.5 Response to perturbations of the submarine melt rate *smr* for an idealized marine-terminating glacier, from warm ice towards cold ice (red to black). Shown are the glacier shape and the corresponding velocities after 1500 years (blue to green) in (**a**), as well as the evolution of grounding line (GRL) position (**b**), grounding line velocity (**c**), calving flux (**d**), grounding line flux (**e**), volume (**f**) and difference between the surface after 1500 years and the steady-state (**g**). The steady-state is marked as dashed line. 33

4.6 Response to perturbations of the rate factor A for an idealized marine-terminating glacier, from warm ice towards cold ice (red to black). Shown are the glacier shape and the corresponding velocities after 1500 years (blue to green) in (**a**), as well as the evolution of grounding line (GRL) position (**b**), grounding line velocity (**c**), calving flux (**d**), grounding line flux (**e**), volume (**f**) and difference between the surface after 1500 years and the steady-state (**g**). The steady-state is marked as dashed line. . . . 35

5.1 Screenshot of the topography (**a**) and velocity (**b**) map of Jakobshavn Isbræ and the produced grid in the interactive webtool by Perrette (2015). The bedrock data is from Morlighem et al. (2014) and the velocity data from Rignot and Mouginot (2012). The resolution of the calculated 1D-data is 5 km. 38

5.2 Initial geometry and forcing of the Jakobshavn Isbræ configuration. (**a**) shows the glacier geometry with the along-flow velocity in steady-state. (**b**) gives the width in planview and (**c**) shows the surface mass balance and submarine melt rate with the same y-axis. 39

5.3 Response to perturbations of the basal sliding A_s for the geometry of Jakobshavn Isbræ, from more to less sliding (red to black). Shown are the glacier shape and the corresponding velocities after 1500 years (blue to green) in (**a**), as well as the evolution of grounding line position (**b**), grounding line velocity (**c**), calving flux (**d**), grounding line flux (**e**), volume (**f**) and difference between the surface after 1500 years and the steady-state (**g**). The steady-state is marked as dashed line. 42

5.4 Response to perturbations of the crevasse water depth cwd for the geometry of Jakobshavn Isbræ, from more to less sliding (red to black). Shown are the glacier shape and the corresponding velocities after 1500 years (blue to green) in (**a**), as well as the evolution of grounding line position (**b**), grounding line velocity (**c**), calving flux (**d**), grounding line flux (**e**), volume (**f**) and difference between the surface after 1500 years and the steady-state (**g**). The steady-state is marked as dashed line. . . . 43

5.5 Response to perturbations of the sea ice factor f_{si} for the geometry of Jakobshavn Isbræ, from more to less sliding (red to black). Shown are the glacier shape and the corresponding velocities after 1500 years (blue to green) in (**a**), as well as the evolution of grounding line position (**b**), grounding line velocity (**c**), calving flux (**d**), grounding line flux (**e**), volume (**f**) and difference between the surface after 1500 years and the steady-state (**g**). The steady-state is marked as dashed line. 44

5.6 Response to perturbations of the submarine melt rate smr for the geometry of Jakobshavn Isbræ, from more to less sliding (red to black). Shown are the glacier shape and the corresponding velocities after 1500 years (blue to green) in (**a**), as well as the evolution of grounding line position (**b**), grounding line velocity (**c**), calving flux (**d**), grounding line flux (**e**), volume (**f**) and difference between the surface after 1500 years and the steady-state (**g**). The steady-state is marked as dashed line. 45

5.7 Response to perturbations of the rate factor A for the geometry of Jakobshavn Isbræ, from more to less sliding (red to black). Shown are the glacier shape and the corresponding velocities after 1500 years (blue to green) in (**a**), as well as the evolution of grounding line position (**b**), grounding line velocity (**c**), calving flux (**d**), grounding line flux (**e**), volume (**f**) and difference between the surface after 1500 years and the steady-state (**g**). The steady-state is marked as dashed line. 47

5.8 Time evolution of the glacier for the first 200 years after a perturbation in the rate factor (**a**), viscosity (**b**), and lateral resistance (**c**), with values corresponding to to $-20\,°\mathrm{C}$. Time steps are 10 years from black (green) to red (blue). The steady-state glacier and velocity are plotted in black with a dashed line. 48

6.1 Combined presentation of property changes for the perturbed parameters after 200 model years: crevasse water depth (cwd, red), sliding factor (A_s, blue), rate factor (A, green), submarine melt rate (smr, orange) and sea ice factor (f_{si}, black). (**a**) and (**b**) show change in glacier volume and temperature in case of changed parameters towards higher temperatures, where the temperatures are only to be taken relatively. (**c**) presents the change in thickness at the ice divide versus length and (**d**) shows the change in calving and submarine melt flux versus grounding line flux. . . 50

6.2 Sketch of the impacts of the five parameter perturbations on a marine-terminating glacier. The panels show the impact of the rate factor (**a**), basal sliding (**b**), crevasses water depth (**c**), buttressing by sea ice (**d**), and submarine melt rate (**e**). 52

6.3 Time evolution of the idealized glacier and Jakobshavn Isbræ for the first 500 years after a reduction in buttressing by sea ice by a factor 3.5. Shown are the evolution of the glacier shape and velocity (**a** and **b**) and the change in length on a planview (**c** and **d**). The time step is 5 years from black to red. The steady-state is illustrated with a dashed line. . . . 58

7.1 Reconstructions of the ice margins of Jakobshavn Isbæ and the Greenland Ice Sheet back to 9500 B.P (Weidick and Bennike, 2007). 62

A.1 Comparison of the unsmoothened bed topography data by Bamber et al. (2013) and Morlighem et al. (2014) along the flowline of Jakobshavn Isbæ, calculated by cross-sections with the interactive webtool by Perrette (2015) 66

B.1 The four stress components along the flowline of the idealized glacier for the steady-state solution. 67

B.2 The four stress components along the flowline of Jakobshavn Isbræ for the steady-state solution. 68

C.1 Time evolution during the first 200 years of the surface and velocity after a perturbation to increased basal sliding ($A_s = 40\,\mathrm{Pa\,m^{-2/3}\,s^{-1/3}}$). The time step is 10 years from black to red (green to blue). The steady-state profile is drawn as dashed line. 69

C.2 Time evolution during the first 200 years of the surface and velocity after a perturbation to reduced basal sliding ($A_s = 160\,\mathrm{Pa\,m^{-2/3}\,s^{-1/3}}$). The time step is 10 years from red to black (blue to green). The steady-state profile is drawn as dashed line. 69

D.1 Glacier response during the first 3000 years to parameter perturbations in viscosity (left column) and lateral resistance (right column) towards values representative for ice temperatures of 0 °C (red) to −20 °C (black). Showing the surface elevation and velocity (**a** and **b**), the change in the surface elevation between first year and last year (**c** and **d**), evolution of grounding line position with time (**e** and **f**), the calving flux (**g** and **h**) and grounding line flux (**i** and **j**). 70

E.1 Model run of the perturbation to a rate factor corresponding to −5 °C for 20,000 years, showing stabilization. Shown are the glacier shape and the corresponding velocities in time steps of 500 years (black to red and green to blue, respectively) in (**a**), as well as the evolution of grounding line position (**b**), volume (**c**), calving flux (**d**) and grounding line flux (**e**). 71

F.1 Combined presentation of property changes for the perturbed parameters after 1500 model years: crevasse water depth (*cwd*, red), sliding factor (A_s, blue), rate factor (A, green), submarine melt rate (*smr*, orange) and sea ice factor (f_{si}, black). (**a**) and (**b**) show change in glacier volume and temperature in case of changed parameters towards higher temperatures, where the temperatures are only to be taken relatively. (**c**) presents the change in thickness at the ice divide versus length and (**d**) shows the change in calving and submarine melt flux versus grounding line flux. . . 72

F.2 Combined presentation of property changes for the perturbed parameters of the approximate geometry of Jakobshavn Isbræ after 1500 model years: crevasse water depth (*cwd*, red), sliding factor (A_s, blue), rate factor (A, green), submarine melt rate (*smr*, orange) and sea ice factor (f_{si}, black). (**a**) and (**b**) show change in glacier volume and temperature in case of changed parameters towards higher temperatures, where the temperatures are only to be taken relatively. (**c**) presents the change in thickness at the ice divide versus length and (**d**) shows the change in calving and submarine melt flux versus grounding line flux. 73